# Numerical Simulation of Dispersion of Emissions from Tema Oil Refinery in Ghana

A dissertation presented to the:
Department of NUCLEAR SCIENCES AND APPLICATIONS

SCHOOL OF NUCLEAR AND ALLIED SCIENCES

COLLEGE OF BASIC AND APPLIED SCIENCES

UNIVERSITY OF GHANA

by

HANNAH ASAMOAH AFFUM (ID: 10174319)
BSc (KNUST), 2002
MPhil (UG), 2006

In partial fulfillment of the requirements for the degree of
DOCTOR OF PHILOSOPHY

in

APPLIED NUCLEAR PHYSICS

2015

# Declaration

This thesis is the result of research work undertaken by Hannah Asamaoh AFFUM in the Department of Nuclear Sciences and Applications, School of Nuclear and Allied Sciences, University of Ghana, under the supervision of Prof. Emeritus E.H.K. Akaho (SNAS, UG - Legon, Ghana), Prof. Joseph J.J. Niemela (ICTP, Trieste, Italy), Prof. Vincenzo Armenio (UT, Trieste, Italy) and Dr. K. A. Danso (SNAS, UG - Legon, Ghana).

Sign: .....

Hannah Asamaoh Affum
(Student)

Sign: ..... Sign: .....

Prof. Emeritus E.H.K. Akaho
(Supervisor)

Prof. J.J. Niemela
(Co-Supervisor)

Sign:..... Sign: .....

Prof. Vincenzo Armenio
(Co-Supervisor)

Dr. K.A. Danso
(Co-Supervisor)

*Dedicated to my amazing children, Aseyenedi Esi Tamakloe, Woedem Dzidula Tamakloe and Alesineyram Aku Tamakloe...*

# *Acknowledgements*

I would like to express my greatest appreciation to Almighty God without whom the subsequent happenings would not have been possible.

This PhD project was funded by the International Atomic Energy Agency (IAEA) through the International Centre for Theoretical Physics (ICTP) Sandwich Training and Exchange Programme(STEP) in Trieste, Italy. It is, as such, befitting for these kind sponsors to be the next receipient of my heart-felt gratitude.

The author would like to express profound thanks to her home principal supervisor, Prof. Emeritus E.H.K. Akaho and home co-supervisor, Dr. K.A. Danso both of School of Nuclear and Allied Sciences(SNAS), University of Ghana. Their constant encouragement and strong belief in my ability to go through this academic exercise is truly appreciated. For agreeing to supervise this thesis and ensuring that I had all that was needed to carry out this research work successfully, my next thanks go to Prof. J.J. Niemela and Prof. Vincenzo Armenio of the International Centre for Theoretical Physics and the University of Trieste respectively. The great exposure acquired through my association is deeply cherished. The intellectual support from my entire supervisory committee is very much appreciated.

Further appreciation is extended to some technical staff of the Residual Fluid Catalytic Cracking Unit of the Tema Oil Refinery, Ghana, especially

the manager Engineer Kwaku Darko, Randy and Priscilla Antwi for willingly commiting to our mini-project of estimating refinery emissions in the absence of data from flow meters.

I would want to specially thank all the doctoral students and staff of the fluids laboratory of the University of Trieste whom I came into contact with and exchanged ideas during my attachment to the laboratory. Ahmad Fakari and Anna Brunetti deserve special mention for their patience they displayed in coaching me through the various codes I used at various stages in this research work. For assisting me to build the Latex code for the write-up of this thesis and others, I also say a big thanks to Christian Nuviadenu and Ernest Asare.

A special thanks also goes to Dr. Clement Onime, whom I affectionately call 'Uncle Clement', Addisu Semie and Grazianno Giancula whose instrumentality is helping with the set-up and running the WRF model can simply not be overemphasized.

I would also like to thank Jake Doku of the Remote Sensing laboratory of the University of Ghana for willingly providing elevation and base maps of my study area. Appreciation is also extended to my colleagues at the Nuclear Application Centre of the Ghana Atomic Energy Commission for their assistance. I specifically mention Simon Adzaklo, Alexander Coleman and Godred Appiah who took turns to pick up my children from school.

Dorotea Calligaro and all staff of the ICTP who in one way or another helped make life comfortable for me while in ICTP, Trieste are also gratefully acknowledged. Spiritual support from members of the ICTP fellowship and the Chiesa di Evangelica especially Ettore Panizon and family, Tonino Cuschito and family is very much appreciated.

Last but not least, my sincere gratitude is to all of my family especially my kind and loving husband Emmanuel for all he sacrificed to care for our children, Aseye, Woedem and Alesi, whiles I was on fellowship in Trieste, Italy. How can I forget the unparalled support from Mawuli, my parents and my in-laws. I would like to thank them for their love, care and encouragements. Truly, I could not have done this without you.

All friends who gave support deserve my sincerest thanks, especially my colleagues who encouraged me during the finalisation of this PhD study.

# Abbreviations

| | |
|---|---|
| ABL | Atmospheric Boundary Layer |
| AFWA | Airforce Weather Agency |
| AMS | Accra Meteorological Station |
| AQM | Air Quality Model |
| BID | Buoyancy-Induced Dispersion |
| CALMET | California Meteorological |
| CALPOST | California Post-Processing |
| CALPUFF | California Puff |
| CDU | Crude Distillation Unit |
| CTDM | Complex Terrain Dispersion Model |
| DEM | Digital Elevation Model |
| DOAS | Differential Optical Absorption Spectrometry |
| EIPPCB | European Integration Pollution Prevention Control Bureau |
| EPA | Environmental Protection Agency |
| FB | Fractional Bias |
| FSL | Forecast Systems Laboratory |
| GC | Gas Chromatography |
| GFS | Global Forecast System |
| GLCC | Global Land Cover Characterization |
| GM | Geometric Mean |
| GSS | Ghana Statistical Service |
| GV | Geometric Variance |

| | |
|---|---|
| IAEA | International Atomic Energy Agency |
| ICTP | International Centre for Theoretical Physics |
| IOA | Index Of Agreement |
| IS | Inertial Sub-layer |
| ISCST | Industrial Source Complex Short-Term |
| KNUST | Kwame Nkrumah University of Science and Technology |
| LULC | Land Use Land Cover |
| MB | Mean Bias |
| NCAR | National Centre for Atmospheric Research |
| NCEP | National Centres for Environmental Prediction |
| MESOPUFF | Mesoscale Puff |
| NMSE | Normalised Mean Square Error |
| NWP | Numerical Weather Prediction |
| PBL | Planetary Boundary Layer |
| PG | Pasquill-Gifford |
| PM | Particulate Matter |
| PRF | Premium Reforming |
| R | Correlation Coefficient |
| RFCC | Residual Fluid Catalytic Cracking |
| RS | Roughness Sub-layer |
| SNAS | School Of Nuclear and Allied Sciences |
| SRTM | Shuttle Radar Topography Mission |
| TMS | Tema Meteorological Station |
| TOR | Tema Oil Refinery |
| UCL | Urban Canopy Layer |
| UG | University of Ghana |
| UNEP | United Nations Environment Programme |
| USAID | United States Agency for International Development |
| USEPA | United States Environmental Protection Agency |

| | |
|---|---|
| USGS | United States Geological Survey |
| UT | University of Trieste |
| UTM | Universal Transverse Mercaptan |
| VOC | Volatile Organic Compound |
| WRF | Weather Research and Forecasting |

# Physical Constants

| **Constant Name** | **Symbol** | = | **Constant Value** |
|---|---|---|---|
| Acceleration due to gravity | $g$ | = | 9.8 $m/s^2$ |
| Universal Gas Constant | $R$ | = | 8.314 $kJK^{-1}mol^{-1}$ |
| pi | $\pi$ | = | 3.14 |
| Von Karman constant | $\kappa$ | = | 0.41 |

# Symbols

| Symbol | Name |
|---|---|
| $\sigma$ | Standard deviation |
| $\theta$ | Potential temperature |
| $\xi$ | Virtual source matrix |
| $\beta$ | Entrainment parameter |
| $\rho$ | Density |
| $U_\tau$ | Friction velocity |
| $d$ | Displacement |
| $z$ | Roughness height |
| $u$ | Velocity |
| $C$ | Concentration |
| $V$ | Volume |
| $Q$ | Emission rate |
| $H$ | Mixing depth |
| $r_G$ | Ground reflection coefficient |
| $D$ | Molecular diffusivity |
| $S$ | Source/Sink |
| $p$ | Probability distribution function |
| $Z$ | Terrain-following vertical coordinate |
| $h_t$ | Terrain height |
| $N$ | Brunt-Vaisala frequency |

| | |
|---|---|
| $k$ | Coefficient of exponential decay |
| $F_r$ | Local Froude number |
| $F$ | Buoyancy |
| $F_m$ | Momentum flux |
| $T_a$ | Ambient Temperature |
| P | Pressure |

# Table of Contents

# List of Tables

# List of Figures

# Abstract

The petrochemical industry is a major contributor of industrial air pollutants which are known to have dire consequences on human health and the environment, neccesitating research into their dispersion and transport. The objective of the study, therefore, is to simulate the dispersion and transport of pollutants emitted during the processing of crude oil by the Tema Oil Refinery in the Greater Accra region of Ghana using the California Puff (CALPUFF) modeling system. This thesis couples the Weather Research and forecasting Model (WRF) with the non-steady state California Puff(CALPUFF) modelling system to simulate the dispersion and transport of emissions from the refinery in a coastal urban/industrial area in Ghana. The mass balance approah was employed to estimate the refinery emission rates which were used as input for the dispersion model. Emission rates of five species were estimated - $SO_2$, $NO_2$, $PM_{2.5}$, $CO_2$ and VOCs. The transport and dispersion of $SO_2$, $NO_2$ and $PM_{2.5}$ were modelled over the period between 2008 - 2013 and their impact on 38 identified receptors investigated. Simulation results showed that the radius of impact of the emissions is approximately 10 km. As a result of the prevailing predominant south-westerly winds in the study area, concentrations of emissions at receptors located upwind of the emission source were found to be higher as the winds carried the pollutant clouds in their direction. Conversely, south and south-western receptors, relative to the refinery, on the other hand,

were minimally impacted. Concentrations of $SO_2$ and $NO_2$ at 2 out of the 38 receptors exceeded the regulatory limit of the World Health Organisation and Ghana's Environmental Protection Agency. It can be concluded, therefore, that $SO_2$ and $NO_2$ emissions from the refinery do not pose any danger to the larger population and the general environment nearby. $PM_{2.5}$ levels at 36 receptors however exceeded the WHO guideline value leading to the conclusion that the refinery operations could pose some dangers to the environment regarding $PM_{2.5}$. The dispersion model results were compared with measurements at the same location in order to validate the model. Similarly, observations from two meteorological stations were compared with results from the meteorological model. The performance evaluation, with the aid of statistical measures revealed that the models' performance were acceptable.

# Chapter 1

# General Introduction

## 1.1 Introduction

This thesis deals with the modeling and simulation of the long-range transport and dispersion of refinery emissions over a defined study area. The first chapter of the dissertation provides a brief background of the thesis subject area, gives the problem statement, the justification and scope of this research and finally outlines the objectives of the study.

## 1.2 Background

All life forms on this planet depend on clean air. Air quality not only affects human health but also components of environment such as water, soil and forests which are the vital resources for human development. A major

threat to the availability of clean air is urbanisation. Urbanization is a process of relative growth in a country's urban population accompanied by an even faster increase in the economic, political and cultural importance of cities relative to rural areas. As an integral part of economic development, urbanisation brings in its wake a number of challenges including the increase in urban population, industrial activities, high rise buildings and vehicular movement. All these activities contribute to air pollution (de Leeuw et al., 2001, Fenger, 1999).

Exposure to such air pollutants may adversely affect human health. Short term exposure to peak levels of particulate matter has been strongly associated with adverse respiratory health impacts (e.g., respiratory diseases such as asthma and pulmonary function insufficiency) (Brunekreef and Holgate, 2002, Guilbert et al., 2003, Hansard et al., 2011). Furthermore, particulate matter, hereafter referred to as PM, is known to degrade atmospheric visibility. High concentrations of sulphur dioxide, $SO_2$, which are also emitted from power plants, industrial processes and during the combustion of fossil fuels, can aggravate respiratory diseases as well as cause problems such as acid rain and damaged vegetation in the form of foliar necrosis (Khamsimak et al., 2012). Additionally, air pollution is not only a human health problem: its effects on ecosystems and materials are well identified and documented (Fowler et al., 2009). Economic costs can also be associated with poor air quality as well as political/governmental measures taken to

prevent or reduce pollution (Muller and Mendelsohn, 2007).

## 1.3 Problem Statement/Research Gap

The USEPA, USAID and UNEP as far as July 2004, selected Accra, Ghana as one of two cities in Africa to benefit from an Air Quality Monitoring Capacity Building Project with the aim to build and establish local capacity on air quality monitoring that will provide policy-makers with information on the air quality in Accra and its impacts on health. Subsequent to this, the EPA, Ghana replicated the project in a few more cities in Ghana with emphasis on PM measurements. $SO_2$ and $NO_2$ emissions from vehicular traffic have also been monitored in parts of Accra. Apart from the EPA's efforts, similar monitoring activities have been carried out, especially within the Accra metropolis, by students and groups of scientists for different periods of time largely on heavy metals. For example, Arku et al. (2008) conducted a study for an initial assessment of the levels and spatial and/or temporal patterns of multiple pollutants in the ambient air in two low-income neighborhoods in Accra, Ghana over a 3-week period while Ofosu et al. (2012) characterized fine particulate sources at Ashaiman in Greater Accra, Ghana. Others include the assessment of particulate matter and heavy metals along major highways and in mining areas (Affum et al., 2008, Bansah and Amegbey, 2012, Safo-Adu et al., 2014). Quite recently, Sackey

(2012) employed Differential Optical Absorption Spectroscopy (DOAS) in the measurement of atmospheric constituents as a result of combustion, vehicular emissions and industrial activities around the Tema Oil refinery. There is, however, limited or no information about the behaviour and spread of these pollutants from specific sources in the atmosphere within the country. This is because none of the research works focussed on a specific industry, its air emissions and rates and the transport of the emissions within its catchment area. A gap therefore exists in this area of research which thesis seeks to fill through atmospheric dispersion modelling.

## 1.4 Justification and Scope of Work

The simplest technique for evaluating patterns of local-scale urban air pollution concentration involves the interpolation of ambient concentrations from existing monitoring networks (Ferretti et al., 2008, Perez Ballesta et al., 2008). However, the measured data from these stations or study areas are not necessarily representative of areas beyond their immediate vicinity. This is because concentrations of pollutants in urban areas may greatly vary on spatial scales that range from tens to hundreds of metres.

Moreover, the establishment and operation of monitoring stations are expensive and can only be expected to be established in few locations. At the same time, the temporal behaviour of primary and secondary pollutants

changes considerably between day and night due to solar radiation, so that daily average measurements become unsatisfactory in determining or explaining high pollution episodes. In such instances, air pollution dispersion models become necessary.

Dispersion modelling studies, in combination with air quality monitoring, are essential and complementary tools for long and short term air pollution control strategies in effective air quality management. Air quality and dispersion models become valid instruments for environmental managers in many activities, such as setting emission control regulations, testing the compliance of actual pollution levels, predicting the impact of new facilities on human health, selecting the best location for monitoring stations and assessing the impact of different emissions scenarios on selected locations (Puliafito et al., 2011). Modelling studies are crucial as they provide useful data on the dynamics of pollutant dispersion and transport among others, which feed into the formulation of environmental policies as well as management processes. Furthermore, they improve the limitations of monitoring networks by providing predictions of the temporal and spatial distribution of actual pollution levels. The focus of this thesis, therefore, is to utilize air quality modeling to fill the gap that presently exists in the area of air pollution studies within the country.

Due to the significant contribution of petroleum refineries to air pollution, this thesis investigates the long-range transport of emissions from Ghana's

only refinery, Tema Oil Refinery, using numerical models.

## 1.5 Objectives of the Study

The main objective of the study is to simulate the dispersion and transport of pollutants emitted during the processing of crude oil by the Tema Oil Refinery, hereafter referred to as TOR, in the Greater Accra region of Ghana using the California Puff (CALPUFF) modeling system. This will be achieved through the following specific objectives:

1. To estimate the emission rates of $CO_2$, $SO_2$, $NO_2$, volatile organic compounds (VOCs) and $PM_{2.5}$ during refinery operations at the TOR.
2. To simulate the transport and dispersion of the emissions and
3. To access the impact of meteorological conditions on the dispersion of the emissions.

## 1.6 Dissertation Outline

This thesis is organized as follows: The first chapter of the dissertation provides a brief background of the thesis area, gives the problem statement, the justification and scope of this research and finally outlines the objectives of the study.

In Chapter 2, a literature review of the subject area is presented. Emissions and their sources are discussed briefly after which an overview of some air quality models and their applications as well as their strengths and limitations are presented. A detailed description of the CALPUFF/CALMET models used for the simulation is also included in this chapter. A short presentation of the prognostic mesoscale WRF model used to simulate the wind fields is also provided.

In Chapter 3, the methodology for the simulation of the pollutants dispersion in the study area is presented. First of all, the methodology for the estimation of pollutants from the refinery is presented. This is followed by a description of the various data resources used for the simulation. The validation methodology of all simulation results is also described using some statistical tools.

A thorough discussion of the research results and its contribution to the wider literature are presented in Chapter 4.

Finally in Chapter 5, conclusions and recommendations are presented. The limitations and challenges of the work are also discussed and future work outlined.

# Chapter 2

# Literature Review

## 2.1 Introduction

This Chapter presents some general concepts and theoretical frameworks in air pollution studies. Various air quality models in literature are also reviewed. A detailed description of the numerical models used for the simulations in this thesis, namely the California Puff (CALPUFF) modelling system and WRF, a description of the study area and the emission source of interest, TOR are also presented. The equations forming the basis of the models are presented as well as an overview of the Residual Fluid Catalytic Cracking (RFCC) process in petroleum refining at the TOR.

## 2.2 Description and Characteristics of the Atmosphere Boundary Layer

A discussion of the layers in the earth's atmosphere is needed to better understand where air pollution dispersion takes place. The main layers of the earth's atmosphere, from the surface of the ground upwards, as shown in Fig.2.1 are the troposphere (0 to 15 km), the stratosphere (15 to 50 km), the mesosphere (50 to 85 km), the thermosphere and others (more than 85 km). The lowest part of the troposphere is the Atmospheric Boundary Layer (ABL) or Planetary Boundary Layer (PBL) which extends from the earth's surface to about 1.5 to 2.0 km in height (Stull, 2012). The ABL is made up of the mixing layer, capped by the inversion layer, and is separated by a change in temperature behaviour in the vertical direction as shown in Fig.2.2.

Human activity is generally confined to the ABL such that pollutant sources are created in this area. Thus the challenge of modeling pollutant dispersion is understanding how materials are mixed by turbulence and transported from the release point to larger scales (Fernando, 2010). Fundamentally, it is characterized by a large shearing stress resulting from momentum transfer at the surface. The exact structure of the ABL is determined by both the character of the surface and the geostrophic winds aloft driving it. Geostrophic winds are a global scale phenomena derived from a basic

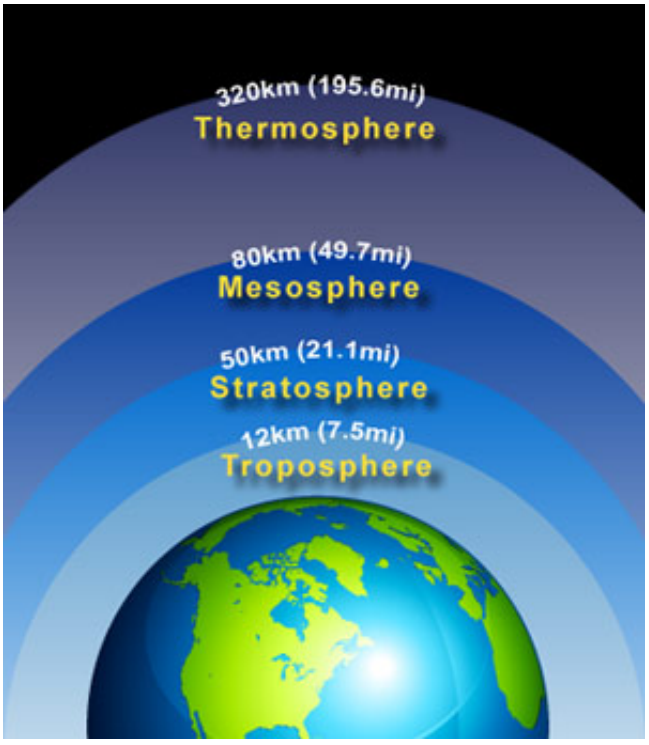


Figure 2.1: Description of the atmospheric layers of the earth (Stull, 2012)

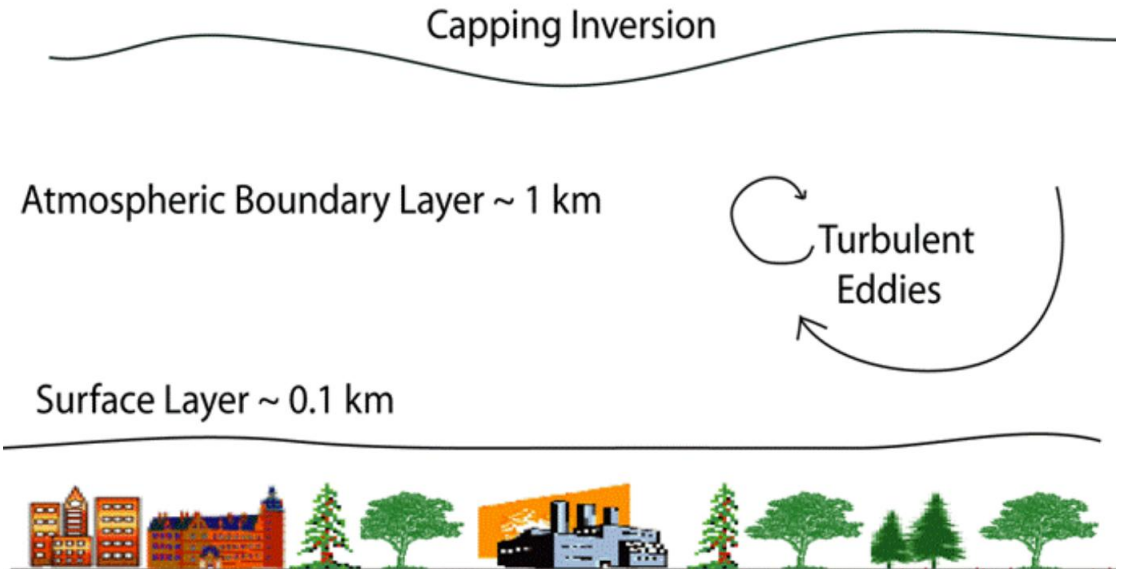


Figure 2.2: Description of the atmospheric boundary layer (Stull, 2012)

balance between pressure and Coriolis force which is the apparent deflection of objects moving in a straight path relative to the earth's surface. For conditions of neutral stability, the depth of the ABL can vary from several hundred meters to over a thousand meters depending on the speed of the geostrophic wind (Pasquill and Smith, 1983). Neutral stability is often a fair assumption for the ABL over urban areas, especially at night, as physical factors like surface drag force due to roughness and heat-storage promote these conditions (Britter and Hanna, 2003).

### 2.2.1 Multi-Scale Considerations

To do a better analysis of the fluid dynamics of the lower atmosphere, it is helpful to recognize the multi-scale phenomena present. The global processes that drive regional weather conditions and atmospheric boundary layer formation will not be the focus of this Thesis. Instead, flow phenomena affecting dispersion at the cities/neighbourhood scale will be considered.

At the city/neighborhood scale, the ABL is further divided into regions describing the impact of the urban environment. The effect of individual buildings on the flow at this scale is conceptualized as flow over a series of roughness elements such as buildings, trees and hills. Closest to the ground, the buildings are said to reside in the canopy layer which extends to the

height of the tallest building. After the canopy layer is the Roughness Sublayer (RS) followed by the Inertial Sublayer (IS) as seen in Fig.2.3.

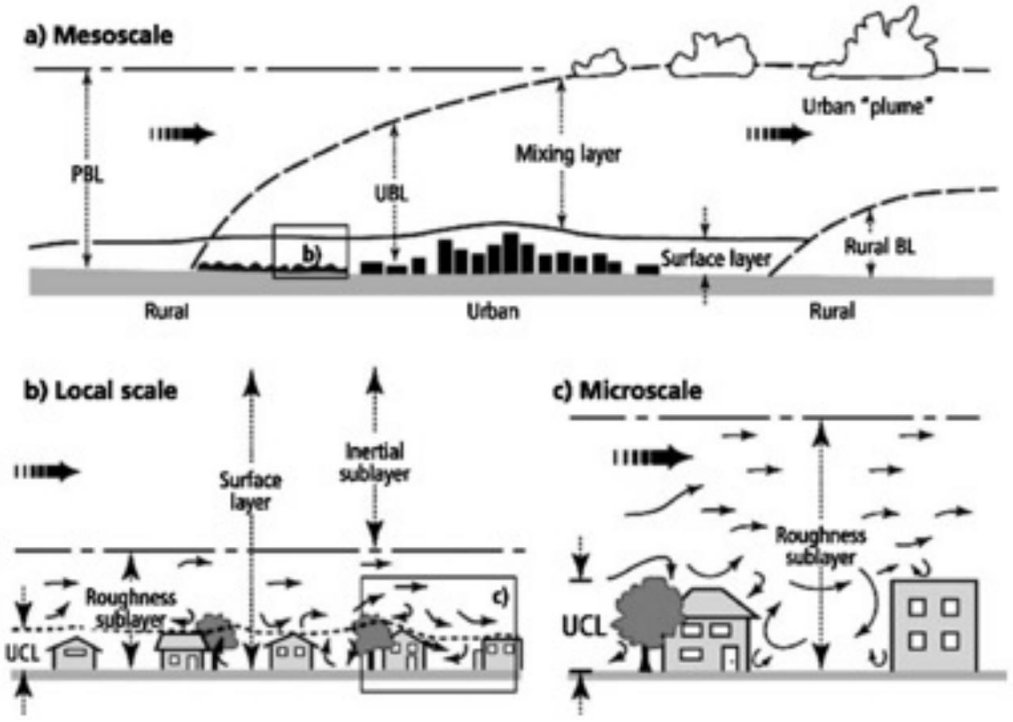


Figure 2.3: Flow layers over an urban environment (Raupach and Thom, 1981)

The RS, as defined by Raupach and Thom (1981), is the region over which mean flow and turbulence properties depend on the specific details of the roughness (i.e. the buildings) itself. As such, the exact definition of its extent varies throughout the literature. The lower boundary is sometimes considered to be the mean building height and in other cases the zero-plane displacement, d, which is defined based on a logarithmic velocity profile (Rotach, 1994). The upper boundary of the RS occurs when the horizontal variation in flow and turbulence parameters caused by the canopy subsides, though exact applications of this concept vary.

The IS, is by definition, a layer of constant shear stress where Monin-Obukhov similarity arguments apply (Monin and Obukhov, 1954). For stable conditions over a rough surface, this leads to a logarithmic velocity profile of the form as depicted by Eqn.( 2.1):

$$u(z) = \frac{u_\tau}{\kappa} ln\left(\frac{z-d}{z_0}\right) \tag{2.1}$$

where

$u_\tau$ is the friction velocity,

$z_0$ is the characteristic roughness height

d is the previously mentioned zero-plane displacement and

$\kappa$ is the Von Karman constant.

Jackson (1981) showed that d represents the level at which the mean surface drag acts, while $z_0$ is a measure of the magnitude of that drag. Values of $z_0$ and d have been tabulated from experimental data for a range of surfaces from croplands and forests to concrete roads and towns (Wieringa et al., 2001). The range reported for any one given surface type illustrates the approximate nature with which $z_0$ and d are often interpreted. The complexity in determining a precise value stems from the fact that $z_0$ and d depend not only on the specific geometrical properties of the roughness elements, but also on the flow conditions. Nevertheless, the logarithmic

velocity profile is typically used not only in the range where it is strictly valid, but is extended into the roughness sublayer. Macdonald (2000) noted that this is done out of a lack of information about flow within the canopy and is generally an acceptable approximation for studies of larger, elevated plumes.

## 2.3 Air Quality Models

In basic applications of air quality models, the processes of air pollution transport are considered as a distributed parameter system, which is governed by a set of transport equations, along with respective boundary and initial conditions. The exact form and structure of a model usually depend on its practical application, type of the polluting compounds considered and the scale of modelling. A model usually takes into account the input data (emission field and meteorological data) as well as the main physical and chemical processes which determine the transport in the atmosphere and transformations of air pollution components (Holnicki, 2011). The characteristics of each specific problem will define the physical and chemical processes involved, and consequently, the best model to use. The main criteria for choosing appropriate software are:

1. The dimension of the area under study

2. The number of pollution sources

3. The chemical species involved and

4. The time scale of the episode.

The spatial and temporal scales of the environmental impact of air pollution are correlated with the lifetime of a pollutant. Thus, depending on the analysis scale, there are respective categories of modelling: local, regional and global. Regarding the practical application and the scale of modelling, the most common types (implementations) of air pollution models are discussed in the following section.

### 2.3.1 Box Models

Box models are derived by simply applying a control volume-based mass conservation approach to determining concentration levels in a domain of interest. This leads to a uniform prediction of concentration without providing information about spatial variation in concentration within the box (Holmes and Morawska, 2006). The domain is treated as a box into which pollutants are emitted and undergo chemical and physical processes. They require the input of simple meteorology and emissions and the movement of pollutants in and out of the box is allowed. The model also assumes that the incoming pollution is instantaneously mixed with the surrounding

air, creating a homogeneous concentration throughout the airshed (Venkatram, 1978). The mass conservation constraint permits the construction of a mass balance equation of the form as shown in Eqn.(2.2):

$$\frac{dcV}{dt} = QA + uc_{in}WH - ucWH \tag{2.2}$$

where

V is the volume described by the box,

c is the homogeneous species concentration within the airshed,

$c_{in}$ is the species concentration entering the airshed,

Q is the emission rate per unit area of sources within the box,

u is the average wind speed normal to the box,

A is the horizontal area of the box (L $\times$ W ),

W is the width of the box and

H is the mixing depth.

Integrating Eqn.( 2.2) provides a steady state estimation of species concentration (Venkatram, 1978) assuming the dynamics of the mixing depth to be quasi-stationary and the source emissions to be constant. In the case of reactive species, the chemical reaction dynamics can be incorporated into the mass balance equation as well as wet and dry deposition effects.

It is incapable of imparting any spatial information regarding the dispersive nature of a pollutant. This precludes the box model approach from a significant proportion of air quality modelling applications. Nevertheless, the method is computationally fast and is capable of providing satisfactory predictions, particularly for scenarios where detailed information on the domain and meteorological conditions is unavailable.

### 2.3.2 Gaussian Models

The Gaussian model forms the basis for the majority of air pollution models, and is the most well known and documented approach. The model presupposes that the dispersion associated with the polluting species can be described by a modified Gaussian or normal distribution curve as shown in Fig.2.4.

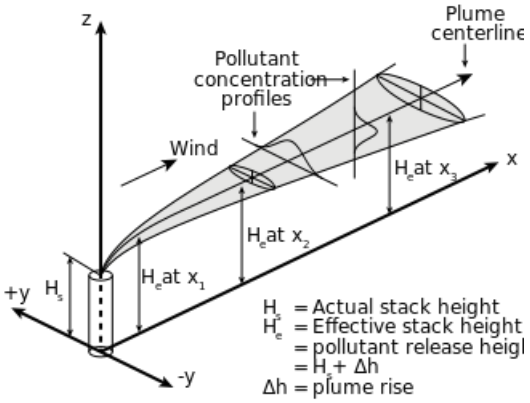


Figure 2.4: Visualization of a buoyant Gaussian air pollutant dispersion plume (Holmes and Morawska, 2006)

A three-dimensional axis system is employed to provide a downwind, cross-wind and vertical resolution. The species concentration is defined as being proportional to the emission rate of the source, diluted by the wind velocity at the source of emission. The dispersion behaviour of a pollutant is determined by the standard deviations associated with the Gaussian distribution function. These standard deviations which are related to the turbulent diffusivities are typically functions of atmospheric stability, localised turbulence and distance downwind from the source. Since the turbulent diffusivity is unknown, however, the deviations are parameterized based on experimental measurements and observations. The parametrization is typically a function of conditions like atmospheric stability (Holmes and Morawska, 2006). The model is usually aligned so that the downwind axis corresponds to the direction of the prevailing wind (Collett and Oduyemi, 1997). The model equation is derived from basic considerations of the diffusion of gaseous matter in three-dimensional space as shown in Eqn.(2.3):

$$C = \frac{Q}{2\pi u \sigma_y \sigma_z} exp\left(\frac{-y^2}{2\sigma_y^2}\right)\left[exp\left(\frac{-(h-z)^2}{2\sigma_y^2}\right) + r_G exp\left(\frac{-(h+z)^2}{2\sigma_y^2}\right)\right] \tag{2.3}$$

where

C is the species concentration at a location (x, y, z),

Q is the source emission rate,

u is the average wind speed normal to the box,

$\sigma_y$ is the standard deviation of the horizontal crosswind distribution of the plume concentration and is a function of the downwind distance x,

$\sigma_z$ is the standard deviation of the vertical crosswind distribution of the plume concentration and is a function of the crosswind distance z,

h is the effective source height to which the plume has risen,

$r_G$ is the ground reflection coefficient where $0 \leq r_G \geq 1$,

y is the crosswind distance and

z is the receptor height above ground.

The effective source height (h) or plume rise is the height to which an emission will initially rise as a result of thermal buoyancy and vertical momentum. The upward movement of the plume is retarded on mixing with ambient air reaching an equilibrium point when the internal energy of the plume is equal to that of the surrounding atmosphere. A review of various semi-empirical methods for the estimation of plume rise can be found in Zannetti (2013). Several assumptions are implied in the derivation of Eqn.(2.3), including the uniformity and time invariance of the emission characteristics of the source, the homogeniety of the meteorological conditions within the domain of interest and the weakness of the topography of the domain so as not to affect pollutant dispersion on plant operation. In

the light of such limitations, the Gaussian model can only be considered workable when such factors are static enough to be regarded as homogeneous.

The behaviour of the Gaussian model depends heavily upon the correct calculation of the dispersion coefficients, $\sigma_y$ and $\sigma_z$. Various approaches currently exist and a summary of the methods for the estimation of $\sigma_y$ and $\sigma_z$ can be found in Zannetti (2013) and Boubel et al. (2013). The limitations of the Gaussian model precludes its use in cases where the short term prediction of species concentration (i.e.sub-hourly averaged values), or the prediction of species concentrations relative to complex environmental constraints are required.

### 2.3.3 Eulerian Models

The Eulerian approach to dispersion modelling solves the conservation of mass equation for a given pollutant species of concentration c. A stationary or normal frame of reference is assumed, with the dispersion phenomena calculated as a concentration field relative to the domain. The physical conditions within the reference domain are generally regarded as turbulent (Brown, 1991). Therefore any dependent variable is composed of an average component, denoted by an overbar, and a fluctuating component, denoted

by a prime, as shown in Eqn.(2.4):.

$$U = \overline{U} + U' \tag{2.4}$$

where

U is the Eulerian wind field vector U(x,y,z).

Given that

$\langle \overline{U} \rangle = \overline{U}$ and $\langle \overline{U'} \rangle = 0$

where

$\langle\rangle$ represents the ensemble average or theoretical mean and

$c = \langle c \rangle + c'$,

then the general form for the equation of conservation of pollutant species c is shown in Eqn.(2.5):

$$\frac{\partial \langle c_i \rangle}{\partial t} = -\overline{U} \cdot \nabla \langle c_i \rangle - \nabla \cdot \langle c_i' U' \rangle + D\nabla^2 \langle c_i \rangle + \langle S_i \rangle \tag{2.5}$$

where

$c_i$ is the concentration associated with the i$^{th}$ species,

D is the molecular diffusivity and

$S_i$ is the sink/source term of the $i^{th}$ species and accounts for chemical reactions, deposition and emission sources.

The first, second and third terms on the right hand side of Eqn.(2.5) represent the rate of advection, turbulent diffusion and molecular diffusion of pollutants respectively.

The term $\langle c_i' U' \rangle$ represents the turbulent atmospheric diffusion eddies whose magnitude and effects are significantly greater than that of molecular diffusion. For the majority of cases it is usual to ignore the molecular diffusivity term as its overall contribution will be negligible. The eddy diffusivity term is unresolvable as $c'$ is unknown and a suitable description of $U'$ is more often than not impossible to obtain. Consequently, the diffusivity term, $\langle c_i' U' \rangle$, has to be modelled if Eqn.(2.5) is to be closed.

After selection of a suitable closure method, Eqn.(2.5) is typically solved in one, two or three dimensions on a discrete mesh architecture, using a suitable numerical method including finite difference, finite element or finite volume (Versteeg and Malalasekera, 2007). Eulerian models suffer the disadvantage that their resolution is confined by the spatial and temporal discretisation of the mesh on which they are solved. The use of a mesh is computationally expensive and traditionally requires some form of optimisation to achieve any degree of efficiency. The approach is, however,

information-rich, providing a description of the relevant transport dynamics at all defined points throughout the domain (Collett and Oduyemi, 1997).

### 2.3.4 Lagrangian Models

The Lagrangian approach to atmospheric dispersion modelling differs from its Eulerian counterparts in that its reference system follows the prevailing vector of atmospheric motion. The term Lagrangian is applied to a wide range of models which simulate pollutant dispersal relative to a shifting reference frame. The general equation of motion describing the atmospheric dispersion of a single pollutant species is given by Eqn.(2.6) according to Zannetti (2013):

$$\langle c(r,t)\rangle = \int_{-\infty}^{t} \int p(r,t|r',t')S(r',t')dr'dt' \tag{2.6}$$

where

$\langle c(r,t)\rangle$ is the ensemble average concentration at r, at time t,

$S(r',t')$ is the source term and

$p(r,t|r',t')$ is the probability density function that an air parcel is moving from $r'$ at $t'$ to r at time t.

Lagrangian models incorporate changes in concentration due to mean fluid velocity, turbulence of the wind components and molecular diffusion. They work well both for homogeneous and stationary conditions over flat terrains and for inhomogeneous and unstable media condition for complex terrains (Tsuang, 2003, Venkatesan et al., 2002).

A fundamental problem that workers have encountered with Eqn.(2.6) and in a wider sense, Lagrangian dispersion models generally, is the relative interpretation of their results. It is fair to assume that the great majority of real-time meteorological and air quality measurements are obtained relative to a stationary reference frame. As a consequence, the results from Lagrangian based models cannot be easily compared with observed measurements. This often presents difficulties during the initial validation and verification phases of model development and throughout the post-development period, where simulation results have to be mapped to real life scenarios if they are to be considered useful. This has resulted in a trend where those atmospheric dispersion models which have adopted a Lagrangian approach have typically utilised Lagrangian methods which can be more readily compared to an Eulerian reference frame (e.g. particle/puff models). Those which have been successfully developed have been required to include some form of Eulerian mapping of their results, in order to achieve a wider application (Collett and Oduyemi, 1997).

### 2.3.5 Data Requirements for Air Quality Models

At this stage, it will be helpful to recognise some data requirements for air quality models notably meteorological, geophysical and emission source data.

#### 2.3.5.1 Meteorological data

Meteorological data is a critical input for AQMs, as it is necessary to obtain accurate description of winds, turbulence fields and radiation in order to correctly describe transport, dispersion, deposition and chemical reactions of a released pollutant (Demuzere et al., 2009, Pearce et al., 2011, Schürmann et al., 2009). Perhaps the most important meteorological element controlling levels of atmospheric pollution is the wind, according to Abdul-Wahab (2003). Wind moves in three dimensions. However, usually the horizontal component is dominant and its important properties are speed and direction. Wind speed determines the travel time from a source to a given receptor and the total area over which the plume will be dispersed. Other effects of wind speed include a dilution in the downwind direction. Usually wind speed has two opposing effects on the dispersion of pollutants. It affects both the spread of the plume (rate of dilution of pollutants) and the height to which the plume will rise. Thus, with a high wind speed, a plume will be diluted quickly, but it will not be able to rise

since higher wind speeds tend to bend a plume, retarding its vertical motion. In calm winds, the dilution factor will be small, but a hot plume may be able to rise to a considerable height. The wind direction determines the course the effluents will take or the area to which the plume will be directed. The correlation of wind direction and pollution concentration at any site can therefore help to identify the sources mainly responsible for the pollution measured at that site. The effects of other meteorological elements like precipitation, temperature and relative humidity cannot be overemphazised.

Meteorological data requirements for local scale models (i.e., steady-state Gaussian, Puff-models) and more complex models, vary considerably. Steady-state Gaussian plume models need data only from a single station, since they assume that meteorological conditions do not vary throughout the domain up to the top of the boundary layer (Cimorelli et al., 1998). More advanced models (both puff and grid models) allow meteorological conditions to vary across the modelling domain and up through the atmosphere, thus requiring more complex meteorological data.

#### 2.3.5.2 Geophysical Data

The next data resource needed is geophysical data consisting mainly of terrain and land use/land cover. The elevation of a geographic location is its

height above or below a fixed reference point, most commonly a reference geoid, a mathematical model of the Earth's sea level as an equipotential gravitational surface. Terrain features around a pollutant source can significantly affect the pattern of dispersion. Steady-state Gaussian models contain limited algorithms that include terrain effects. Advanced models contain more sophisticated procedures for modelling the effects of terrain, with a correspondingly greater effort required by the user to specify the static data. Since terrain data will be required for every receptor on the grid, there are several pre-processing tools that extract and format the Digital Elevation Model (DEM) data.

Land use plays an important role in air dispersion modelling from meteorological data processing to defining modelling characteristics such as urban or rural conditions. Land use data can be obtained from digital and paper land-use maps. The maps provide an indication into the dominant land use types within an area of study, such as industrial, agricultural, forest and others. This information can then be used to determine dominant dispersion conditions and estimate values for the critical surface characteristics which are surface roughness length, albedo and the Bowen ratio.

The most common global data sets are: the United States Geological Service (USGS) GTOPO30 with a horizontal grid spacing of 30 arc-seconds (approximately 1km); USGS SRTM30, with the same horizontal grid spacing, but covering the globe only from 60°N latitude to 56°S latitude, with

a seamless and uniform representation; and SRTM3 data with a horizontal grid spacing of 3 arc-seconds (about 90 m). Land Use and Land Cover (LULC) data are also available from the USGS, at the 1:250,000 scale, or in some cases at the 1:100,000 scale. The USGS Global Land Cover Characterization (GLCC) Database is developed on continental basis for land use, while land cover maps are classified into 37 categories, with a spatial resolution of 1 km (USGS, 2010).

#### 2.3.5.3 Emission Data

Emission inventories are also a key input for AQMs. There are numerous ways of estimating emissions of air pollutants with the popular ones being direct measurements, use of mass balances or fuel analysis, emission factors and emission models.

The most accurate way of estimating emissions is directly measuring the concentration of air pollutants from the source. Source tests and continuous emission monitoring systems (CEMS) are two methods of collecting actual emission data (USEPA, 2010, 2011). A CEMS involves the installation of the monitoring equipment that accumulates data on a pre-determined time schedule in a source (for example a stack or duct). It provides a continuous record of emissions over an extended and uninterrupted period of time. Data from source-specific emission tests or continuous emission

monitors are usually preferred for estimating pollutant releases because the data provide the best representation of emissions from tested sources. However, test data from individual sources are not always available, and may not even reflect the variability of actual emissions over time. Thus, emission factors are frequently used for estimating emissions, in spite of their limitations (Puliafito et al., 2011).

Emission factors are generally derived from measurements made on a number of sources representative of a particular emission sector and are usually expressed as the weight of pollutant divided by a unit weight,volume, distance, or activity duration that releases the pollutant (e.g., kilograms of particulate emitted per megagram of coal burned). Such factors facilitate estimation of emissions from various sources of air pollution. In most cases, these factors are simply averages of all acceptable quality data available, and are generally assumed to be representative of long-term averages for all facilities in the source category (i.e., a population average). Emission factors are founded on the premise that there exists a linear relationship between the emissions of air contaminant and the activity level pollutant (e.g., kilograms of particulate emitted per megagram of coal burned). Such factors facilitate estimation of emissions from various sources of air pollution. In most cases, these factors are simply averages of all acceptable quality data available, and are generally assumed to be representative of

long-term averages for all facilities in the source category (i.e., a population average). Emission factors are founded on the premise that there exists a linear relationship between the emissions of air contaminant and the activity level (Puliafito et al., 2011, USEPA, 2001).

Mass balance involves the quantification of total materials into and out of a process, with the difference between inputs and outputs being accounted for in terms of releases to the environment, or as part of the facility waste. Mass balance is particularly useful when the input and output streams can be quantified, and this is most often the case for individual process units and operations. Mass balance techniques can be applied across individual unit operations, or across an entire facility. These techniques are best applied to systems with prescribed inputs, defined internal conditions and known outputs (USEPA, 2011).

### 2.3.6 Model Evaluation

Evaluation of an AQM is the process of assessing its performance in simulating spatial-temporal features embedded in the air quality observations. When evaluating air quality management strategies, policy-makers need information about relative risk and likelihood of success of different options. In these cases, a range of values reflecting the model uncertainties, is more important than the model best guess, or actual output. End users are

more likely to work with operational and dynamic evaluation tools, while the other two categories of evaluation are more related to model development.

The kind of data needed for verifying model output, will depend on the model itself and the users needs. For models with meteorological preprocessors, like CALMET, or coupled meteorological/chemical models like WRF/Chem, atmospheric variables observation in some points of the domain would be required in order to validate results. Observations can be made at ground level or with a vertical profile, in the case of three dimensional simulations. In the case of chemical species concentration, monitoring stations could supply data needed to check model results. Some ground or satellite instruments can also provide vertical profile for chemical species (Martin, 2008). In any case, a consistent procedure should be applied in order to evaluate the model performance. The most usual practice is to use the information content shown between the observed and the model-predicted values. In this respect, Willmott (1982) and Seigneur et al. (2000) propose some statistical performance measures namely: correlation coefficient(R), mean bias(MB), fractional bias(FB), normalised mean square error(NMSE), geometric mean(GM), geometric variance(GV) and index of agreement(IOA).

The coefficient of correlation is the measurement of the relationship between observed and predicted values. It indicates the tendency of the predicted

values to change with a change in the observed values. A value of R close to unity implies good model performance. The NMSE measures the random spread of the values around the mean. It characterises the amount of deviation between predictions and observations. A good model will have an NMSE value of 0. The IOA reflects the degree to which the observed variable is accurately predicted. The IOA varies from 0 (the theoretical minimum for an inadequate prediction) to 1(perfect accuracy between the predicted and observed values). The FB is a measure of the systematic bias of the model. It indicates the tendency and the sign of the deviation. A negative FB value indicates model over-prediction and a positive value, an under-prediction.

Air quality modelers do not agree fully upon the magnitude of standards for accepting or rejecting model performance. In most cases, a model is considered acceptable if most of its predictions are within a factor of 2 of the observations (Hanna et al., 1993, 1991). On the other hand, studies by Ahuja (1996), Kumar et al. (1993), Zawar-Reza et al. (2005) report that a model can be deemed acceptable if: NMSE $\leq$ 0.5, -0.5 $\leq$ FB $\leq$ +0.5, and IOA $>$ 0.5.

## 2.4 CALPUFF Modeling System

The model used for the simulation studies in this research, the CALPUFF modelling system, is described at this point. Many dispersion models typically assume steady, horizontally homogeneous wind fields instantaneously over the entire modeling domain and are usually limited to 50 kilometers from a source. However, for applications with emission source hundreds of kilometers away, other models or modeling systems. At these distances, the transport times are sufficiently long that the mean wind fields cannot be considered steady or homogeneous. CALPUFF is one such modeling system, consisting of three components: CALMET, a meteorological preprocessor that utilizes surface, upper air, and on-site meteorological data to create a three-dimensional wind field and derive boundary layer parameters based on gridded land use data; CALPUFF, a puff dispersion model that can simulate the effects of temporally and spatially varying meteorological conditions on pollutant transport, removes pollutants through dry and wet deposition processes and transforms pollutant species through chemical reactions; and CALPOST, a postprocessor that takes the hourly estimates from CALPUFF and generates estimates at specified hours as well as tables of maximum values (Scire et al., 2000b).

CALPUFF is a transport and dispersion model that advects puffs of material released from modelled sources. It requires 3-dimensional fields of wind

and temperature, along with associated 2-dimensional fields such as mixing heights, surface characteristics and dispersion properties. To develop these fields, a deterministic meteorological processor (CALMET) was created. CALMET requires both hourly surface and twice-daily upper-air data to construct the meteorological fields. CALMET cannot forecast meteorology, but has a Diagnostic Wind Module (DWM) that adjusts wind and temperature fields due to the influence of terrain and vegetation. There are several switches in the CALMET model that must be set by the modeller to reflect the unique geophysical characteristics within an airshed (Scire et al., 2000b). The model accounts for a variety of effects such as spatial variability of meteorological conditions, causality effects, dry deposition and dispersion over different types of land surfaces, plume fumigation, low wind-speed dispersion, primary pollutant transformation and wet removal. CALPUFF has various algorithms to include the use of turbulence-based dispersion coefficients derived from a similarity theory or observations.

The individual components of the modeling system are described in detail in the following sections.

### 2.4.1 CALMET Diagnostic Meteorological Model

CALMET is a diagnostic meteorological model that develops hourly wind and temperature fields on a three-dimensional gridded modelling domain,

including two-dimensional fields such as mixing height, surface characteristics and dispersion properties. The CALMET model operates in a terrain-following vertical coordinate system using Eqn.(2.7):

$$Z = z - h_t \tag{2.7}$$

Where

Z is the terrain-following vertical coordinate (m),

z is the Cartesian vertical coordinate (m) and

$h_t$ is the terrain height (m).

The vertical velocity, W, in the terrain-following coordinate system is defined by Eqn.(2.8):

$$W = w - u\frac{\partial h_t}{\partial x} - v\frac{\partial h_t}{\partial y} \tag{2.8}$$

Where

w is the physical vertical wind component (m/s) in Cartesian coordinates and

u , v are the horizontal wind components (m/s).

The diagnostic wind field module in CALMET uses a two-step approach in the computation of wind fields (Scire et al., 2000a). In the first step, an initial-guess wind field is adjusted for kinematic effects of terrain, slope

flows and terrain blocking effects to produce a Step-1 wind field. CALMET parameterizes the kinematic effects of terrain using the approach of Liu and Yocke (1980).

The Cartesian vertical velocity is computed by Eqn.(2.9):

$$w = (V \cdot \nabla h_t) exp(-kz) \tag{2.9}$$

Where

V is the domain-mean wind speed,

$h_t$ is the terrain height,

k is a stability-dependent, coefficient of exponential decay and

z is the vertical coordinate

The exponential decay coefficient, k, increases with increasing atmospheric stability and is given by Eqn.(2.10):

$$k = \frac{N}{|V|} \tag{2.10}$$

Where

$|V|$ is the speed of the domain-mean wind and

N is the Brunt-Vaisala frequency (1/s) and is given by Eqn.(2.11):

$$N = \left[ (\frac{g}{\theta}) \frac{d\theta}{dz} \right]^{\frac{1}{2}} \tag{2.11}$$

Where

$\theta$ is the potential temperature (K) and

g is the acceleration due to gravity $(m/s^2)$

The kinematic effects of the terrain on the horizontal wind components are evaluated by applying a divergence-minimization procedure to the initial guess of the wind field.

The thermodynamic blocking effects of terrain on the wind flow are parameterized in terms of the local Froude number given by Eqn.(2.12):

$$F_r = \frac{V}{N \Delta h_t} \tag{2.12}$$

Where

$F_r$ is the local Froude number,

V is the wind speed(m/s) at the grid point,

N is the Brunt-Vaisala frequency $(1/s)$ and

$\Delta h_t$ is the effective obstacle height(m) and is given by Eqn.(2.13):

$$\Delta h_t = (h_{max})_{ij} - (z)_{ijk} \tag{2.13}$$

Where

$(h_{max})_{ij}$ is the highest gridded terrain height within a radius of influence of the grid point (i,j) and

$(z)_{ijk}$ is the height of level k of grid point (i,j) above the ground.

The second step consists of an objective analysis procedure to introduce observational data (surface and upper-level observational) into the step 1 wind field in order to produce the final wind field.

An option is provided to allow gridded prognostic wind fields to be used by CALMET, which better represents regional flows and certain aspects of sea breeze circulations. The prognostic data, as a 3D.DAT file, can be introduced into CALMET in three ways: as a replacement for the initial guess wind field, as a replacement for the step 1 field or as observations in the objective analysis procedure. In order to improve the initialization of the diagnostic model, the wind fields from the WRF prognostic model are ingested every hour by CALMET as the initial-guess wind field. This step is expected to improve the models performance by providing equally spaced data points both at the surface and upper levels within the modelling domain where observational data are not available (Chandrasekar et al., 2003). The prognostic winds are interpolated to the fine-scale CALMET grid. The diagnostic module in CALMET then adjusts the initial-guess

wind field for kinematic effects of terrain, slope flows and terrain blocking effects using fine-scale CALMET terrain data.

CALMET reads hourly surface observations of wind speed, temperature, cloud cover, ceiling height, surface pressure, relative humidity, and precipitation (only if wet removal is to be computed). The twice-daily upper air observations required by CALMET include vertical profiles of wind speed, wind direction, temperature, pressure, and elevation. CALMET also requires geophysical data, including gridded fields of terrain elevations and land use categories. Gridded fields of other geophysical parameters, such as the surface roughness length, albedo, Bowen ratio, soil heat flux parameter, anthropogenic heat flux and vegetation leaf area index are also required. CALMET consists of two boundary layer meteorological modules for overland and over water applications (Scire et al., 2000b). For overland surfaces, the energy balance method of Holtslag and Van Ulden (1983) is used to compute hourly gridded fields of the heat flux, surface friction velocity, Monin-Obukhov length, and convective velocity scale. Mixing heights are determined from the computed hourly surface heat fluxes and observed temperature soundings. The model also determines the Pasquill-Gifford stability classes and optional hourly precipitation rates.

### 2.4.2 CALPUFF Model

The basic equation for the contribution of a puff at a receptor by CALPUFF is by Eqn.(2.14):

$$C = \frac{Q}{2\pi\sigma_x\sigma_y} g \left\{ exp\left(\frac{-{d_a}^2}{2\sigma_x^2}\right) exp\left(\frac{-d_c^2}{2\sigma_y^2}\right) \right\} \tag{2.14}$$

Where

C is the ground-level concentration $(g/m^3)$,

Q is the pollutant mass (g),

$\sigma_x$, $\sigma_y$ and $\sigma_z$ are the standard deviations (m) of the Gaussian distribution in the along-wind direction, cross-wind and vertical directions respectively,

$d_a$ and $d_c$ are the distances (m) from the puff center to the receptor in the along-wind and cross-wind directions respectively and

g is the vertical term (m) of the Gaussian equation.

The vertical term, g, is given by Eqn.(2.15):

$$g = \frac{2}{(2\pi)^{\frac{1}{2}}\sigma_z} \sum_{n=-\infty}^{\infty} exp\left[-(H_e + 2nh)^2/(2{\sigma_z}^2)\right] \tag{2.15}$$

Where

$H_e$ is the effective height (m) above the ground of the puff center and

h is the mixed-layer height (m).

#### 2.4.2.1 Dispersion

The key modelling consideration in CALPUFF is the specification of the horizontal and vertical Gaussian dispersion coefficient, $\sigma_y$ and $\sigma_z$, for a puff (or each end of a slug) at the start and end of a sampling step, and also for each receptor at which the cloud has a computed contribution during the step. The coefficients for the puff location at the start of a step are equal to those found at the end of the preceding sampling step, because cloud-size is continuous between sampling steps. Those at the end of the step, or at nearby receptors during the step, are computed according to an ambient turbulence growth relationship and possibly a source-related constant variance. The growth due to ambient turbulence may be formulated as either a function of time, or as a function of distance. Therefore, a generic metric $\xi$ which stands for either one is used (Scire et al., 2000b).

The dispersion coefficients for an incremental 'position' $\Delta\xi$, relative to the beginning of sampling step n are given by Eqn.(2.16):

$$\sigma^2_{y,n}(\Delta\xi_y) = \sigma^2_{yt}(\xi_{yn} + \Delta\xi_y) + \sigma^2_{ys} + \sigma^2_{yb} \tag{2.16}$$

and Eqn.(2.17):

$$\sigma^2_{z,n}(\Delta\xi_z) = \sigma^2_{zt}(\xi_{zn} + \Delta\xi_z) + \sigma^2_{zb} \tag{2.17}$$

Where

$\xi_{yn}$ and $\xi_{zn}$ are the virtual-source metrics (time;distance) defined implicitly by the requirement that the sigmas match those at the end of the previous step when $\Delta\xi = 0$,

$\sigma_{y,n}$ and $\sigma_{z,n}$ are the total horizontal and vertical dispersion coefficients (m) respectively at some position during sampling step n,

$\sigma_{yt}$ and $\sigma_{zt}$ are the functional forms of the dispersion coefficients (m) of $\sigma_y$ and $\sigma_z$ respectively due to atmospheric turbulence. $\sigma_{yb}$ and $\sigma_{zb}$ are the components (m) of $\sigma_y$ and $\sigma_z$ respectively due to plume buoyancy at the time of release and

$\sigma_{ys}$ is the component of the horizontal dispersion coefficient (m) due to the lateral (cross-wind) scale of an area-source.

The increment $\Delta\xi$ is positive when describing the growth of the puff during the sampling step, but can be either positive or negative for receptor-specific sigmas. For example, $\Delta\xi$ would be negative for a receptor located just upwind of the puff at the start of a sampling step. This allows CALPUFF to reproduce plume-like features during steady meteorological conditions,

using very few puffs. Negative $\Delta\xi$ could also drive the argument of $\sigma_{yt}$ and $\sigma_{zt}$ through zero if a lower limit on the size of the sigmas at the source were not enforced. So there is an initial $\xi_0$ imposed, defined implicitly by Eqn.(2.18) and Eqn.(2.19):

$$\sigma_{yt}^2(\xi_{oy}) = \sigma_{yo}^2 \tag{2.18}$$

and

$$\sigma_{zt}^2(\xi_{oz}) = \sigma_{zo}^2 \tag{2.19}$$

Where

$\sigma_{yo}$ and $(\xi_{oz})$ are the initial values (m) of $\sigma_y$ and $\sigma_z$ respectively due to the nature of the source (e.g., volume source) or the rapid initial dilution associated with building downwash of point sources and

$\xi_o$ is the initial virtual-source metric defined implicitly and separately for y and z.

Thus, quadratic addition of initial dispersion components for buoyant rise effects and for the lateral size of an area source are assumed, but other initial cloud dimensions and the subsequent growth of the puff or slug are accomplished using the virtual-distance or virtual-transport time approach. This virtual- source approach is necessary if current puff growth is to be dependent only on the current size of the puff and not on how it reached

that size. The concept of a virtual source is particularly important when a puff can move between substantially different dispersion regimes in just one sampling step. For example, land use varies by grid cell, so a puff may go from an overwater cell with weak dispersion into an overland cell with substantial vertical convection. Or a young puff in the late afternoon mixed layer may see the turbulence decay rapidly. In both cases, CALPUFF computes subsequent growth during the step using the appropriate turbulence (actual or parameterized), and the growth rate appropriate to its size (Scire et al., 2000b).

#### 2.4.2.2 Atmospheric Turbulence Components

In the calculation of the atmospheric turbulence components, the basic strategy in the design of the dispersion module is to allow the use of the most refined data available in the calculation of $\sigma_{yt}$ and $\sigma_{zt}$. For situations in where this data is not available, backup algorithms not requiring specialized data are provided. The five dispersion options are:

1. Dispersion coefficients computed from measured values of turbulence, $\sigma_v$ and $\sigma_w$.

2. Dispersion coefficients from internally calculated $\sigma_v$ and $\sigma_w$ using micrometeorological variables.

3. Pasquill-Gifford(PG) dispersion coefficients for rural areas (computed using the Industrial Source Complex Short-Term (ISCST) multi-segment approximation) and McElroy-Pooler coefficients in urban areas.

4. Same as 3 except PG coefficients are computed using the MESOPUFF II equations.

5. Complex Terrain Dispersion Model(CTDM) sigmas used for stable and neutral conditions (assumes that measured $\sigma_v$ and $\sigma_w$ are read). For unstable conditions, sigmas are computed as in Dispersion Option 3.

#### 2.4.2.3 Buoyancy-Induced Dispersion

The effect of plume buoyancy on the dispersion coefficients are parameterized in terms of the plume rise (Irwin, 1983). It is given by Eqn.(2.20):

$$\sigma_{yb} = \sigma_{zb} = \frac{\Delta H}{3.5} \tag{2.20}$$

Where

$\Delta H$ is the plume rise(m).

Buoyancy-induced dispersion (BID) is automatically included for all the dispersion coefficient options described in Section 2.4.2.2.

The basic point source plume rise relationships are based on the Briggs equations (Briggs, 1975). The plume rise due to buoyancy and momentum during neutral or unstable conditions, $z_n$ is calculated using Eqn.(2.21):

$$z_n = \left[3F_m x/(\beta_j{}^2 u_s{}^2) + 3F_x{}^2/(2\beta_1{}^2 u_s{}^3)\right]^{1/3} \tag{2.21}$$

Where

$F_m$ is the momentum flux ($m^4/s^2$),

F is the buoyancy ($m^4/s^3$),

$u_s$ is the stack height wind speed (m/s),

x is the downwind distance (m),

$\beta_1$ is the neutral entrainment parameter ($\sim 0.6$),

$\beta_j$ is the jet entrainment coefficient ($\beta_j = 1/3 + u_s/w$),

w is the stack gas exit speed (m/s).

During stable conditions, the plume rise, $z_s$ is determined by Eqn.(2.22):

$$z_s = \left[3F_m/(\beta_j{}^2 u_s S^{1/2}) + 6F/(\beta_2{}^2 u_s S)\right]^{1/3} \tag{2.22}$$

Where

$\beta_2$ is the stable entrainment parameter ($\sim 0.36$) and

S is a stability parameter given by Eqn.(2.23):

$$S = \left(\frac{g}{T_a}\right)\left(\frac{d\theta}{dz}\right) \tag{2.23}$$

Where

g is the acceleration due to gravity $(m/s^2)$,

$T_a$ is the ambient temperature (K) and

$(d\theta/dz)$ is the potential temperature lapse rate (K/m).

### 2.4.3 CALPOST

CALPOST is used to process output files from CALMET and CALPUFF, producing tabulations that summarize the results of the simulation, identifying the highest and second highest 3-hour average concentrations at each receptor for example. Fig. 2.5 is the schematic diagram of the CALPUFF system.

The application of CALMET/CALPUFF modelling system is well known, and several validation tests have been published (Dios et al., 2013, Dresser and Huizer, 2011, Fishwick and Scorgie, 2011, Ghannam and El-Fadel, 2013, Hernández et al., 2014, Levy et al., 2003, Protonotariou et al., 2004). Most of them were based on specific experiments with passive tracers and a large compilation of surface and aloft meteorological measurements during

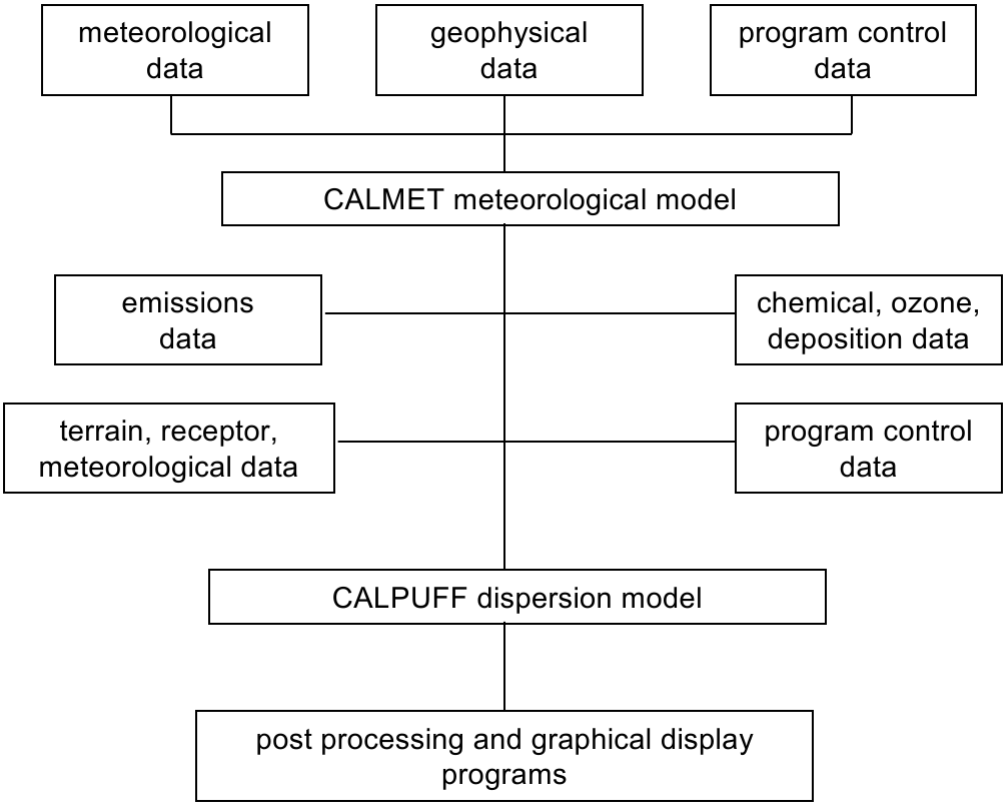


Figure 2.5: A schematic diagram of the program elements in the CALMET/CALPUFF modelling (Scire et al., 2000b)

the experiments, in order to achieve the best model performance evaluation. However, with actual pollutants sources and limited meteorological datasets, uncertainties arise (both in measurements and models results) and worse models performance is expected.

### 2.4.4 Weather Research and Forecasting (WRF) Model

The WRF model is a fully compressible, non-hydrostatic mesoscale model with a hydrostatic option which uses a terrain-following hybrid sigma-pressure vertical coordinate in its meteorology simulation (Janjic, 2003, Janjić, 2002). It was developed in a collaborative effort by the National Center for Atmospheric Research (NCAR), the National Centers for Environmental Prediction (NCEP), the Forecast Systems Laboratory (FSL), the Air Force Weather Agency (AFWA), Oklahoma University (OU) and other university scientists. It is a state-of-the-art numerical weather prediction (NWP) and data assimilation system suitable for horizontal grid scales in the 1 to 10 km range. The model can be run in a nested way with the outer domain on a regional scale, covering distances usually between 500  1,000 km (Michalakes et al., 2004, Shamarock et al., 2008).

# Chapter 3

# Methodology

## 3.1 Introduction

This Chapter describes the study area for the research and the calculations used in the estimation of the emissions from the Tema Oil Refinery. The methodology employed in the meteorological and dispersion simulations are also presented. The mass balance method is employed in the estimation of pollutants from the RFCC unit of the refinery due to the unavailability of such data from the refinery. Based on these calculated rates, emissions from the whole refinery are also derived. The flare and flue stack are also characterised by parameters such as stack/flare height and diameter, emission escape velocity and discharge temperature. The methodology used in validating the CALPUFF/CALMET simulation results are also presented.

### 3.1.1 The Study Area

The study area, capturing Ghana's only refinery in Tema, the emission source for this study and spaning a domain size of 60 km × 60 km, is located in the Greater Accra Region of Ghana stretching along the Ghanaian Atlantic coast and extending a bit north into Ghana's interior as shown by Fig.3.1. The Universal Transverse Mercator (UTM) coordinate of the southwestern corner of the domain in zone 30 are 795 km easting and 600 km northing. The study area covers most part of the Accra Metropolitan area, the Tema municipal area and extends to parts of the Eastern and Volta regions. The southern boundary of the metropolis of Accra which coincides with that of the study area is the Gulf of Guinea.

Tema is the most industrialised city in Ghana on the Gulf of Guinea and Atlantic coast of Ghana. It is located 25 km east of the capital city, Accra, in the region of Greater Accra with a population of approximately 402,637 people (G.S.S, 2012). Tema is locally nicknamed the 'Harbour Town' because of its status as Ghana's largest seaport. It is a major trading center, home to Ghana's only oil refinery and other numerous factories, and is linked to Accra by a highway and railway.

The Greater Accra Region is located in the Dahomeyan Gap, where the coast runs parallel to the prevailing moist monsoonal winds. It features a tropical savanna climate and a savanna vegetation that borders on a

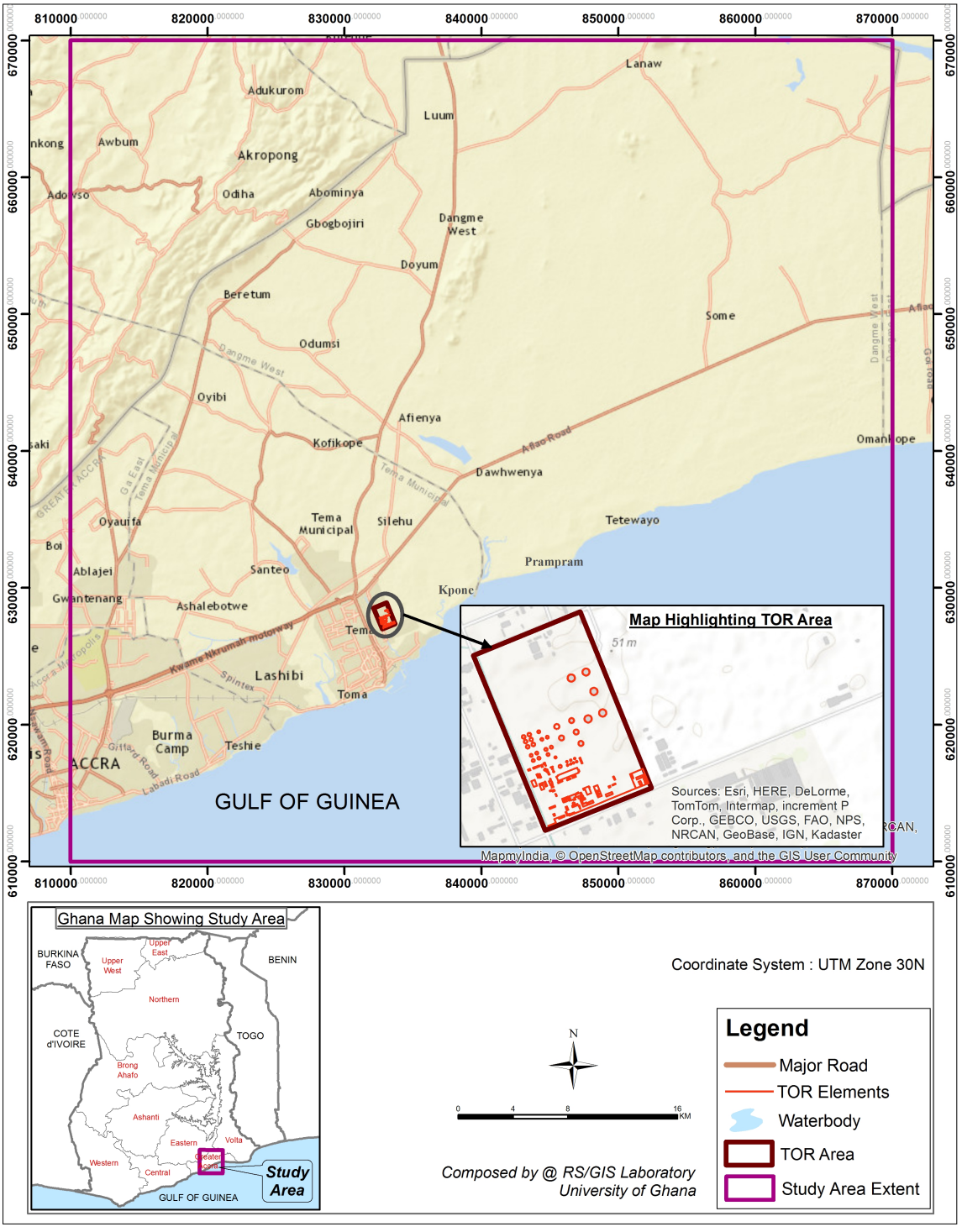


Figure 3.1: Map of Study Area showing the Tema Oil Refinery

semi-arid climate. Accra experiences two rainy seasons: April to June and September to October with the former being the heaviest. The average annual rainfall is about 730 mm which falls primarily during Ghana's two rainy seasons. Variation in temperature throughout the year is recorded to be nominal with mean monthly temperature ranging from 24.7°C in August to 28°C in March and an annual average of 26.8°C. Relative humidity is generally high, varying from 65% in the mid afternoons to 95% at night. Accra experiences a breezy dry heat during windy harmattan seasons usually in December and January (Muff and Efa, 2006).

The landscape is mainly flat with terrain elevations between 200 m and 500 m, except for the low mountain system (Akropong range north of the refinery and the Shai hills) east of the refinery. The traditional land use classification within the study area includes built-up/urbanisation, forestry/agriculture, water, shoreline, protected areas and bare areas inferred from Addo (2013).

### 3.1.2 Tema Oil Refinery

Tema Oil Refinery (TOR) Limited, formerly Ghanaian Italian Petroleum (GHAIP) Limited was commissioned on December 12, 1963. The Government of Ghana became the sole shareholder in 1977 and renamed the company Tema Oil Refinery Limited in 1991. The Refinery predominantly

processes crude oil into refined products like LPG, Gasoline, Jet Fuel, Kerosene, Diesel and Fuel Oils. The refinery is situated on an area of 440,000 square meters located in the industrial hub of the Greater Accra Region. The refinery complex, as a whole, contains the refinery itself, its tank farm containing storage tanks, wastewater treatment plant, gas turbine power generating sets and its utility system of boilers. The refinery has an installed total capacity of 65 000 barrels per stream day(bpsd) equivalent to 3,000,000 tonnes per annum (tpa) with contributions from the Crude Distillation Unit (CDU)- 2,000,000 tpa, Residue Fluid Catalytic Cracker(RFCC)-685,000 tpa and the Premium Reforming unit(PRF)-315,000 tpa (Darko and Quist, 2012).

The RFCC process converts heavy crude oil fractions into lighter, more valuable hydrocarbon products at high temperature and moderate pressure in the presence of finely divided silica/alumina based catalyst in crude refineries. In the course of cracking the large hydrocarbon molecules into smaller molecules, a non-volatile carbonaceous material, commonly referred to as coke, is deposited on the catalyst. The presence of coke on the catalyst deactivates the catalytic cracking activity of the catalyst by blocking access to the active catalytic sites. In order to regenerate the catalytic activity of the catalyst, the coke deposited on the catalyst is burned off with air in the regenerator vessel. The regenerator is normally operated at conditions that achieve complete combustion of C to $CO_2$. Flue gas exits the cyclone

separators to minimize catalyst entrainment prior to discharge from the regenerator through the flue stack (Maya-Yescas et al., 2005). Other stack emissions include $SO_x$, $NO_x$ and unburnt hydrocarbons.

The refinery is also equipped with a flare which primarily burns off flammable gas released by pressure relief valves during unplanned over-pressuring of plant equipment. It is used both for safety reasons during process upsets (start-up, shut down, system blow-down) and for managing the disposal of waste gases with hydrocarbons from routine operations. However, through combustion, the flare also produces other pollutants including $SO_x$, $NO_x$, CO, $CO_2$ and PM (both total PM and micro-particulates- ie, $PM_{10}$ and $PM_{2.5}$). Infact, according to USEPA (2011), it is one of the air pollution sources in a refinery emission inventory followed by the flue stack. It is for this reason that other emissions from stationary combustion sources, including process heaters, boilers, combustion turbines and similar devices, are not calculated but extrapolated, in this study.

## 3.2 Tema Oil Refinery Emission Estimation

The air emissions from the refinery are mainly due to the combustion of fuel gas. In this work, the pollutants of interest are $SO_x$, $NO_x$, $CO_2$, PM and VOCs and the point sources under consideration are the flue stack and the flare. As mentioned early on, the mass balance approach is employed

Table 3.1: Operational Average Flow Parameters of the RFCCU of the Tema Oil Refinery for 2008 - 2013

| **Year** | **Feed Rate ($m^3$/hr)** | **Airflow Rate ($Nm^3$/hr)** | **Fuel Gas rate (kg/hr)** | **Initial Catalyst Inventory(kg/hr)** |
|---|---|---|---|---|
| 2008 | 78.83 | 70989.00 | 6248.93 | 120000 |
| 2009 | 72.02 | 63882.88 | 6239.00 | 120000 |
| 2010 | 80.11 | 63147.37 | 6858.40 | 120000 |
| 2011 | 73.44 | 56954.83 | 6368.20 | 120000 |
| 2012 | 74.71 | 55508.67 | 5853.17 | 120000 |
| 2013 | 74.44 | 55643.80 | 5207.14 | 120000 |

during which the compound being combusted is examined to predict the emissions. The gases involved in the calculations were assumed to be ideal and so the idea gas laws were applied.

For example, the flue stack gas contains products of the combustion of deposited carbon on the catalyst during cracking. Based on the stoichiometric equations of the combustion reactions, products are estimated given the reactant concentrations. In the case of the flare, emissions rates are informed by a gas chromatographic analysis of the fuel gas exiting the flare. Table 3.1 shows the quantities of some parameters used in the calculations.

### 3.2.1 Estimation of Flue Stack Gas Rate and Composition

In the regeneration of the catalyst in the regenerator through combustion, air is used as a source of oxygen. The carbon reacts to form $CO_2$ upon complete combustion as is the case with this refinery. Based on the regenerator

air flow rate, therefore, the emission rates of $CO_2$ and carbon particulates are estimated. The air flow rate provided by the refinery is on a wet basis and was converted to dry basis prior to the calculations.

The larger component of the total FCC PM emitted is as a result of cyclone inefficiency estimated at 0.25% (Harding et al., 2001, Jiménez-García et al., 2011) which is what is used in the calculations. Research also shows that $PM_{2.5}$ is a large fraction of the total particulate emissions even without consideration of primary sulphate or organic emissions (England et al., 2000, Hildemann et al., 1994). Therefore, PM modelled in this study is considered to be of aerodynamic diameter of 2.5.

According to Corma et al. (1997), in the FCC unit, between 45 and 55% of the total sulphur present in the feed, especially the nontiophenic compounds, is converted to $H_2S$, while approximately 35 to 45% stays in the liquid products as sulphur compounds. The remaining 5% is left on the catalyst as part of coke and results in 90% $SO_2$ and 10% $SO_3$ during the coke combustion. The TOR processes mainly light sweet and light sour crude with % feed sulphur between 0.5 - 1.5 (Darko and Quist, 2012, Products, 1997, Zhao et al., 1997). In this study, an average of 1% feed sulphur is used.

Elemental nitrogen typically equals 0.32% of the FCC feed, 15% of which ends up on the catalyst together with the coke. Ninety percent (90%) of

this is converted to NO and the remaining 10% to $NO_2$ and ends up in the flue gas (Jiménez-García et al., 2011, Zhao et al., 1997).

A sample of the calculations, using flow parameters for the year 2009, are shown in Appendix A.

### 3.2.2 Estimation of Flared Gas Composition

When fuel is burnt, carbon in the fuel reacts to form either $CO_2$ or CO, hydrogen forms $H_2O$, sulphur forms $SO_2$ and $SO_3$ and some of the nitrogen in the air forms $NO_2$ at high temperatures (Abdul-Wahab, 2003, Corma et al., 1997). However, when flaring is done in the presence of excess air, CO is not formed which is the case in this study. Small amounts of $NO_2$ are formed at temperatures greater than 1400°C. Since this temperature is greater than the flare temperature, it is also assumed that no $NO_2$ is produced in the flare. The flare emissions therefore contain $H_2$, $O_2$, $N_2$, $CO_2$, $SO_2$ and some unburnt hydrocarbons hereafter referred to as volatile organic compounds (VOCs). VOCs are present in flare emissions as a result of flare efficiency (destruction efficiency) given as 98% (TOR Manual). Flares are designed to operate at 98 - 99% (Al-Fadhli et al., 2011, Martín et al., 2003, Wood et al., 2012). In this methodology, the composition of the flare gas combustion products is calculated through atomic and molecular balances. At constant temperature and pressure, mole % of gases is

equal to volume %. Therefore from the GC analysis report provided by the quality control laboratory of the refinery, the mole fractions of the flare gas components are calculated as shown in Appendix A. Given the average molecular weight of the fuel gas of 20 kg/kmol (Zadakbar et al. (2008)) and its mass flow rate, the total moles of the fuel gas mixture are also calculated. From this, the moles of the components are estimated using their respective fractions. Based on the stoichiometry of the combustion reactions, the combustion products are obtained: $CO_2$, $H_2O$, $SO_2$ and $N_2$. $SO_2$ and VOCs are the flare pollutants considered. Again, the estimation is carried out using operational data for 2009 on an hourly basis and is shown in Appendix A.

Total refinery emissions are then estimated as percentages of the RFCC emissions (EIPPCB, 2012). For the sake of simplicity, $SO_2$ and $SO_3$ from the flue stack are added and considered as $SO_2$. Similarly, NO and $NO_2$ are also lumped together and modelled as $NO_2$.

### 3.2.3 Calculation of Flare and Flue stack Exit Gas Velocities

The flare and flue gas velocities are calculated by dividing their volumetric flow rates by the cross-sectional areas (obtained from their diameters) of

the flare stack and flue stack respectively. The calculations are shown in Appendix A.

### 3.2.4 Modelling Period

A minimum of a year is necessary to capture the time-varying emissions and meteorology during a full cycle of seasons. However, to be able to do a trend analysis to inform future predictions, a six-year period from January 2008 to December 2013, was considered in the study.

### 3.2.5 Model Set-up

As stated earlier in this section, the key program elements and data input requirements for CALPUFF are meteorological wind fields, emissions data, receptor locations (points in the modeling domain where the model will predict concentrations), and CALPUFF modeling parameters. These elements are described below.

#### 3.2.5.1 CALMET Modelling

Due to the unavailability of complete observational meteorological datasets from the local weather stations, the CALMET model was initialised with WRF data to develop the meteorological field for CALPUFF. This option is

available in the CALMET model. Because the prognostic models like WRF are usually run over very large domains with much coarser resolutions, they are not suitable for direct use in CALPUFF. In this case, CALMET will interpolate the gridded prognostic data to develop a 3-D fine scale field of wind speeds, directions and other parameters.

The WRF model runs were performed at the International Centre for Theoretical Physics (ICTP), Trieste, Italy. Two one-way nested computational domains were set with horizontal grid spacing of 24 and 12 km representing horizontal grid dimensions of outer and inner domains respectively as shown in Fig.3.2. The vertical grid contained 29 full sigma levels. The inner domain covered the whole of Ghana within which the study area is located.

The model was run with Global Forecast System (GFS) 1 degree reanalysis as initial and boundary conditions with full physics processes included in order to reproduce real meteorological phenomena. Other options include WRF Single Momentum (WSM) 6 Class Graupel for Microphysics Scheme, Rapid Radiative Transfer Model (RRTM) scheme for long wave radiation, Dudhia scheme for short wave radiation, Monin-Obukhov scheme for surface layer, and Noah model (5 soil layers) for land-surface interactions, while the dynamic options were left as default to produce hourly averages (Skamarock et al., 2005).

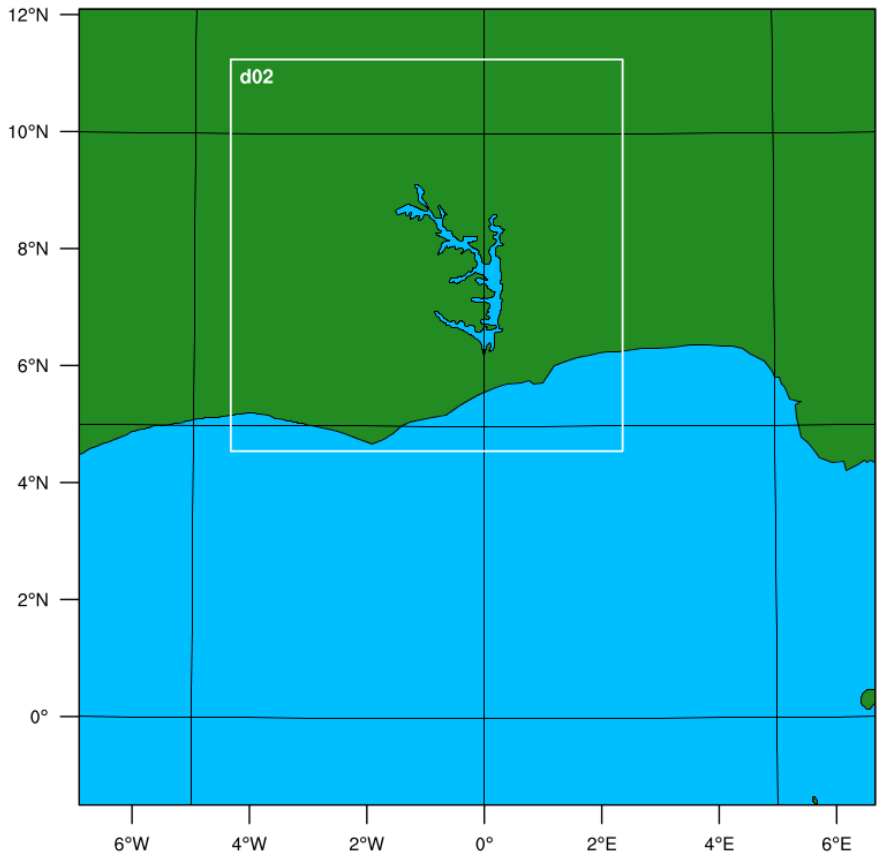


Figure 3.2: Nested Computational domains in the WRF simulations

CALMET-compatible 3D.DAT files containing data of horizontal and vertical velocity components, pressure, temperature and precipitation among others were then created by running CALWRF on the WRF output data. The CALMET meteorological processor was then used to interpolate the 12 km resolution WRF winds to the CALPUFF domain.

A horizontal grid spacing of 1 km was selected for the CALMET simulation; the study area therefore corresponds to 60 rows by 60 columns. With this grid spacing, it was possible to maximize run time and file size efficiencies while still capturing large-scale terrain feature influences on wind flow patterns. CALMET uses fewer vertical layers than WRF, in part because air pollution modeling does not require detailed information on the upper atmosphere. Therefore to adequately characterize the vertical structure of the atmospheric boundary layer (i.e., the layer within about 2000 metres above the Earth's surface), ten vertical layers with cell face heights at 0, 20, 40, 80, 160, 320, 640, 1000, 1500, 2200 and 3000 m were used in the CALMET runs. CALMET defines a vertical layer as the midpoint between two faces (i.e., 11 faces correspond to 10 layers, with the lowest layer always being ground level or 10 m). CALMET automatically interpolated from the WRF model grid system to the CALMET grid (Scire et al., 2000a, Zhou et al., 2003).

#### 3.2.5.2 Geophysical Data Input

Prior to running CALMET, a geophysical file containing information about the land use type, elevation and surface parameters about the domain under study was created. Due to the unavailability of terrain elevation and land use land cover (LULC) data in the required format for Ghana from the local agency in the required format, data from the United States Geological

Survey (USGS) web site at

`http://edcwww.cr.usgs.gov/doc/edchome/ndcdb/ndcdb.html` was used.

Detailed terrain features were incorporated using the USGS global 3 arc-sec SRTM3 data ($\sim$ 90m resolution). Elevations are in meters relative to mean sea level. The spacing of the elevations along each profile is 3 arc-seconds, which corresponds to a spacing of approximately 90 meters. A vertical and horizontal grid spacing of 1km was selected to adequately represent the important terrain features. The raw terrain data were processed into each gridded field. These terrain fields effectively resolve major land features in the model domain.

Land use and land cover (LULC) data were downloaded from the USGS at the 1:250,000-scale with file names corresponding to the 1:250,000-scale map names. Land use data were processed to produce a 1-km resolution gridded field of fractional land use categories and land use weighted values of surface and vegetation properties for each CALMET grid cell. The 14 default CALPUFF land use categories were used (10, 20, 30, 40, 51, 54, 55, 60, 61, 62, 70, 80, and 90). Each land use type has six assigned values, one each for surface roughness, albedo, Bowen ratio, soil heat flux parameter, anthropogenic heat flux, and leaf area index. The surface roughness is a measurement of the average vertical relief and small-scale irregularities of the terrain surface. The surface roughness is low for the areas in the study area classified as water bodies and is high for the areas classified as urban or

built-up land and forest. The albedo is the fraction of light that is reflected by a given surface. For instance, the albedo of a snow-covered area is much higher than that of a paved parking lot. The leaf area index is the ratio of the total area of all leaves on a plant to the area of ground covered by the plant. All areas that have the potential to have plant growth have leaf area indexes assigned to them. A value of zero is assigned to the water bodies. The leaf area index is as high as seven (7) in the areas identified as forest land.

Terrain and land Use data for the modelling domain were then processed through the TERREL and CTGPRO CALMET pre-processors respectively. Since the modeling domain spans both over-water and over-land regions, the global self-consistent hierarchical high-resolution shoreline (GSHHS) was used to define the coastal lines. The CALMET GEO file was then created using the MAKEGEO pre-processor which combines data from TERREL and CTGPROG.

CALMET was configured with the default wind field options and parameters.

#### 3.2.5.3 CALPUFF modelling

Even though emissions of five species were estimated, only three are modelled, namely $SO_2$, $NO_2$ and $PM_{2.5}$. The CALPUFF model predicts concentrations at specific points, or receptors, which are established by the user within the modelling domain. Thirty-eight (38) receptors, whose locations are given in Table 3.2 representing populated areas, schools, a hospital and universities were identified within the domain. In addition, receptors were also located at one ambient monitoring site in order to facilitate the model-to-monitor comparisons that are part of the model validation process.

For modelling purposes, constant emission rates of the pollutants were assumed. The refinery was assumed to process crude throughout the whole year. The model determines average concentration at each of the approximately 38 modelled receptors for each of the 366/365 days within the years considered in this research.

Due to data file size limitations, CALMET was executed for four quaters of each year thus generating four CALMET.dat files per year. The outputs of the CALMET simulation were used as inputs for CALPUFF. CALPUFF was also then executed for all the years under consideration.

The PRTMET, a post-processor of CALMET, was used to analyze and display of meteorological parameters from the binary CALMET output file. The CALPOST was used to process the files from CALPUFF, producing

Table 3.2: Receptor Locations in the Study Area

| **Receptor** | **Code** | **Easting(km)** | **Northing(km)** |
|---|---|---|---|
| Tema Oil Refinery | TOR | 831.699 | 627.210 |
| Tema Steelworks | TSW | 832.215 | 629.955 |
| Ashiaman | ASH | 830.287 | 630.477 |
| Central University | CU | 841.410 | 638.219 |
| Dawenya | DAW | 837.148 | 637.054 |
| Sebrepor | SEB | 831.172 | 633.778 |
| Prampam | PRAM | 843.381 | 632.814 |
| Tema Newtown | TNT | 835.168 | 625.508 |
| Kpone | KP | 837.970 | 630.162 |
| Tema Fishing Harbour | TFH | 834.227 | 624.685 |
| Tema General Hospital | TGH | 829.622 | 628.685 |
| Tema Community 4 | TC4 | 831.463 | 625.952 |
| Tema Community 7 | TC7 | 831.175 | 626.749 |
| Tema Community 10 | TC10 | 829.664 | 626.435 |
| Afienya | AFNY | 832.542 | 641.534 |
| Akropong | AKR | 822.313 | 661.283 |
| Dodowa | DDW | 821.429 | 651.073 |
| Oyibi | OYB | 819.252 | 643.347 |
| New Ningo | NNG | 850.317 | 635.186 |
| Old Ningo | ONG | 852.617 | 636.861 |
| Kpeshie | KPSH | 820.829 | 619.060 |
| Teshie | TSH | 820.860 | 617.597 |
| Adenta | AD | 814.697 | 632.409 |
| Madina | MD | 813.895 | 628.998 |
| University of Ghana | UG | 811.117 | 625.613 |
| Sakumono | SAK | 826.715 | 623.704 |
| Sege | SEG | 866.159 | 651.299 |
| Shai Hills | ShHL | 839.477 | 654.0509 |
| Odumasi Krobo | OdKR | 837.889 | 659.386 |
| Larteh | LT | 823.382 | 656.945 |
| Volta River | VR | 869.021 | 669.86 |
| Osu | OSU | 813.070 | 614.740 |
| Tema Community 20 | TC20 | 824.261 | 625.726 |
| Tema Community 19 | TC19 | 825.599 | 625.599 |
| Tema Community 18 | TC18 | 824.329 | 625.120 |
| Tema Community 25 | TC25 | 834.031 | 633.978 |
| Kotoka Int. Airport | KIA | 813.748 | 620.858 |
| Heavy Industrial Area | HIA | 835.469 | 628.393 |

a summary of simulation results in tabulated as well as in gridded form CALPOST was also used to produce wind roses from the CALMET and WRF output data.

#### 3.2.5.4 Model Evaluation

The most commonly used measures of model performance are the statistics recommended in the U.S.EPA 1992 modeling guidance. To determine the reliability of the simulation data, verification of simulated values using the WRF and CALMET models was conducted for surface wind speed and direction. Datasets from the Tema and Accra meteorological stations were used. Even though there are other stations located within the study domain, many of them are not functional. Therefore, only the two stations mentioned were used. Due to the large number of missing data of the other surface wind parameters, they could not be used for validation. Only wind speed and direction were validated.

To validate the dispersion model, CALPUFF, measured data on $SO_2$, $NO_2$ emissions made from the 10 - 23 January, 2008 were used. The Differential Optical Absorption System (DOAS) used for the measurements was installed on the premises of the Tema Oil refinery to monitor and measure

the concentration of gases emitted into the atmosphere due to its activities and also due to the operations of other industries within its environs. Details of the set-up and results can be obtained in Sackey (2012).

The statistical verification of model performance in this study was performed using four statistical indicators including the Index of Agreement (IOA), Fractional Bias (FB), Normalized Mean Square Error (NMSE), and Pearson correlation coefficient (R). The formulas used to derive these five indicators are given in :Eqn. 3.1 - Eqn. 3.3.

$$R = \frac{\sum_{i=1}^{N}\left(C_{oi} - \overline{C}_o\right)\left(C_{pi} - \overline{C}_p\right)}{\sqrt{\sigma_o \sigma_p}} \tag{3.1}$$

$$FB = \frac{\overline{C}_o - \overline{C}_p}{0.5\left(\overline{C}_o + \overline{C}_p\right)} \tag{3.2}$$

$$NMSE = \frac{\overline{\left(C_o - C_p\right)^2}}{\overline{C_o}\,\overline{C_p}} \tag{3.3}$$

$$IOA = 1 - \frac{\sum_{i=1}^{N}\left(C_{pi} - C_{oi}\right)^2}{\sum_{i=1}^{N}\left(\left|C_{pi} - \overline{C}_o\right| + \left|C_{oi} - \overline{C}_p\right|\right)^2} \tag{3.4}$$

where $C_o$ is the observed quantity, $C_p$ the predicted quantity, $C_{oi}$ and $C_{pi}$ are the observed and predicted quantities respectively for N cases.

# Chapter 4

# Results and Discussions

## 4.1 Introduction

This Chapter presents results of the estimated refinery emission rates and other parameters used for the dispersion simulations. Both the meteorological and dispersion simulation results are also presented and discussed as well as their validation.

## 4.2 Refinery Emissions and Interannual Trends

Plots of estimated emission rates of $CO_2$, VOCs, $PM_{2.5}$, $SO_2$ and $NO_2$ and their averages for 2008 - 2013 are shown in Figs.4.1 - Fig.4.5 respectively.

It can be noticed that total $CO_2$ emissions were the highest of the pollutants estimated from the Tema Oil Refinery ranging from about 130 to 165 t/hr.

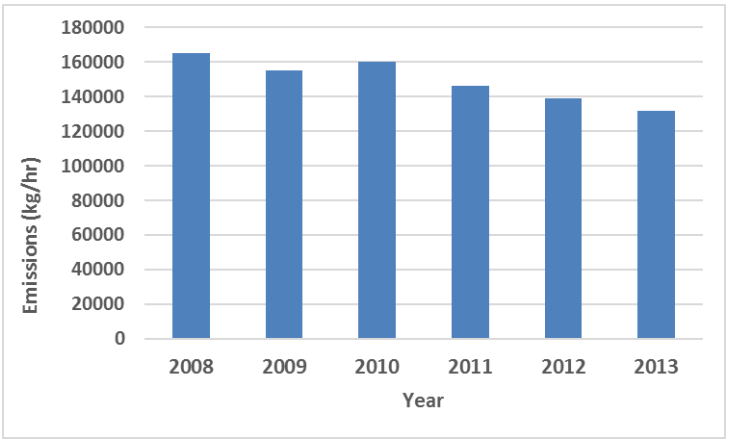


Figure 4.1: Interannual Variation of $CO_2$ Emission Rates from the Tema Oil Refinery

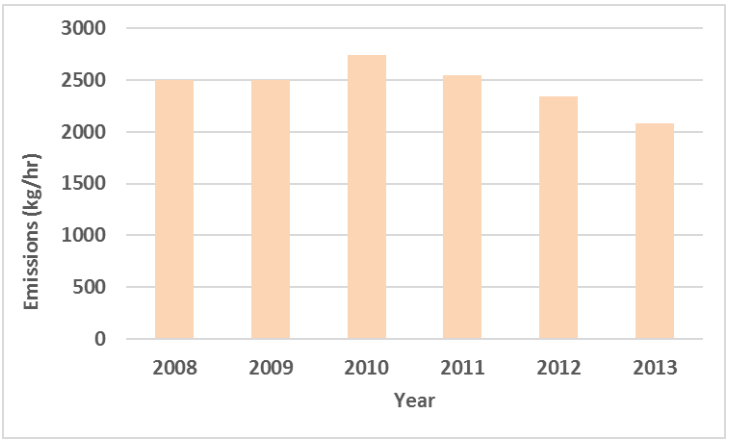


Figure 4.2: Interannual Variation of VOCs Emission Rates from the Tema Oil Refinery

The VOCs are next in line with emission rates ranging between 2083 and 2500 kg/hr. Particulate matter rates were observed to decline marginally over the years with an average rate of 1032 kg/hr followed by $SO_2$ and $NO_2$ with average rates of 776 and 371 kg/hr respectively.

$CO_2$ emissions were highest in 2008, dipped in 2009, increased again in 2010 after which a steady decrease over the remaining years is observed. The highest emissions of $PM_{2.5}$ also occured in 2008 followed by a marginal

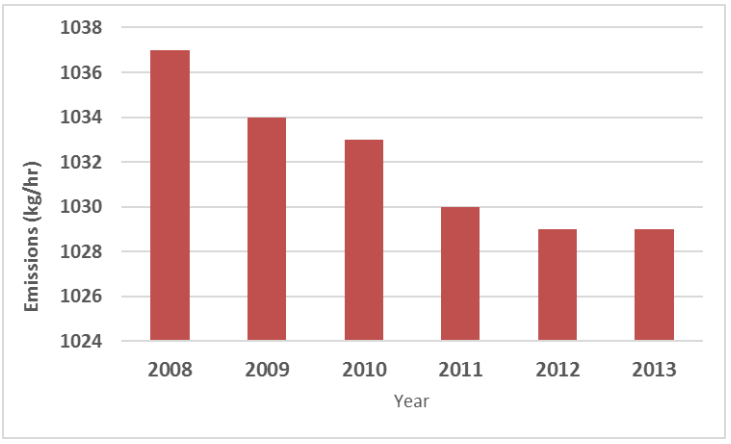


Figure 4.3: Interannual Variation of $PM_{2.5}$ Emission Rates from the Tema Oil Refinery

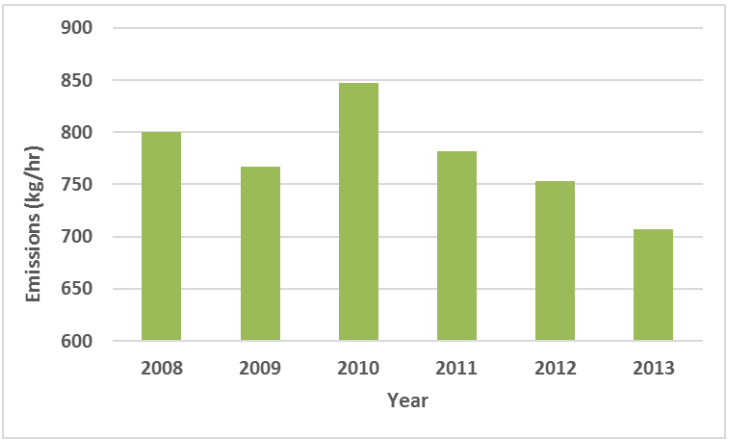


Figure 4.4: Interannual Variation of $SO_2$ Emission Rates from the Tema Oil Refinery

steady decline over the years. However, the other emissions peaked in 2010 and declined steadily over the following years. The decline in emission rates was a result of a reduction in production due to the frequent shortfalls in the refinery's crude oil supply, consequently leading virtually to a halt of refinery operations in 2014 preceded by intermittent shutdowns.

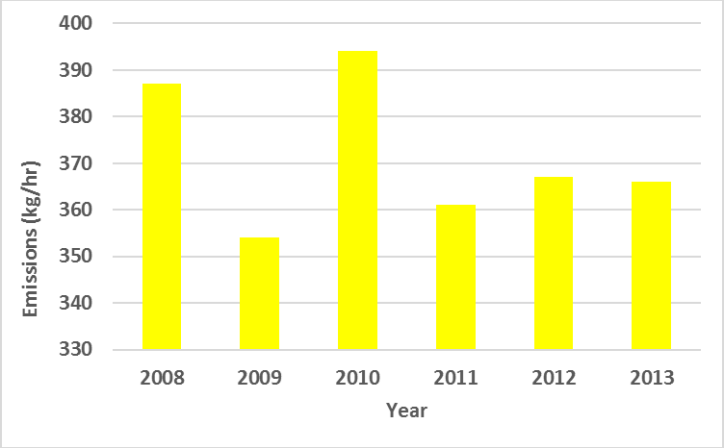


Figure 4.5: Interannual Variation of $NO_2$ Emission Rates from the Tema Oil Refinery

## 4.3 Preliminary Dispersion Simulation

Geophysical inputs, terrain data (with receptor locations relative to the refinery) and Land Use data, are given Figs.4.6 and 4.7 respectively.

The most prominent topographical feature is the Gulf of Guinea that forms the southern boundary of the study area. The other topographical feature with elevated terrain, between 300 - 600 m, is the Akropong-range located at the north-western corner of the study area as shown in Fig.4.6. Land use within the study area is fairly complex, varying from open ocean to the south, marshy and wetlands along the coast to the urban areas of Osu (Fig.4.7). The built-up Tema community is not captured probably due to poor resolution. In addition, there are large tracts of agricultural land also present in the study area.

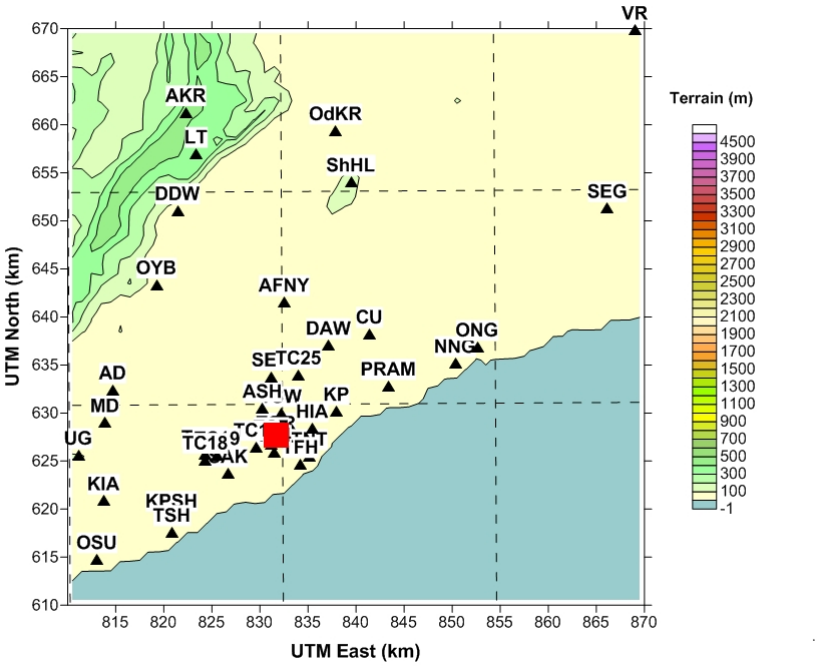


Figure 4.6: Terrain Map of the Study area showing receptor locations and the Refinery (red square)

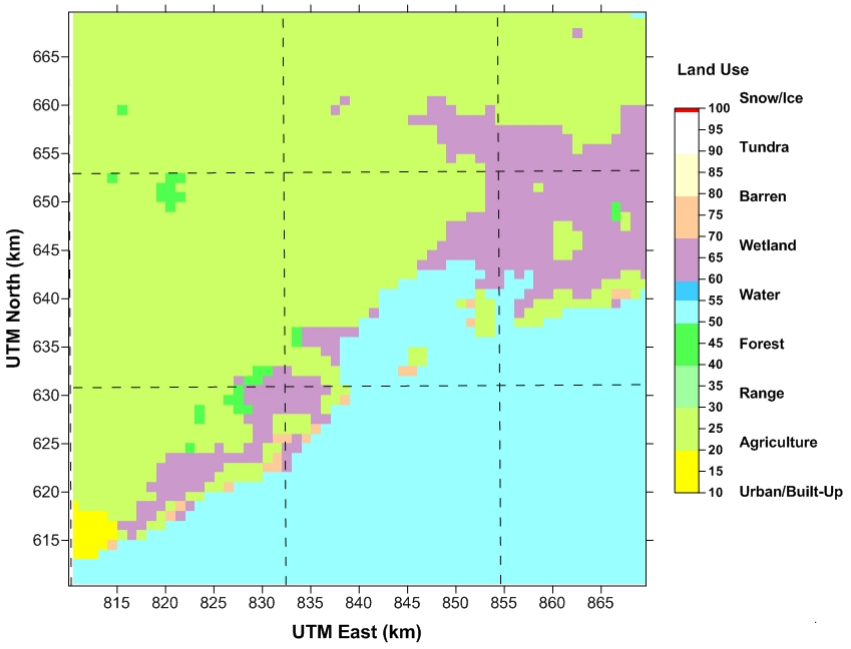


Figure 4.7: LandUse Map of the Study Area

### 4.3.1 Spatial Variation of Pollutants

Results of the preliminary simulations of the dispersion of the refinery emissions in the study domain are presented in the form of daily average concentrations of the modelled emissions at the indicated receptors respectively. Considering the receptor locations within the study area, as shown in Fig.4.6, it was observed that predicted daily average pollutant concentrations were high at receptors closest to the refinery and low at receptors far away from the refinery. This can be explained by the dispersion equation, Eqn.(2.14), which expresses an exponential decay of emissions with distance from emission source.

Considering receptor locations relative to the refinery, predicted concentrations were noted to be high at northern receptors as seen in Fig.4.8. These receptors include Tema Steelworks, Ashiaman and Sebrepor. This was followed by receptors on the north-eastern side up to about 10 km of the refinery including Heavy Industrial Area, Dawenya, Kpone, Prampam, Old and New Ningo and the Central University as shown in Fig.4.9. Tema Newtown and the Tema Fishing Harbour located south east of the refinery also receive significant emissions followed by south western receptors including Tema Communities 4, 7 and 10 and the Tema General Hospital which are located within a distance of about 4 km of the refinery as shown in Figs.4.10 and 4.11. Receptors located on the north western part

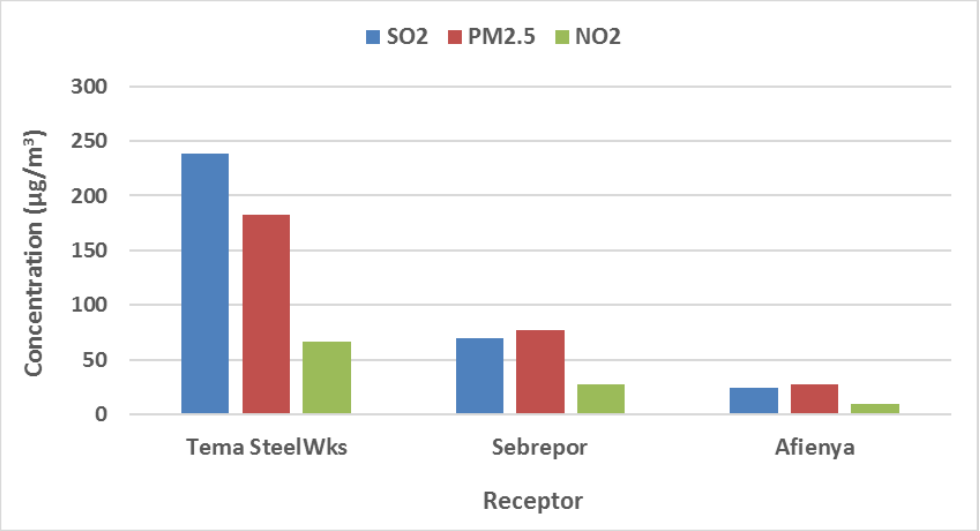


Figure 4.8: Predicted Daily Average Concentrations of $SO_2$, $NO_2$ and $PM_{2.5}$ at northern receptors in the Study area

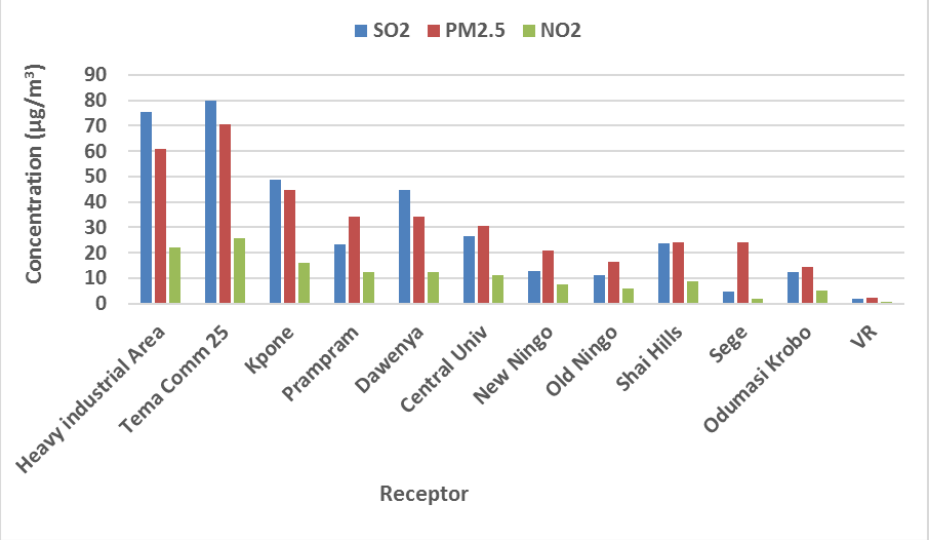


Figure 4.9: Predicted Daily Average Concentrations of $SO_2$, $NO_2$ and $PM_{2.5}$ at north eastern receptors in the Study area

of the refinery are the least impacted by the refinery emissions as they showed very low emission concentrations. These include Madina, Adenta, the University of Ghana, Oyibi, Larteh, Dodowa and Akropong.

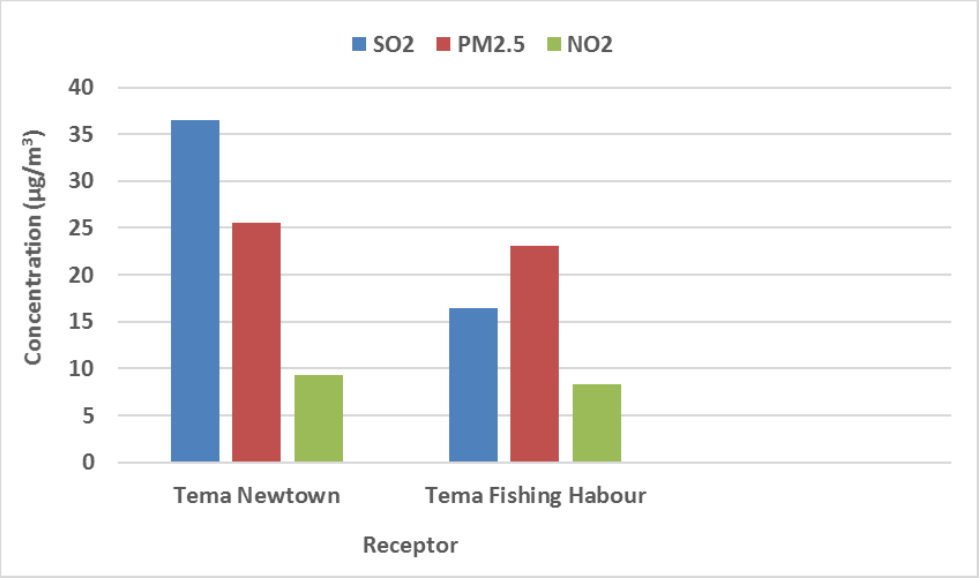


Figure 4.10: Predicted Daily Average Concentrations of $SO_2$, $NO_2$ and $PM_{2.5}$ at south eastern receptors in the Study area

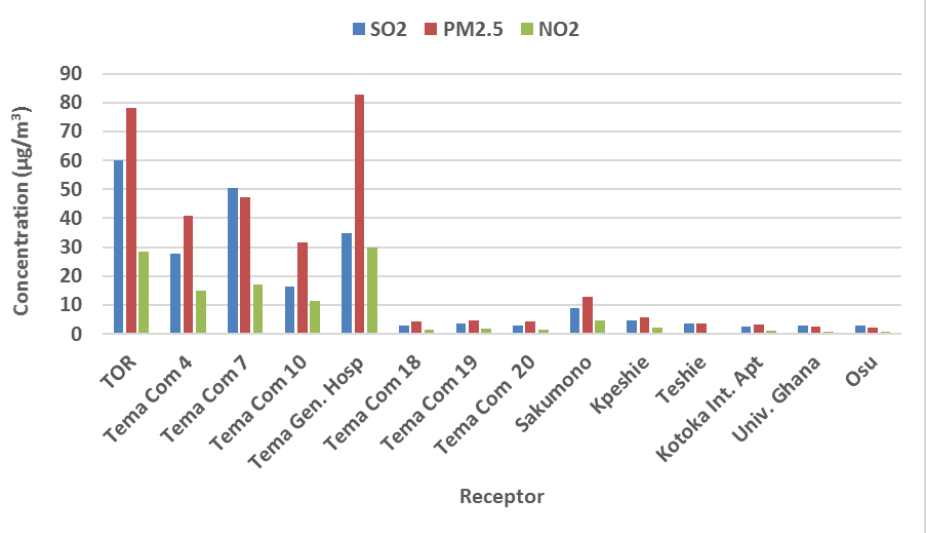


Figure 4.11: Predicted Daily Average Concentrations of $SO_2$, $NO_2$ and $PM_{2.5}$ at south western receptors in the Study area

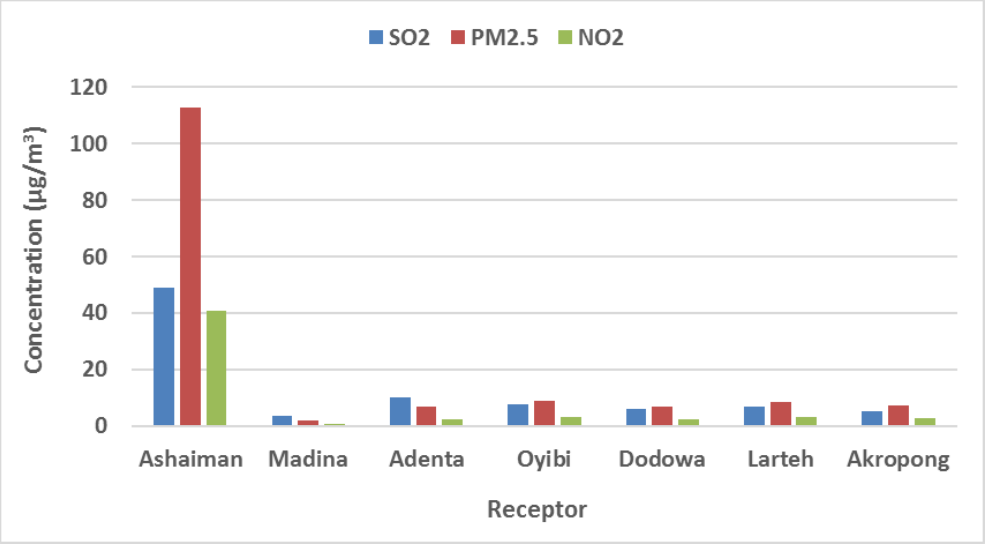


Figure 4.12: Predicted Daily Average Concentrations of $SO_2$, $NO_2$ and $PM_{2.5}$ at northern western receptors in the Study area

The prevailing wind directions during the year under study were south-westerly (87%) of total winds as depicted by Fig.4.13. Therefore, receptors located on the north and north-eastern parts of the refinery show relatively higher emission concentrations than other parts of the study domain because the south-westerly winds carry the pollutant clouds from the refinery towards them. Approximately 77% of winds in the study area are clustered in $3^{rd}$ wind speed classes (3.3 - 5.4 m/s) with winds in the next upper class of (5.4 - 8.5 m/s) being 19%. Winds from 1.8 - 3.3 m/s account for 8% of total winds. The average wind speed is estimated at 3.45 m/s with calm winds forming 0.057% of total winds.

Based on these preliminary results, it can be concluded that emissions from the refinery impact communities located within a radius of about 10-15 km around the refinery. Consequently, subsequent simulations of emissions of

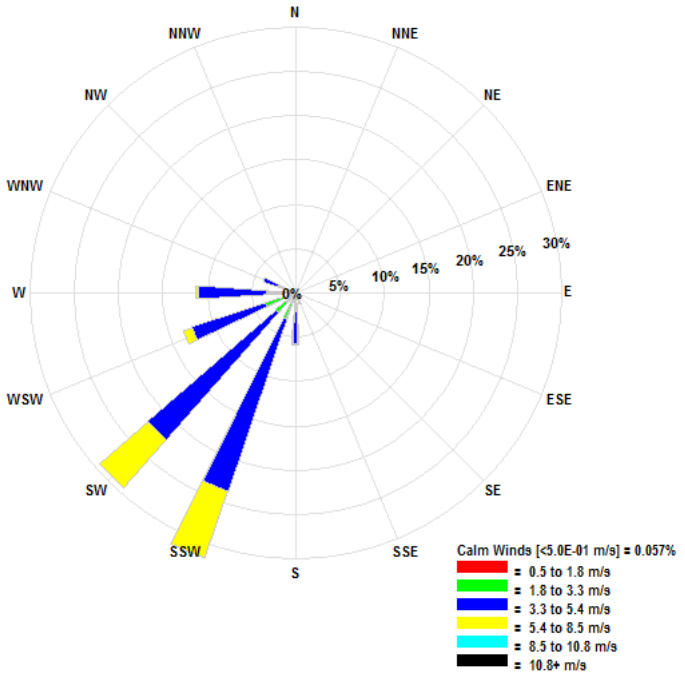


Figure 4.13: Wind Rose Depicting Surface Winds in Tema for 2008

the other years will focus on the receptors which fall within this radius of influence.

## 4.4 Validation of the CALPUFF Model

At this point, results of the performance evaluation of CALPUFF, are presented and discussed. Plot of the comparison between measured and modelled $SO_2$ and $NO_2$ are seen in Fig.4.14 and Fig.4.15 respectively.

The performance assessment of the model, based on direct quantitative comparisons of observed and predicted mean concentrations as seen in

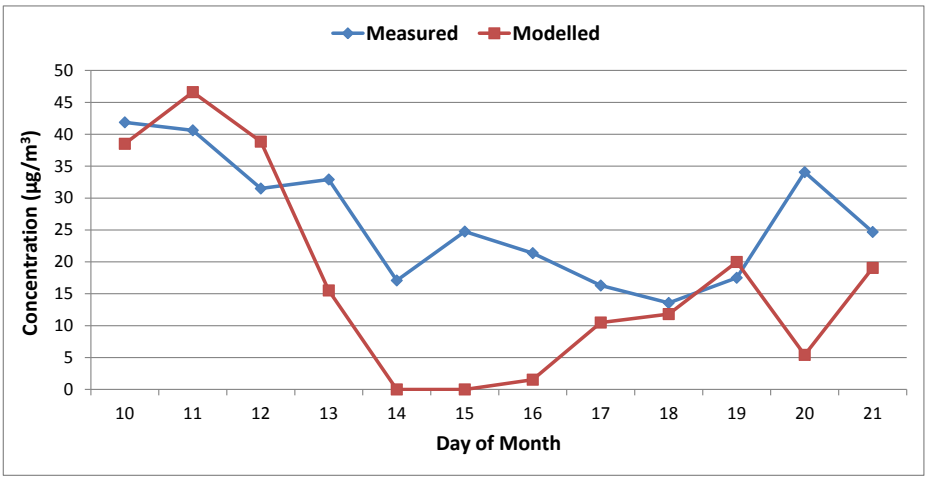


Figure 4.14: Plots of measured and modelled $SO_2$ Concentrations

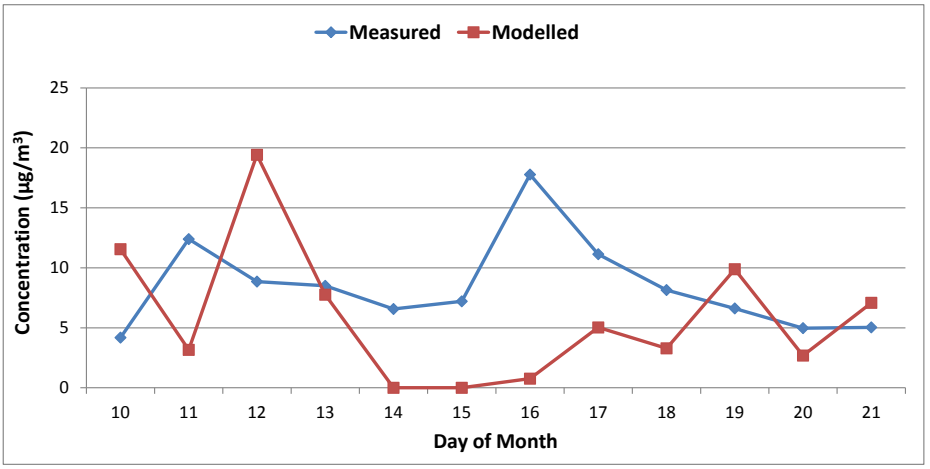


Figure 4.15: Plots of measured and modelled $NO_2$ Concentrations

Figs.4.14 and 4.15, reveals that CALPUFF predictions for $SO_2$ were better than $NO_2$ concentrations. From the 10 - 12, 17 - 19 and 21 January, predicted $SO_2$ concentrations closely approached measurements. Quantitative agreement between predicted and modelled $NO_2$ concentrations is excellent on 13 January and good for 19 - 21. However, from 13-16 January, CALPUFF significantly under-predicted the measured values. Despite these differences between predicted and measured values on some days, the trends in the measurements are accurately predicted especially for $SO_2$. The simulation results did not take into account $SO_2$ and $NO_2$ background concentrations because this data was not available. This may explain the reason for this under-prediction. The measured concentrations are likely to include emissions from other sources which are not considered in the simulations. Another important reason could be the assumption made that emission rates from the refinery are constant. This is unlikely to be representative of actual operating conditions at the refinery. It was, however, necessary to make this assumption using a constant estimated average emission rates for modeling purposes. Additionally, possible errors associated with the measurements of $SO_2$ and $NO_2$ at the measurement location cannot be overlooked.

Results of model performance evaluation after applying the USEPA guidelines pertaining to model evaluation protocol are presented in Table 4.1. The indices are the correlation coefficient (R), the index of agreement

(IOA), the normalised mean square error (NMSE) and the fractional bias (FB).

Table 4.1: Statistical Performance Indices of the CALPUFF model

| **Pollutant** | ***R*** | ***NMSE*** | ***IOA*** | ***FB*** |
|---|---|---|---|---|
| $SO_2$ | 0.66 | 0.73 | 0.39 | 0.41 |
| $NO_2$ | -0.25 | 0.36 | 1.34 | 0.36 |

The index of agreement between predicted concentrations and measurements is better for $SO_2$ and $NO_2$. The correlation coefficient of $SO_2$ with observations is satisfactory but that for $NO_2$ is negatively weak as shown in Table 4.1. The $NO_2$ emissions from automobiles make up a large fraction of ambient $NO_2$ levels. It is therefore probable that a large fraction of the measurements consists of contributions from the vehicular emission, revealed in the weak correlation and the poor index of agreement. CALPUFF under-predicts $NO_2$ by a smaller factor than $SO_2$ as revealed by their FB values. The NMSE values for $SO_2$ is acceptable whiles that of $NO_2$ is not. Therefore, based on these indices, the performance of CALPUFF can be described as good.

## 4.5 Validation of CALMET and WRF Models

Results obtained from CALMET and WRF simulations are compared with available surface observations (wind speed and direction) for January 2008 from the Tema meteorological station (TMS) as shown in Figs.4.16 and 4.17. Wind roses generated from the models for the same period are also presented in Figs.4.18 and 4.19.

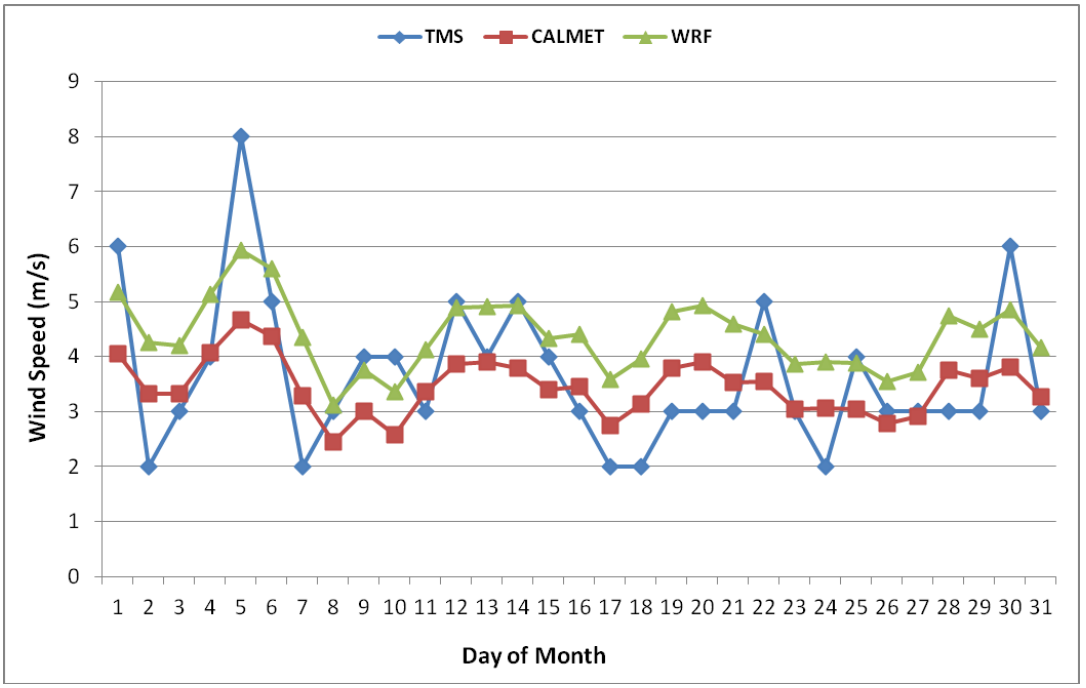


Figure 4.16: Plots of Observed and Modelled Wind Speeds

It is apparent from Fig.4.16 that WRF and CALMET models generally under-predicted wind speeds from January 9 - 14 and over-predicted speeds on January 16 - 24. However, on days 11, 16, 21 and 23, CALMET predictions closely approach observations whiles WRF predicts similar speed on

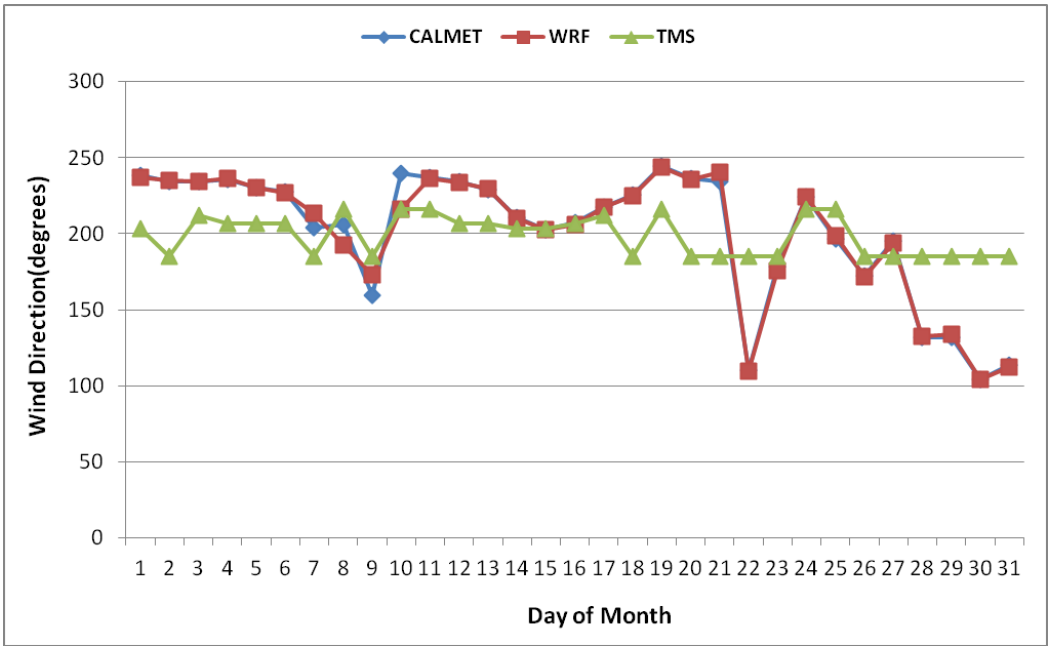


Figure 4.17: Plots of Observed and Modelled Wind Direction

the $15^{th}$ January. Fig. 4.17 reveals the over-prediction of wind direction by both models for most part of the period considered. From the other statistical performance measures given in Table 4.2, it can be observed that both CALMET and WRF share similar indices rating their performances on the same scale with CALMET indicating slightly higher correlation coefficients for both wind direction and speed than WRF. Under-prediction by CALMET is greater than by WRF as seen in the FB values.

Table 4.2: Statistical Performance Indices of CALMET and WRF models

| | CALMET | | | | WRF | | | |
|---|---|---|---|---|---|---|---|---|
| **Parameter** | ***R*** | ***NMSE*** | ***IOA*** | ***FB*** | ***R*** | ***NMSE*** | ***IOA*** | ***FB*** |
| *Speed* | 0.58 | 0.66 | 0.24 | 0.34 | 0.57 | 0.65 | 0.09 | 0.15 |
| *Direction* | 0.29 | 0.66 | 0.02 | -0.10 | 0.28 | 0.66 | 0.02 | -0.10 |

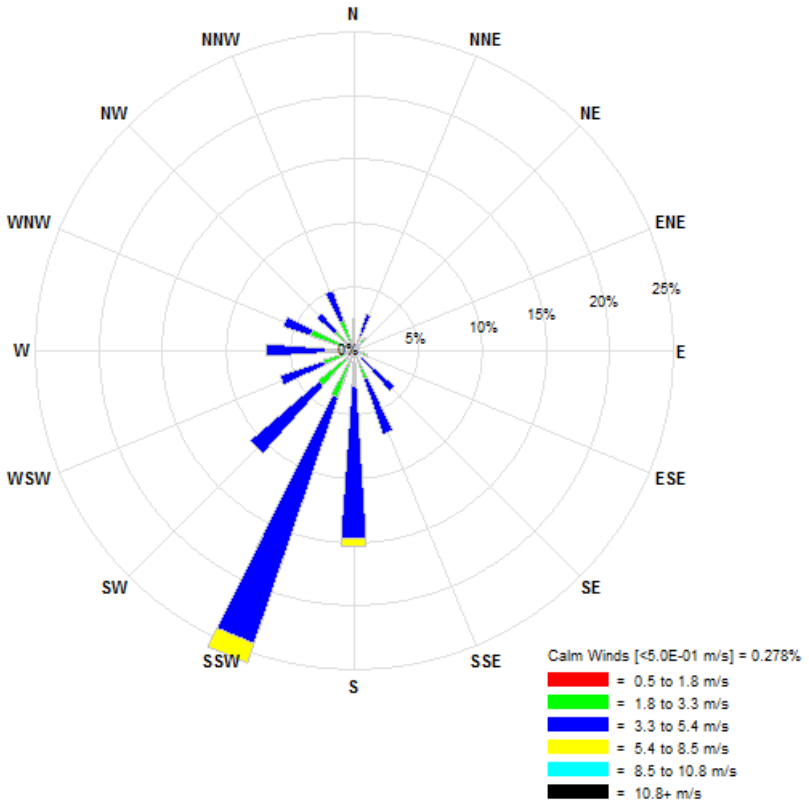


Figure 4.18: Wind Rose Depicting CALMET Surface Winds

The wind rose generated from CALMET (Fig.4.18) indicated the predominant prevailing wind is south south-westerly (26%) whiles southerly and southwesterly represent about 26%. The remaining winds are spread across a wide spectrum ranging from westerly to north north-easterly. WRF wind rose (Fig.4.19) predicted an increased percentage of south south-westerly winds (31%) than CALMET. It also indicates 12% of southerly winds and 12% of south-westerly winds which is lower than CALMET. It is clear that the percentages of the other winds are also lower in the WRF wind rose than

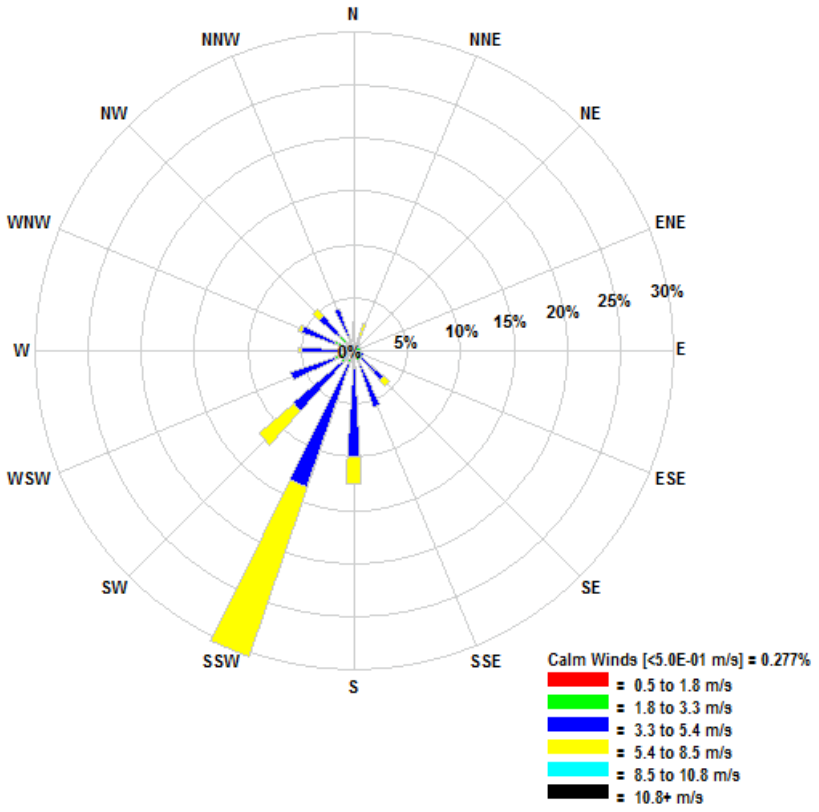


Figure 4.19: Wind Rose Depicting WRF Surface Winds

the CALMET. The predominant wind speed class predicted by both models is 3.3 - 5.4 m/s with CALMET predicting a higher percentage (75%) than WRF (64%). Thirty percent (30%) of the total winds have speeds between 5.4 - 8.5 m/s according to WRF whiles CALMET predicts only 3% of that class. Generally, average wind speeds is higher for WRF than CALMET. Calm winds in both modelled wind (>0.5 m/s) account for only 0.28% of the data. Based on the statistics, it appears that CALMET predictions better approximates observations as it is able to capture small scale effects

which cannot be accounted for by WRF. Numerical meteorological models tend to have spatial and temporal phase errors in simulating surface wind. This is because the lowest-level WRF winds must be extrapolated down to ground-level to initialize CALMET. Thus unless the vertical resolution is quite fine, it would be expected that the near-surface CALMET output winds will be biased towards the trends seen in the lowest level of the WRF data, which has a higher elevation in the region compared to the surface stations (Protonotariou et al., 2004). On this basis, the remaining validation results for only CALMET with data from TMS and AMS for 2008 - 2013 are presented in Table 4.3.

Table 4.3: Statistical Performance Indices of CALMET and Observations from the TMS and AMS

| | | TMS | | | | AMS | | | |
|---|---|---|---|---|---|---|---|---|---|
| **Year** | **Parameter** | ***R*** | ***NMSE*** | ***IOA*** | ***FB*** | ***R*** | ***NMSE*** | ***IOA*** | ***FB*** |
| 2008 | *Speed* | 0.58 | 0.24 | 0.66 | 0.34 | 0.56 | 0.88 | 0.72 | 0.08 |
| | *Direction* | 0.29 | 0.02 | 0.66 | -0.10 | 0.57 | 0.02 | 0.71 | -0.14 |
| 2009 | *Speed* | 0.48 | 0.12 | 0.62 | 0.17 | 0.52 | 0.99 | 0.72 | 0.85 |
| | *Direction* | 0.07 | 0.02 | 0.72 | -0.12 | -0.01 | 0.02 | 0.72 | -0.14 |
| 2010 | *Speed* | 0.32 | 0.17 | 0.60 | 0.24 | 0.64 | 0.80 | 0.72 | 0.77 |
| | *Direction* | 0.06 | 0.01 | 0.68 | -0.09 | 0.03 | 0.02 | 0.69 | -0.11 |
| 2011 | *Speed* | 0.31 | 0.10 | 0.54 | 0.09 | 0.59 | 0.78 | 0.72 | 0.76 |
| | *Direction* | -0.02 | 0.01 | 0.69 | -0.09 | 0.22 | 0.01 | 0.71 | -0.11 |
| 2012 | *Speed* | 0.34 | 0.12 | 0.60 | 0.20 | 0.47 | 1.40 | 0.73 | 0.98 |
| | *Direction* | 0.03 | 0.01 | 0.72 | -0.10 | 0.35 | 0.02 | 0.72 | -0.11 |
| 2013 | *Speed* | 0.45 | 0.16 | 0.64 | 0.28 | 0.61 | 1.33 | 0.73 | 0.96 |
| | *Direction* | 0.03 | 0.01 | 0.70 | -0.1 | -0.01 | 0.03 | 0.69 | -0.14 |

From Figs.4.20 - 4.31, it can be seen that the observed direction by both

stations was almost constant for 2008 - 2010 and showed only slight variations for 2011 - 2013. Observed speeds, on the other, appeared highly variable. It is also clear that the quantitative agreement between wind speeds observed at the TMS and CALMET predictions for all the years was higher than from the AMS.

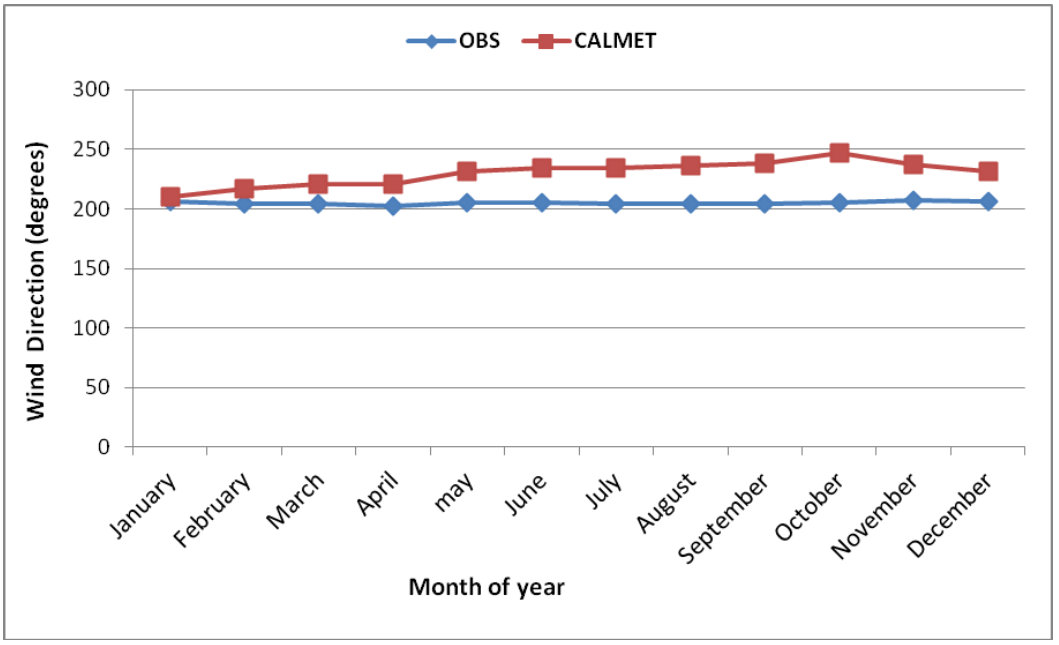


Figure 4.20: Plots of Modelled and Observed(AMS) Surface Wind direction for 2008

The correlation coefficient values between modelled and observed speed for the six-year period were higher for AMS (0.47 - 0.64) than for TMS (0.31 - 0.58) indicating a stronger relationship of the modelled with the observed winds from AMS. The highest R of 0.58 was existed between modelled speeds and TMS speed in 2008 whiles a weakest correlation of 0.31 was found between 2011 modelled and observed data. The highest correlation of 0.64 was obtained with 2010 data at AMS whiles the least value of 0.47

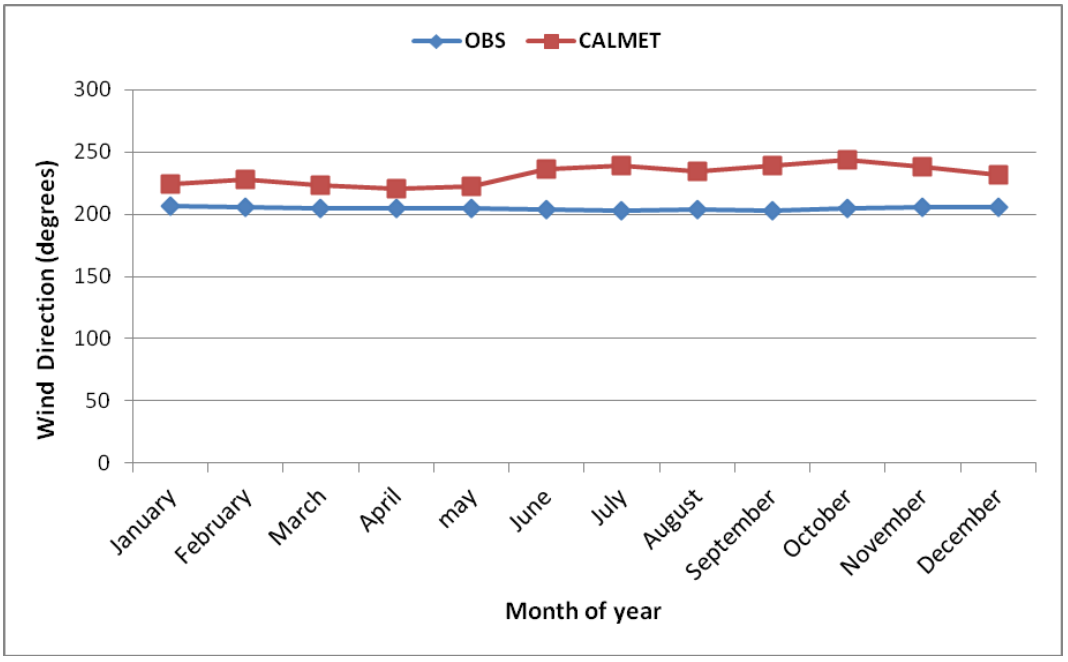


Figure 4.21: Plots of Modelled and Observed(AMS) Surface Wind direction for 2009

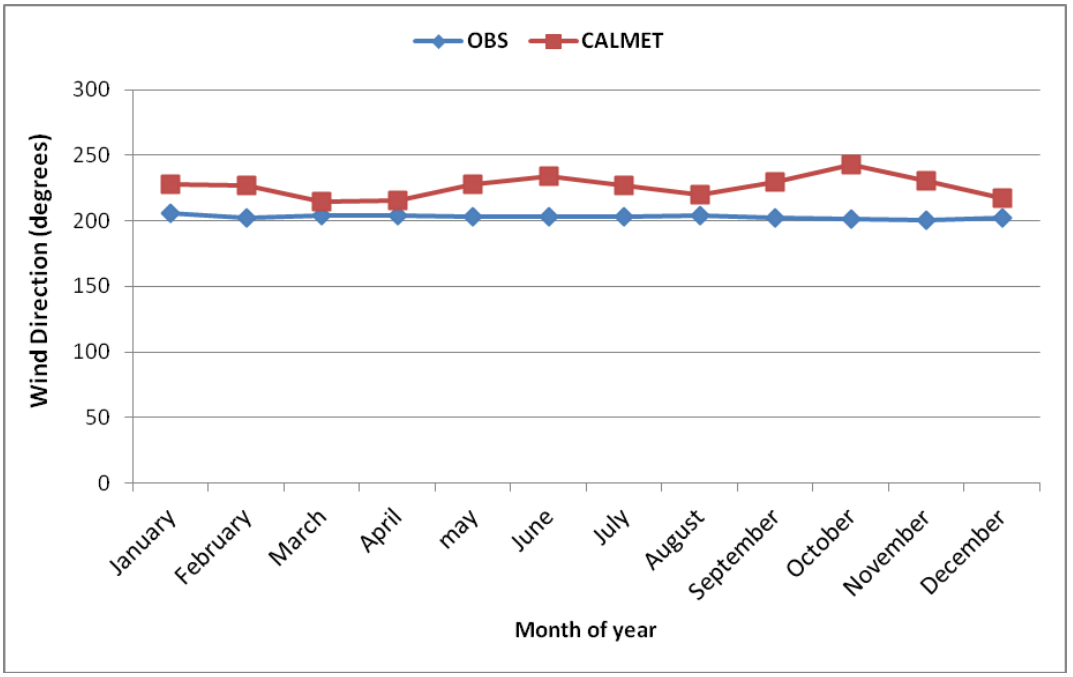


Figure 4.22: Plots of Modelled and Observed(AMS) Surface Wind direction for 2010

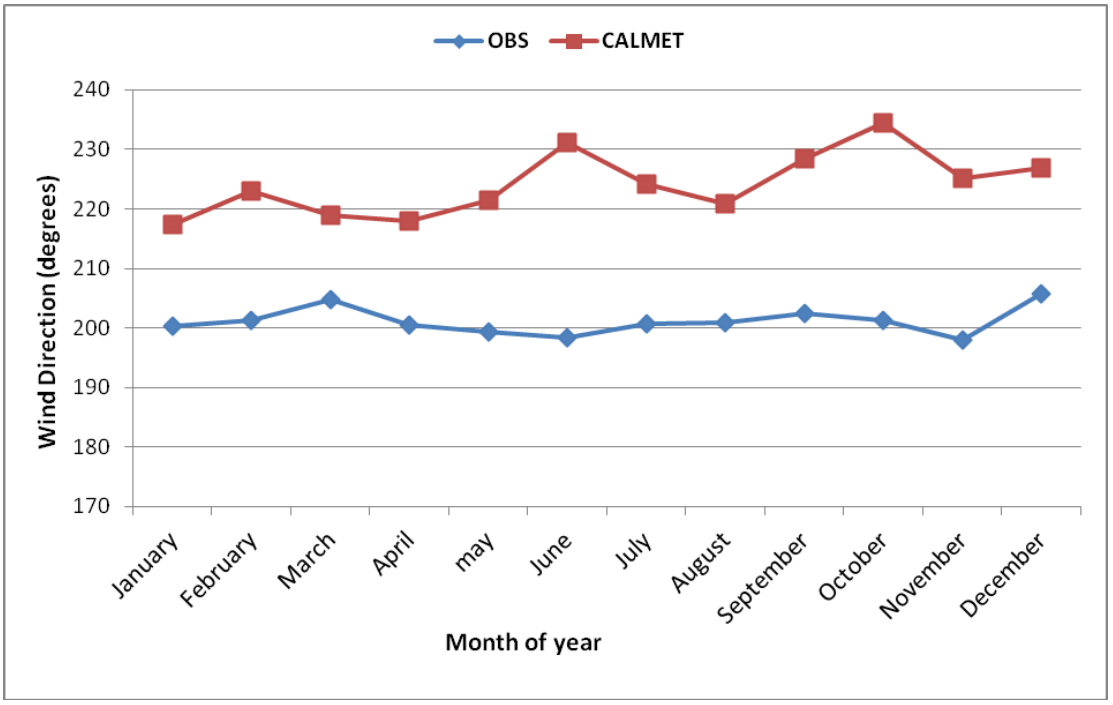


Figure 4.23: Plots of Modelled and observed(AMS) Surface Wind direction for 2011

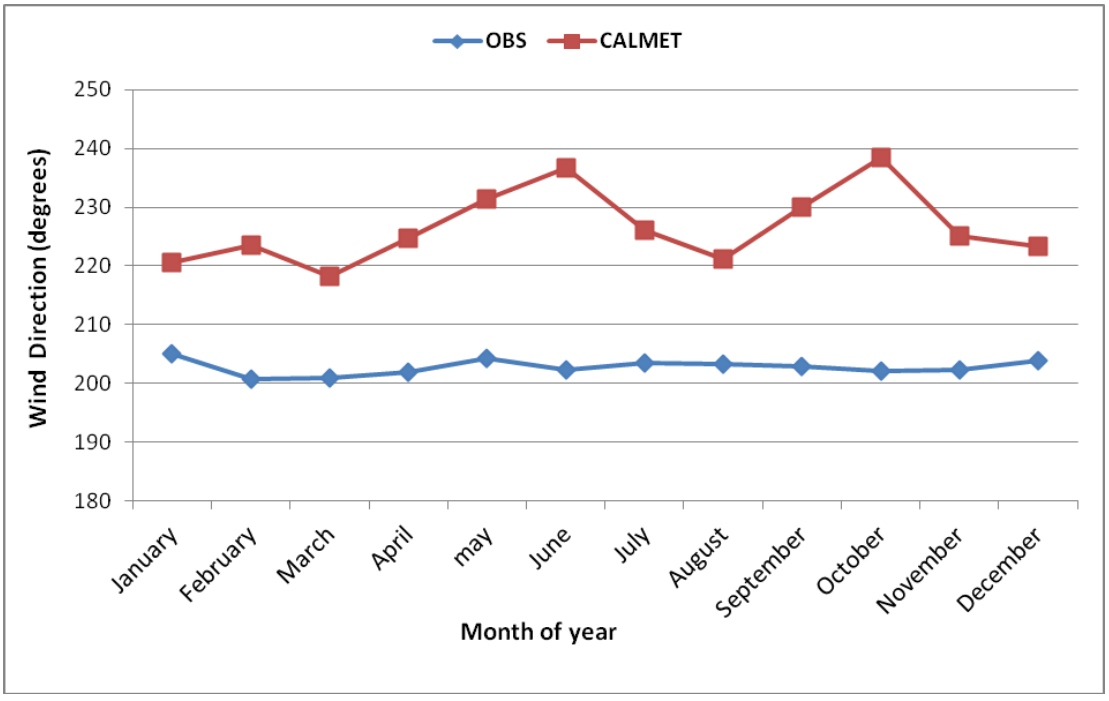


Figure 4.24: Plots of Modelled and observed(AMS) Surface Wind direction for 2012

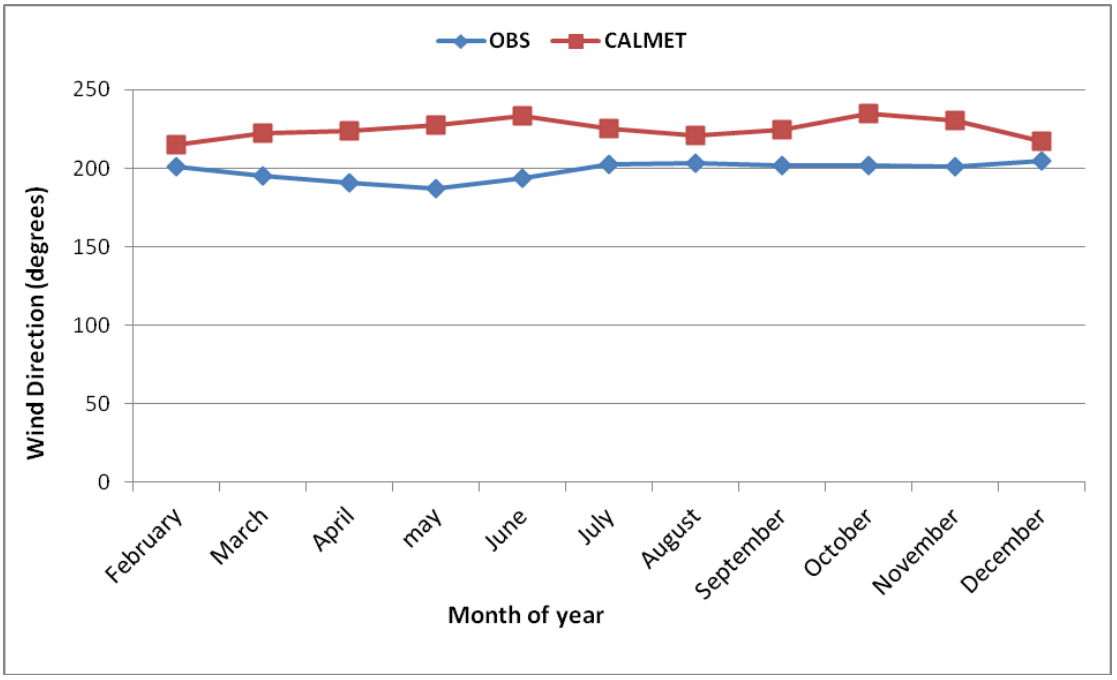


Figure 4.25: Plots of Modelled and observed(AMS) Surface Wind direction for 2013

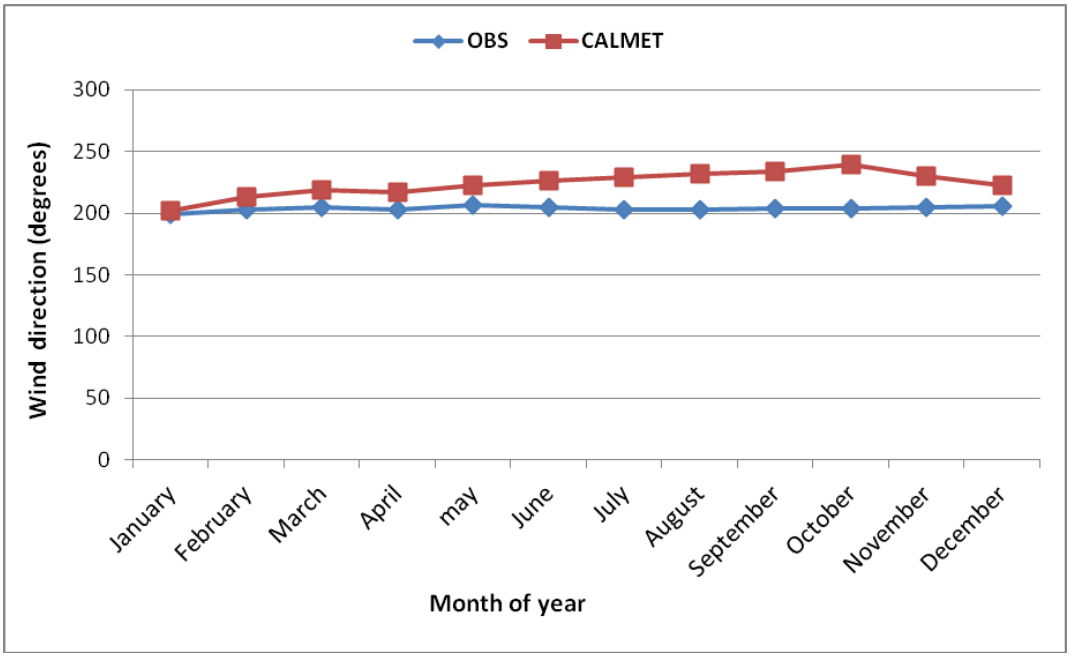


Figure 4.26: Plots of Modelled and Observed(TMS) Surface Wind direction for 2008

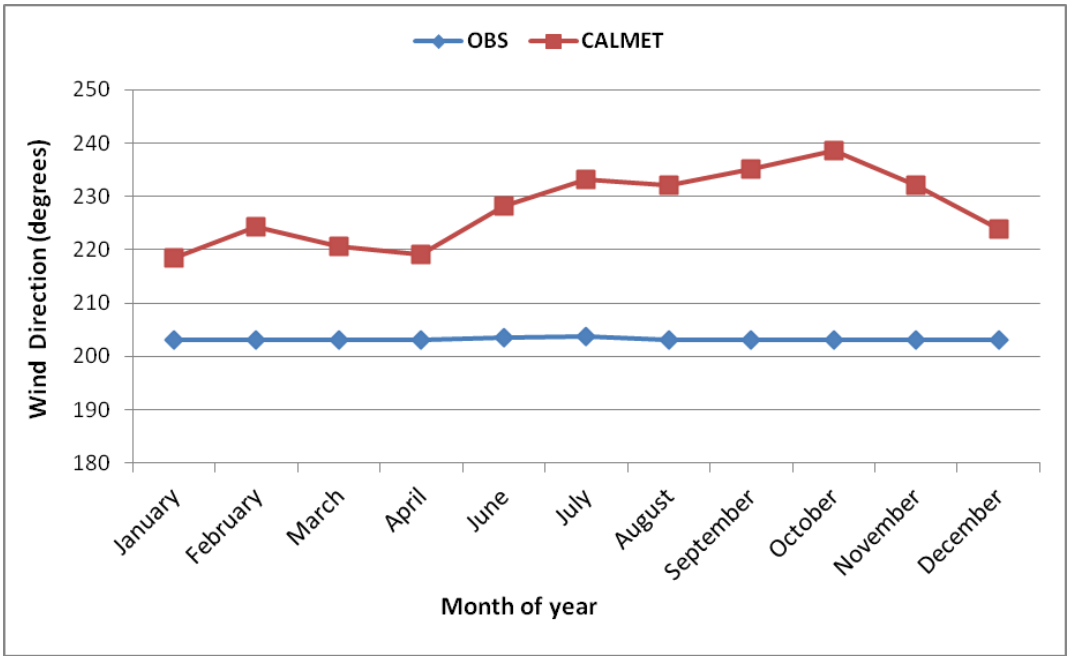


Figure 4.27: Plots of Modelled and Observed(TMS) Surface Wind direction for 2009

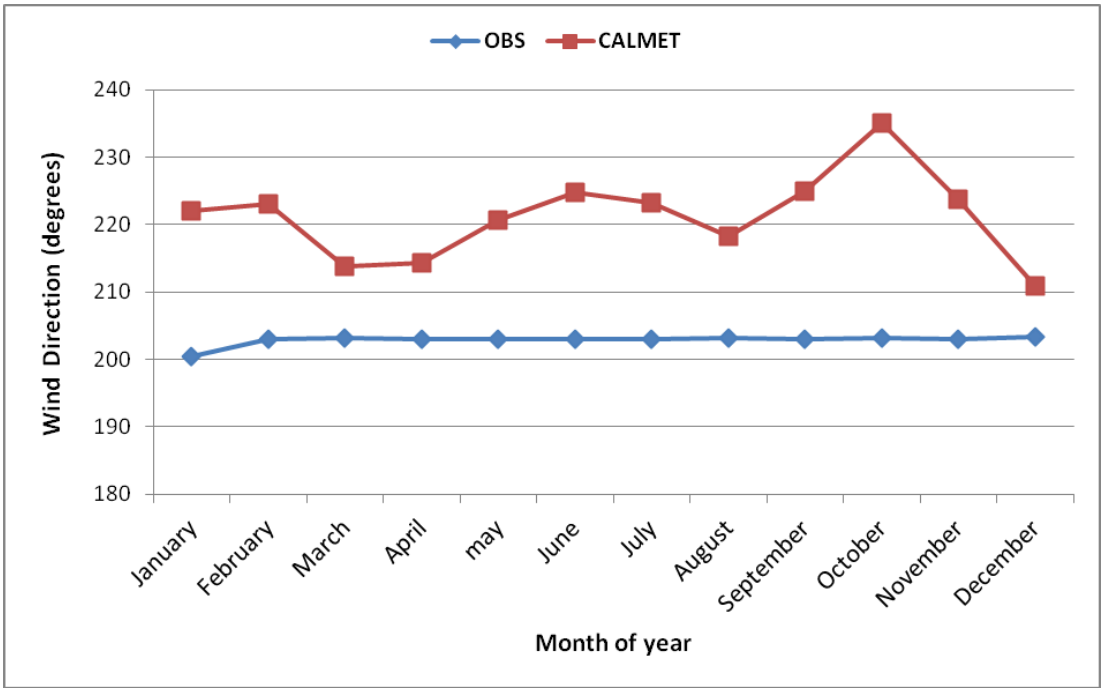


Figure 4.28: Plots of Modelled and Observed(TMS) Surface Wind direction for 2010

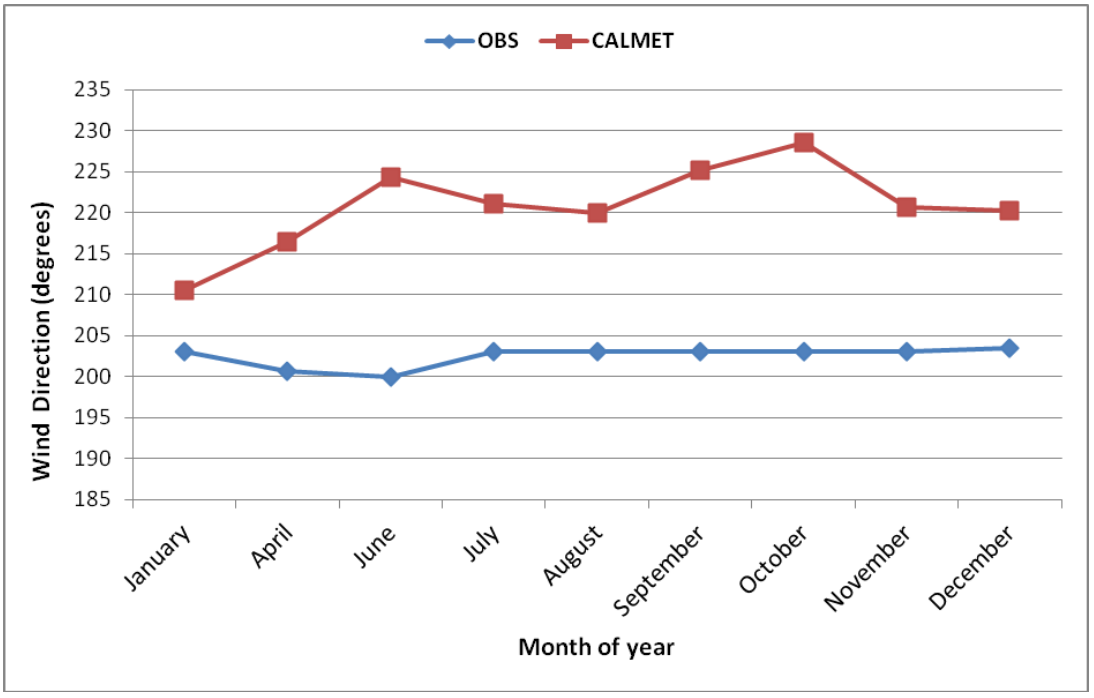


Figure 4.29: Plots of Modelled and observed(TMS) Surface Wind direction for 2011

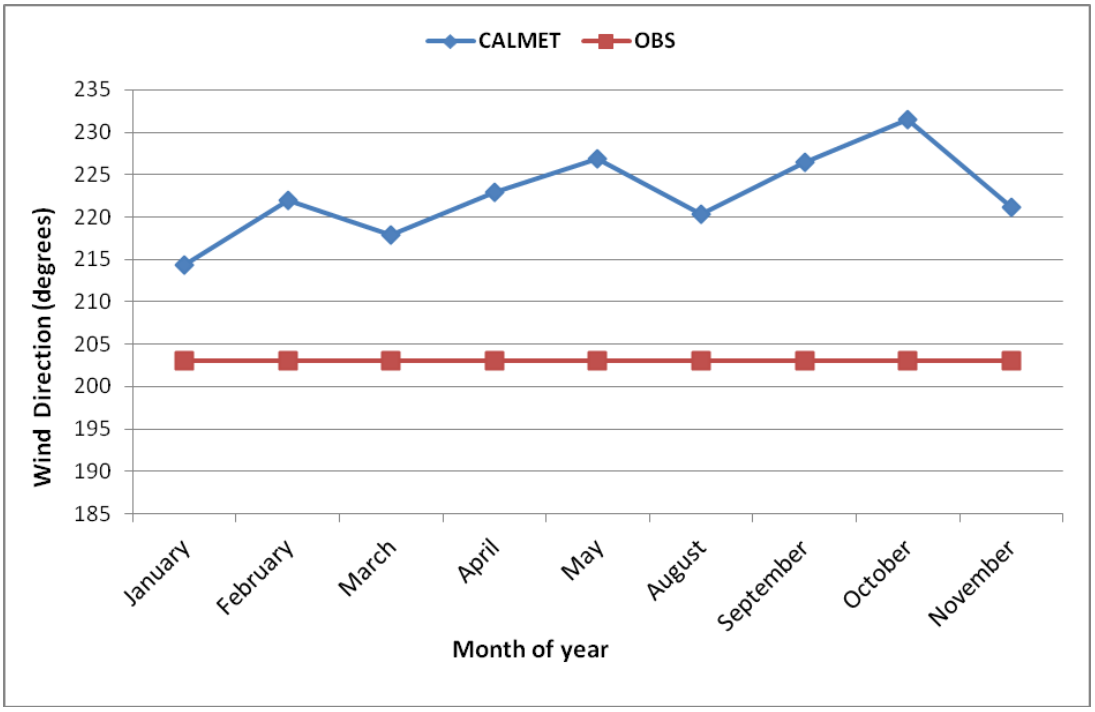


Figure 4.30: Plots of Modelled and observed(TMS) Surface Wind direction for 2012

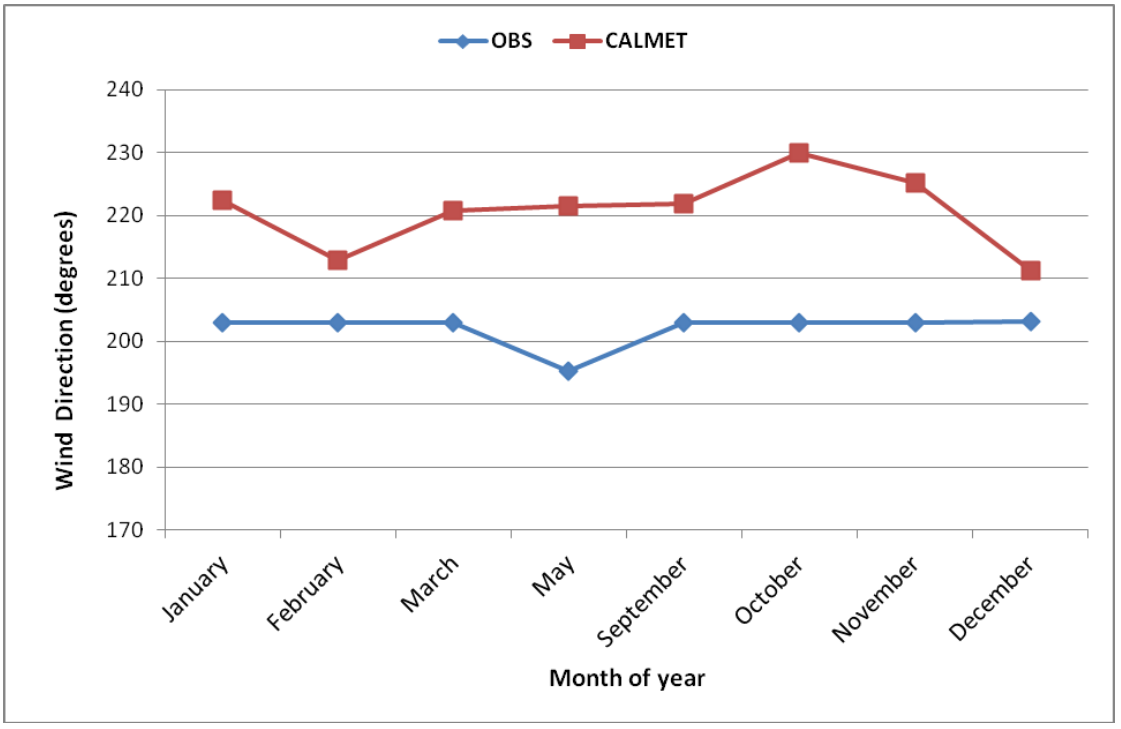


Figure 4.31: Plots of Modelled and observed(TMS) Surface Wind direction for 2013

was found for 2012. Generally, R values for wind direction were lower between model and observed data from both stations.

NMSE values were encouragingly low for wind direction for both stations (0.01 - 0.2) reflecting a low scatter in the entire data set. However, nmse values obtained for speed for AMS were high (0.88 - 1.4) indicating a large scatter in the speed data. NMSE value for speed for TMS were satisfactory (0.1 - 0.24).

IOA between modelled and observed data for all the years was above 0.60 for both variables from both stations except for 2011 speeds.

The negative FB values for direction are indicative of the overpredictions

by CALMET of the observed wind direction from both meteorological stations as shown in Figs.4.20 - 4.25 for AMS and Figs.4.26 - 4.31 for TMS. CALMET clearly under-predicts observed speeds as is seen in the positive FB values. Whiles CALMET overpredicts surface wind direction, it underestimates wind speeds as shown in Figs.4.32 - 4.37 for AMS and Figs.4.38 - 4.43 for TMS.

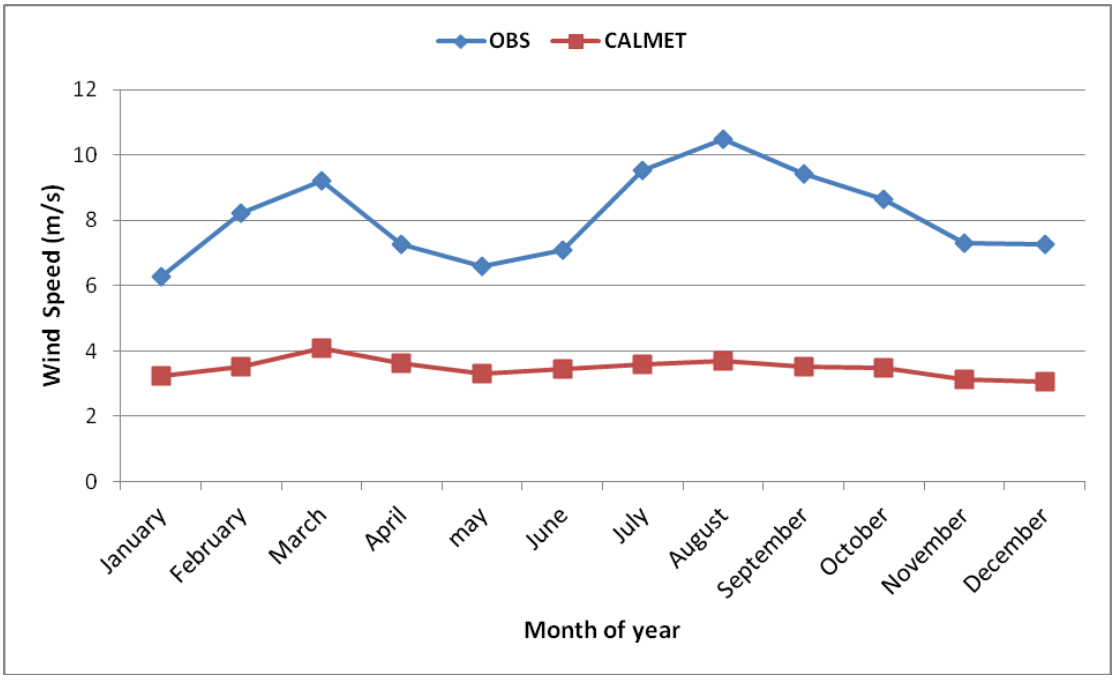


Figure 4.32: Plots of Modelled and Observed(AMS) Surface Wind Speed for 2008

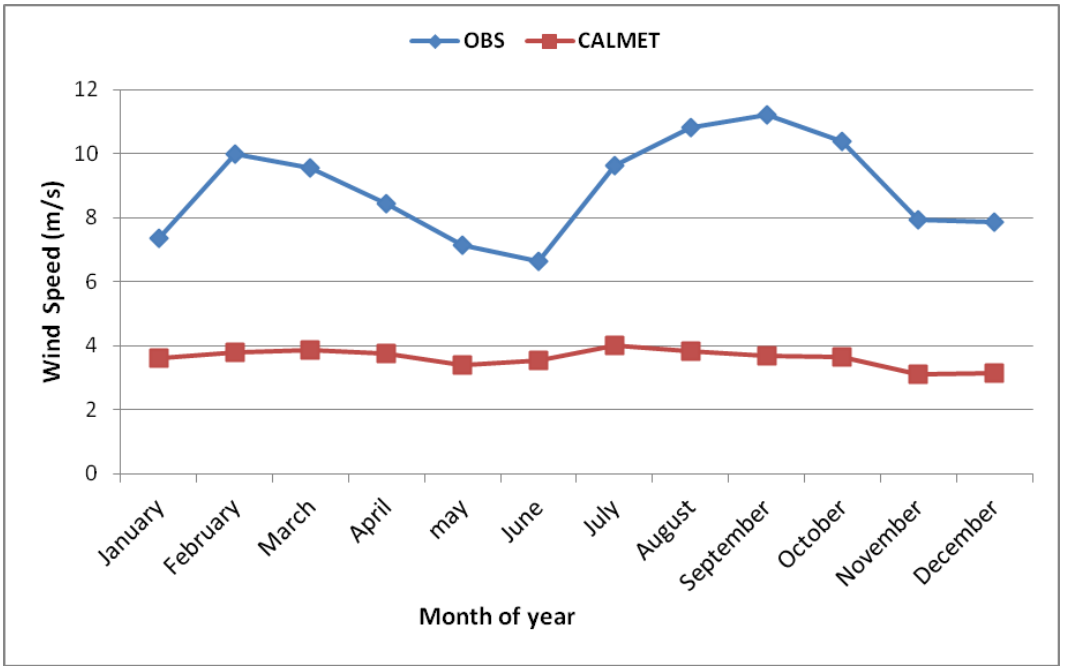


Figure 4.33: Plots of Modelled and Observed(AMS) Surface Wind Speed for 2009

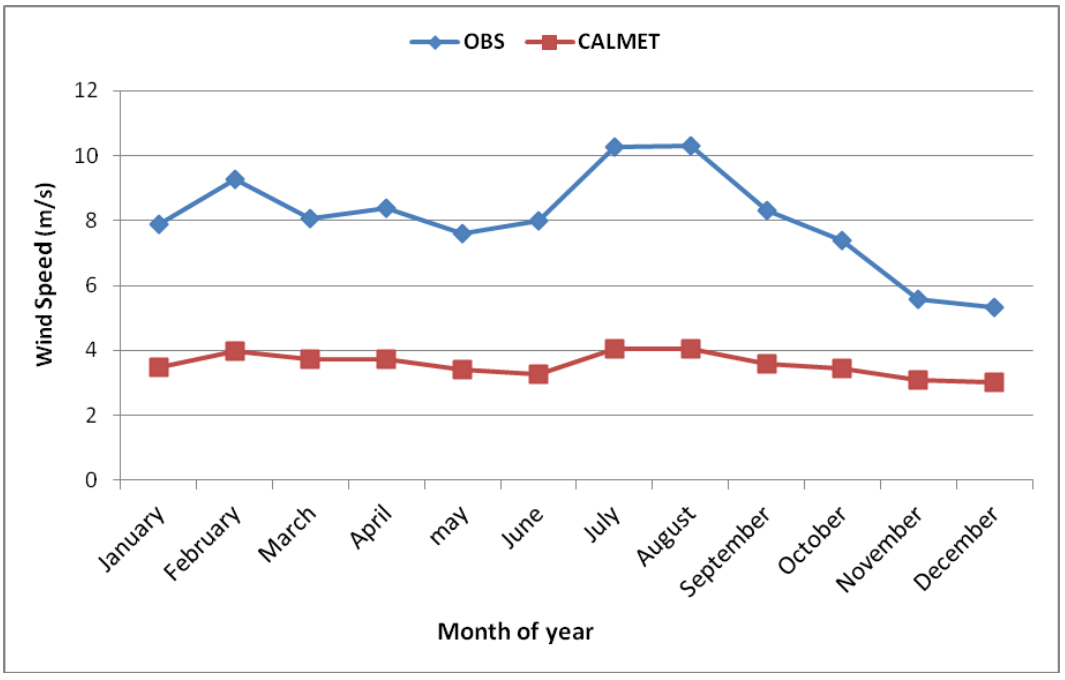


Figure 4.34: Plots of Modelled and Observed(AMS) Surface Wind Speed for 2010

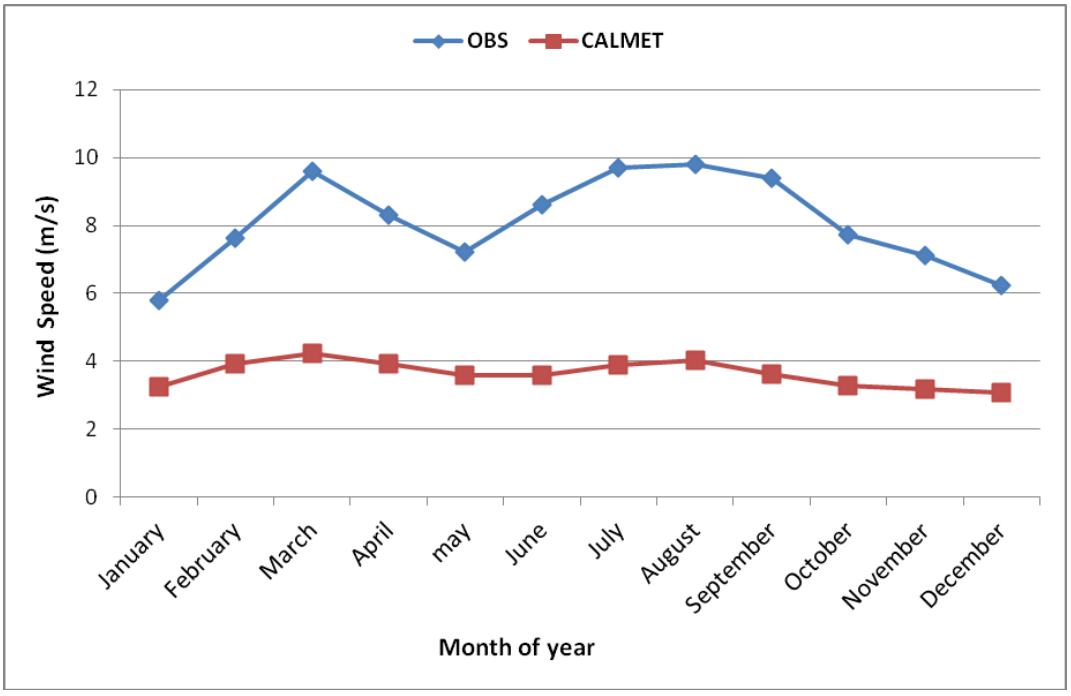


Figure 4.35: Plots of Modelled and Observed(AMS) Surface Wind Speed for 2011

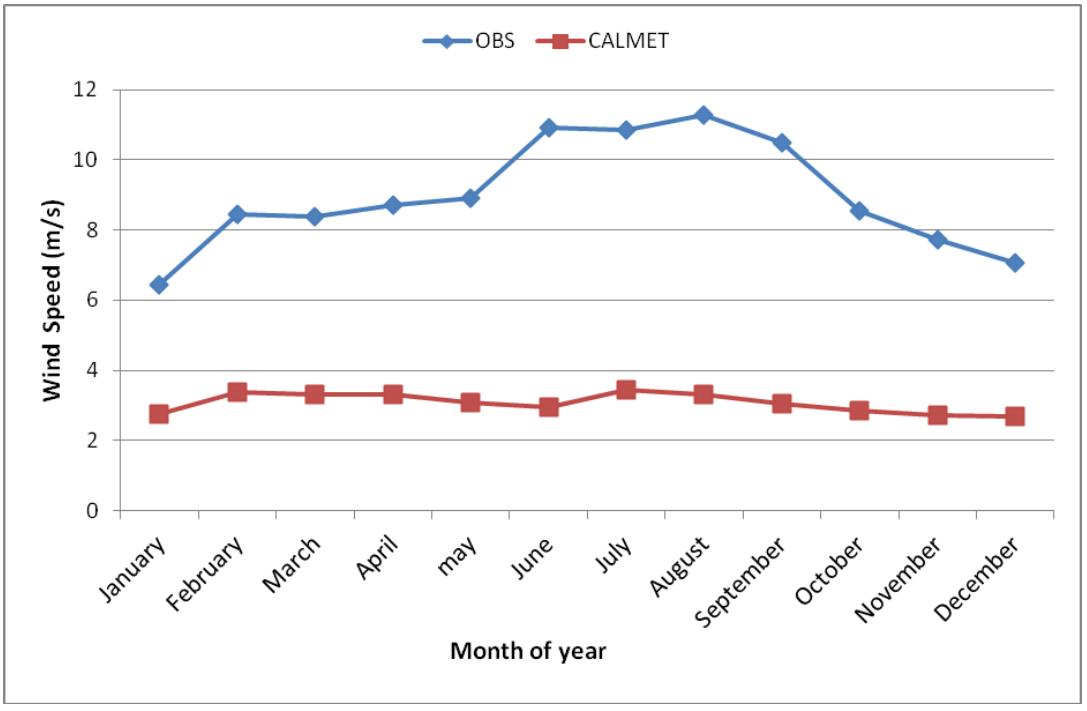


Figure 4.36: Plots of Modelled and Observed(AMS) Surface Wind Speed for 2012

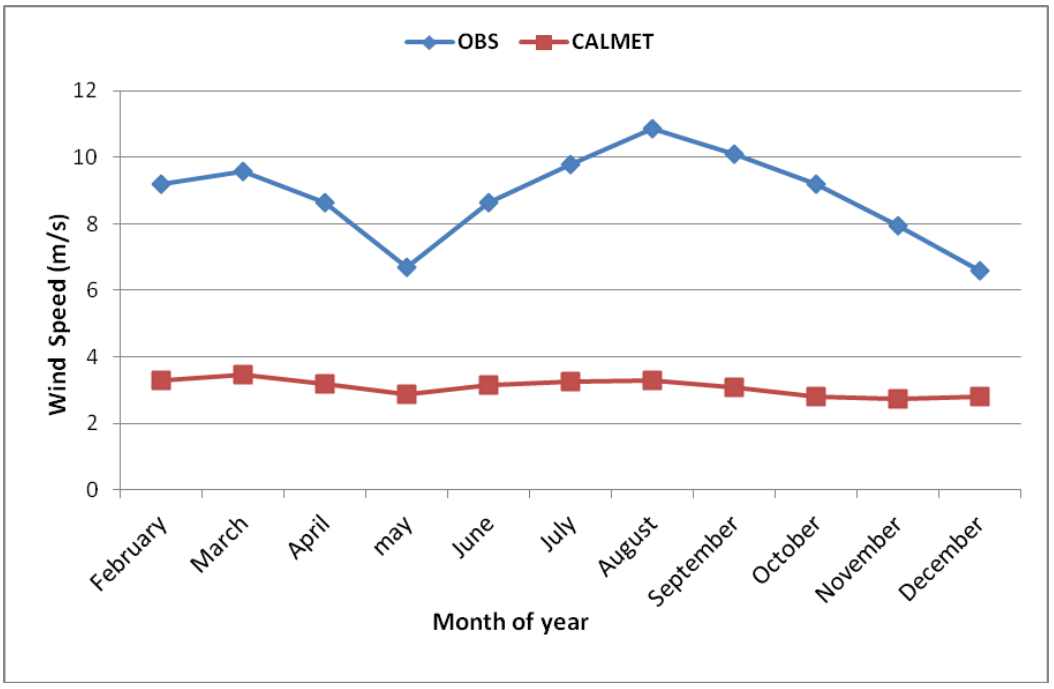


Figure 4.37: Plots of Modelled and Observed(AMS) Surface Wind Speed for 2013

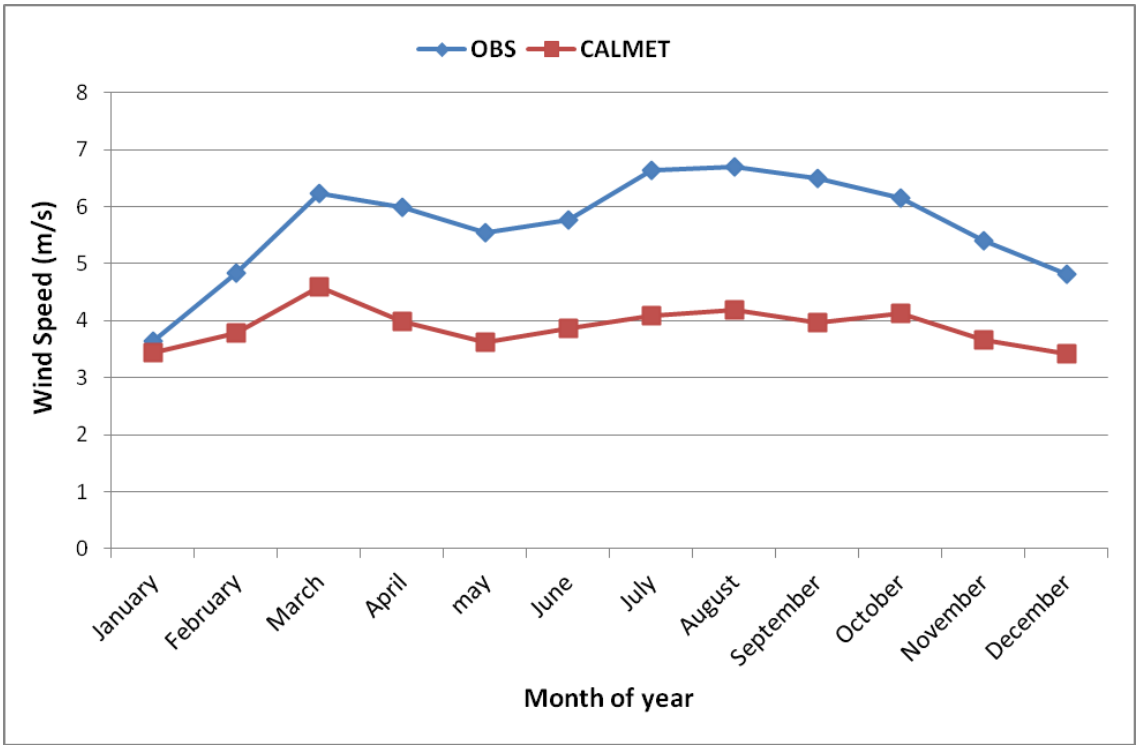


Figure 4.38: Plots of Modelled and Observed(TMS) Surface Wind Speed for 2008

These challenges can be attributed to the quality of the initial winds. The quality of the initial wind fields of the diagnostic model (from WRF) is of vital importance for the resultant wind fields. While CALMET is able to add value to even 5 km WRF fields, a resolution reduction of WRF to 10 km grid spacing induces errors with respect to unresolved air flows which CALMET is unable to correct in most cases (Truhetz et al., 2007).

These statistical measures, generally, suggest a good performance of CALMET .

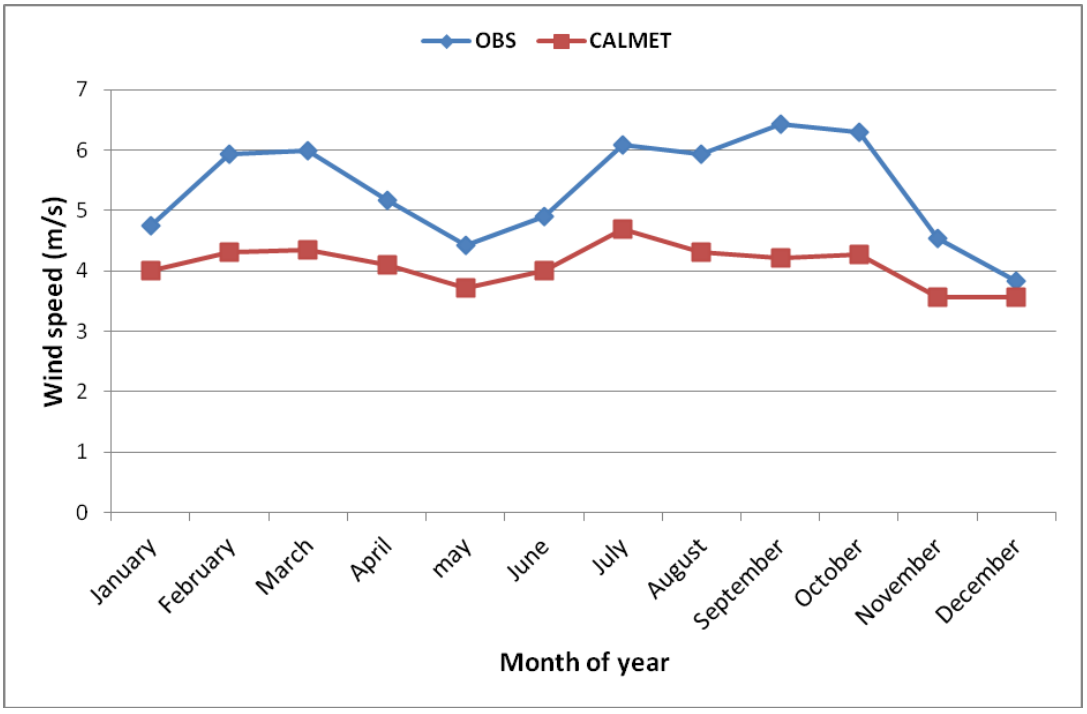


Figure 4.39: Plots of Modelled and Observed(TMS) Surface Wind Speed for 2009

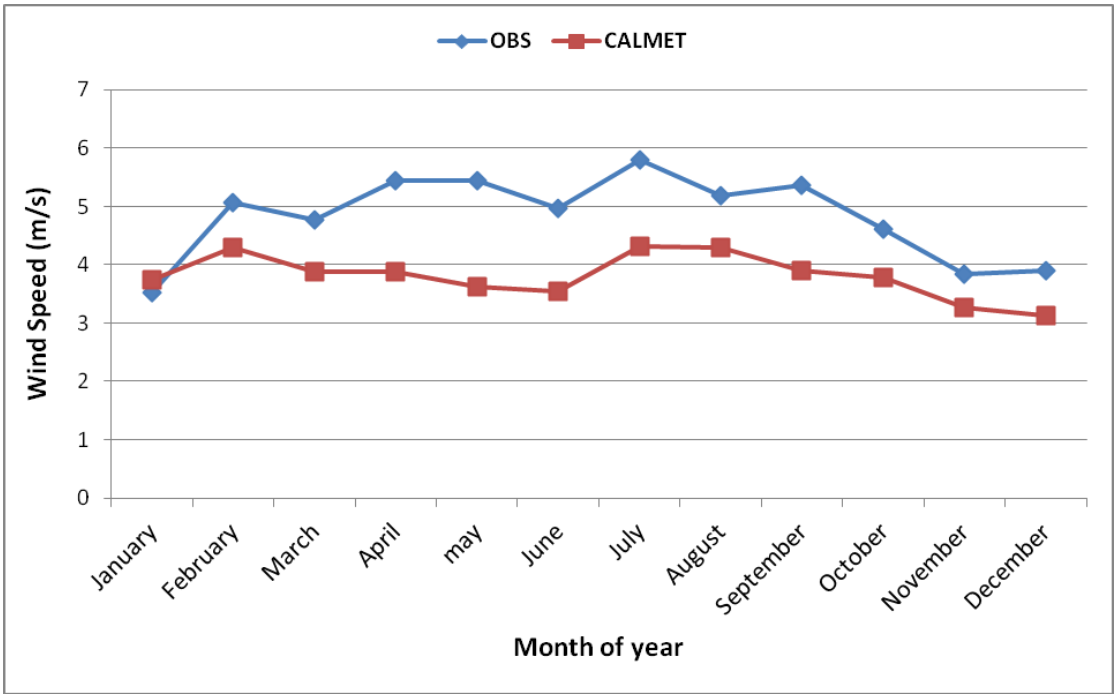


Figure 4.40: Plots of Modelled and Observed(TMS) Surface Wind Speed for 2010

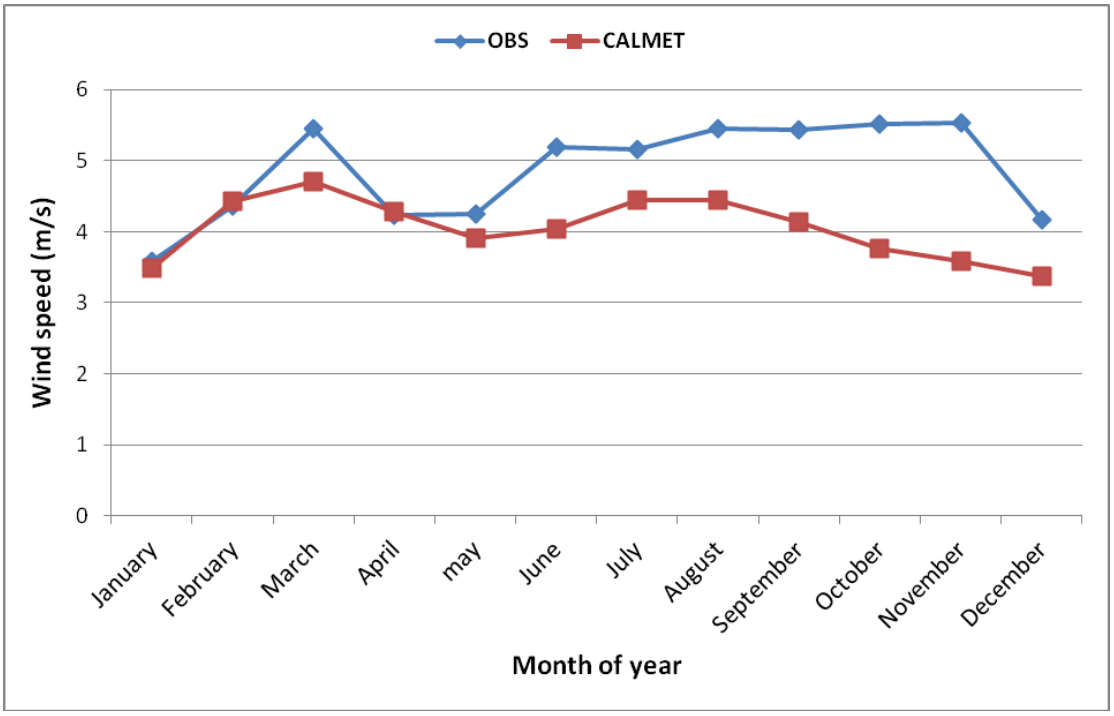


Figure 4.41: Plots of Modelled and Observed(TMS) Surface Wind Speed for 2011

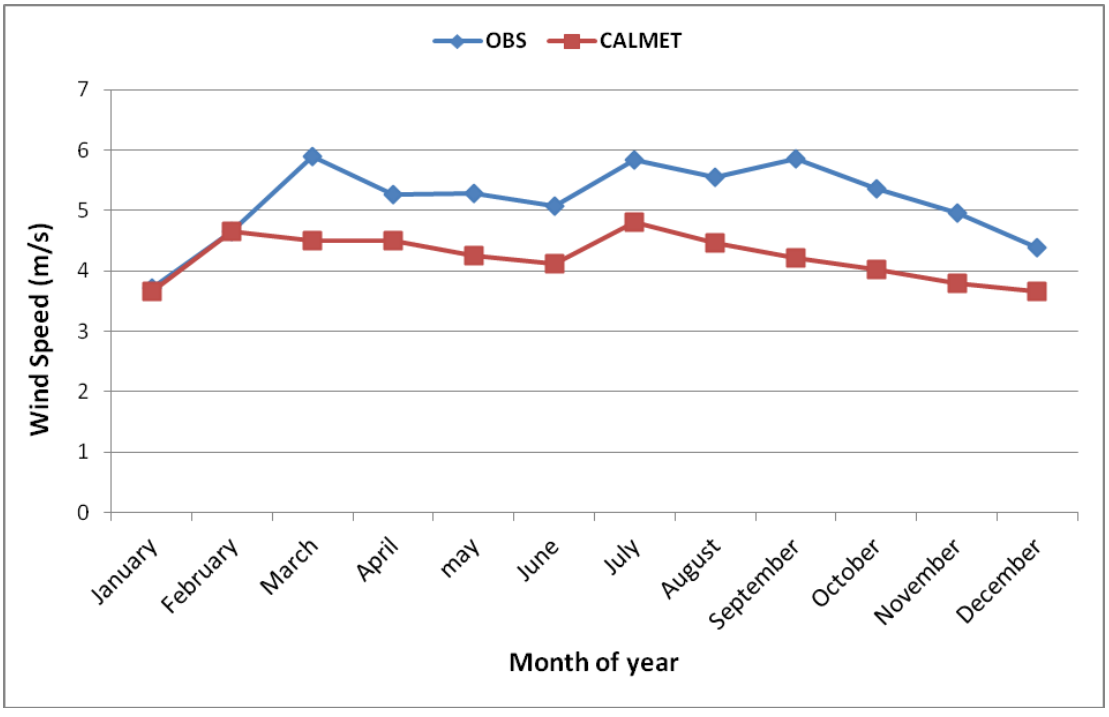


Figure 4.42: Plots of Modelled and Observed(TMS) Surface Wind Speed for 2012

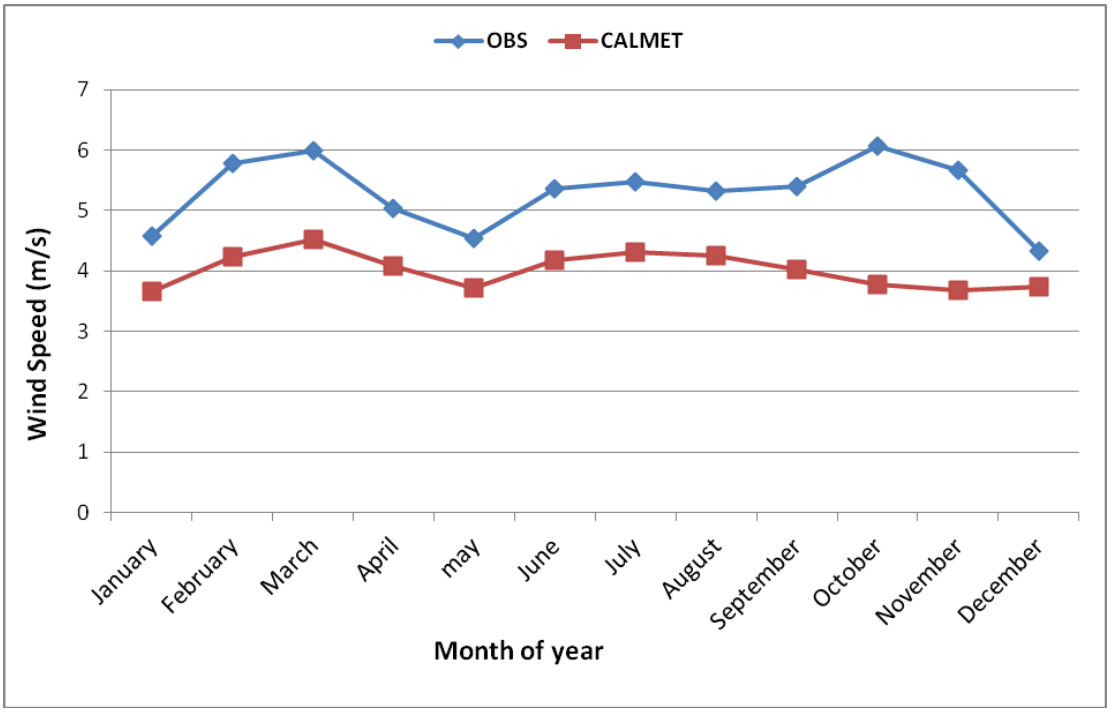


Figure 4.43: Plots of Modelled and Observed(TMS) Surface Wind Speed for 2013

## 4.6 Spatial Distribution of Emissions

Concentrations contours of annual averages of the modelled emissions for the 6-year period are presented in Figs.4.44 - 4.46. The plots reflect the spread of the pollutants and also shows the likely wind direction prevalent in the study area for 2008. The spread of the $SO_2$ plume is larger due to its high diffusivity and low density compared with $NO_2$ and $PM_{2.5}$. Consequently, it impacts a larger part of the study area with maximum contours of 610 $\mu g/m^3$ near the souce of emission and minimum contours of 10 $\mu g/m^3$. Due to the predominant south westerly winds of the year

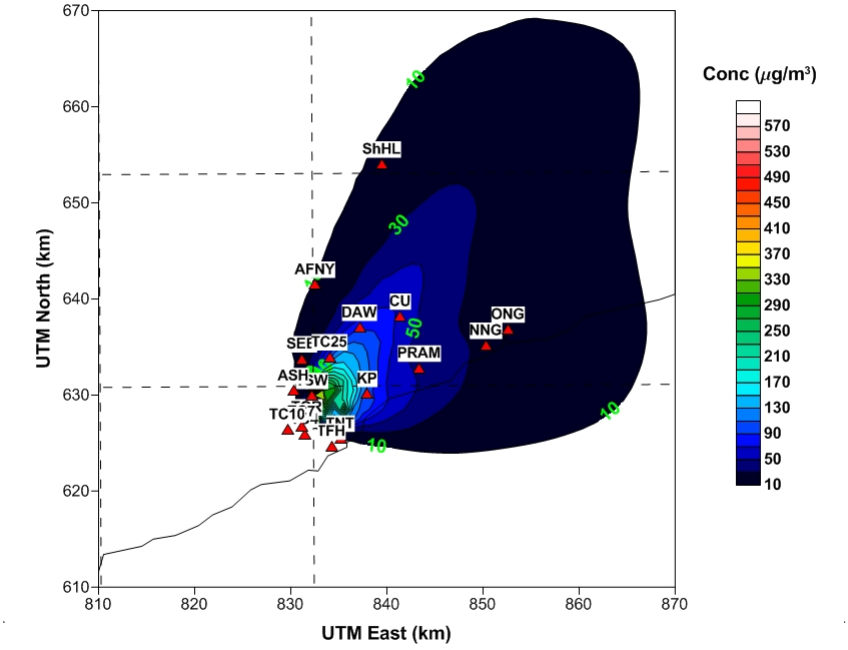


Figure 4.44: 2008 Annual Average Concentration contours of $SO_2$ in the Study Area

(windrose shown earlier), receptors located upwind are the most hit. According to Chan and Kwok (2000), fine and especially ultra-fine particles are expected to disperse in the air like gases. The larger-sized particles, however, are greatly affected by gravity and thus have a shorter residence time in the air. This explains the fairly elevated $PM_{2.5}$ levels.

Even though the emission rates for 2009 is similar to that of 2008, the concentration contours of pollutants are lower with maximum $SO_2$, $NO_2$ and $PM_{2.5}$ contours of 75 $\mu g/m^3$, 72 $\mu g/m^3$ and 62 $\mu g/m^3$ respectively as shown in Figs.4.47, 4.48 and 4.49 respectively. Since emission rates are assumed to be constant, the differences could be attributed mainly to

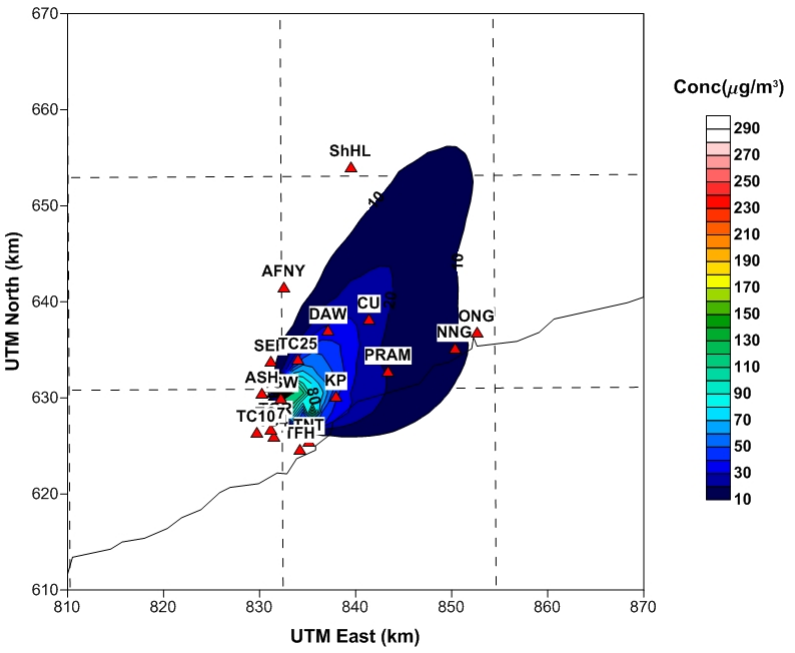


Figure 4.45: 2008 Annual Average Concentration contours of $NO_2$ in the Study Area

meteorological conditions. The wind rose for 2009 is shown in Fig.4.50. The predominant south westerly winds of the year represent 90% of total winds. Wind speed class of 3.3-5.4 m/s constitutes 73% followed by 22% of speeds between 5.4 - 8.5 m/s and 3% of total winds falling into class 1.8 - 3.3 m/s . Total calm winds are nil. A comparison of wind roses for 2009 and 2008 shows that the average wind speed was higher in 2009 than in 2008. Strong winds tend to increase pollutant mixing and dispersion and hence decreasing ground level concentrations. The year 2008 experienced more low wind speeds and calm periods. This meteorological condition favours increased ground level concentrations of pollutants as evidenced by the 2008 contour plots. Low synoptic winds create a well-known meteorological

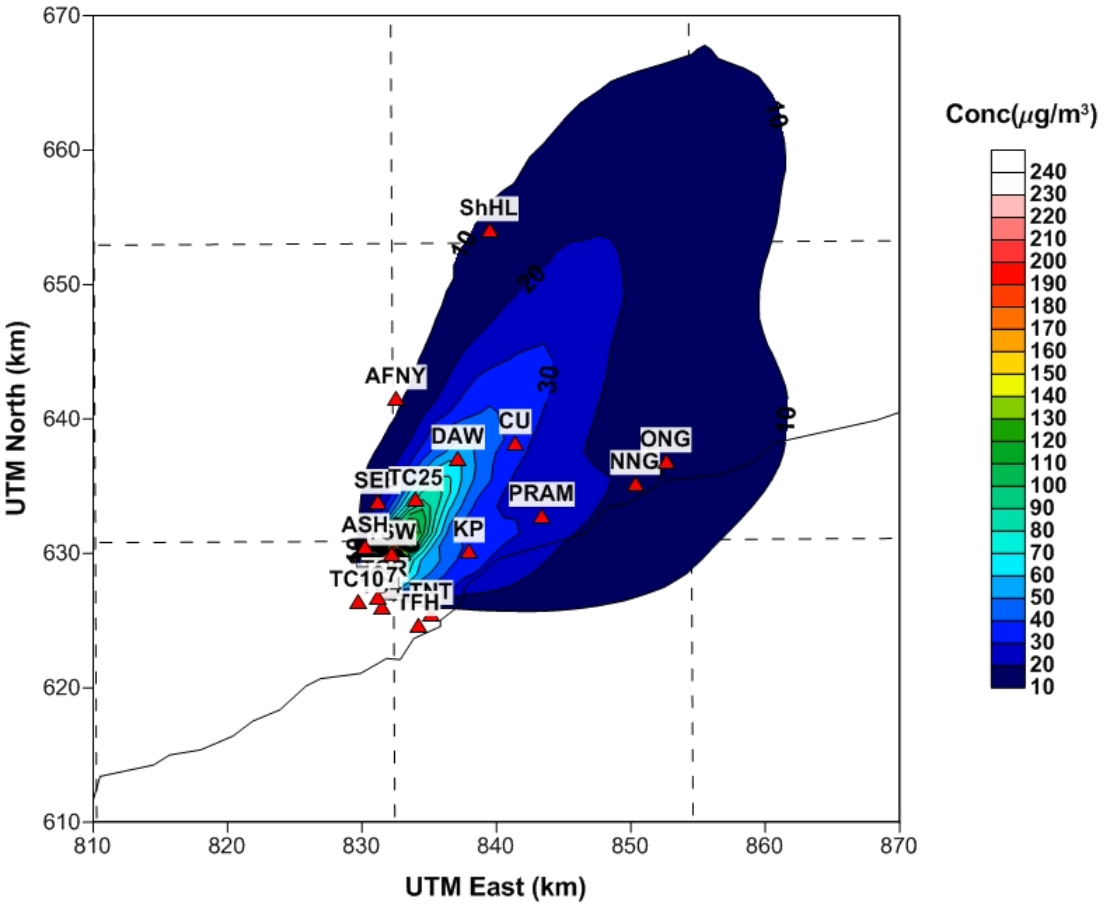


Figure 4.46: 2008 Annual Average Concentration contours of $PM_{2.5}$ in the Study Area

situation that favours air pollution built-up in urban areas (Jones et al., 2000, Qin and Kot, 1993).

Figs.4.51 - 4.53 present concentration contours of the pollutants for 2010 with its accompanying wind rose in Fig. 4.54. Emission rate of the pollutants for 2010 was the highest. However, the positive influence of the prevailing winds for the year was seen in the generally low concentrations similar to those in 2009. The statistics of the 2010 surface winds are quite

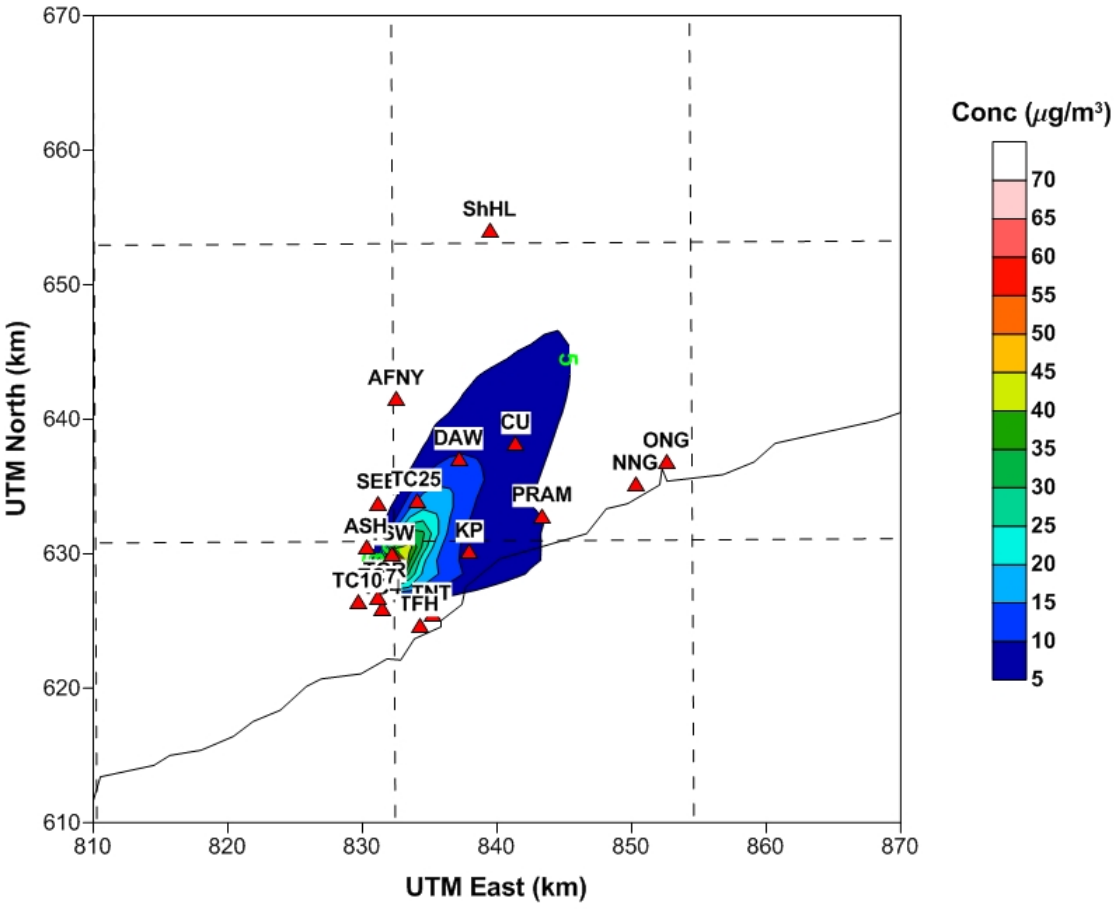


Figure 4.47: 2009 Annual Average Concentration contours of $SO_2$ in the Study Area

similar with 2009 winds.

Concentration contours for the remaining years and their corresponding windroses are shown by Figs. 4.55 - 4.66.

It can be seen from Fig. 4.58, Fig.4.62 and Fig. 4.66 that the percentage of the upper wind speed class, 5.4 - 8.5 m/s, of total winds decreased giving rise to an increase in low speed percentages. Infact, 2013 recorded a low

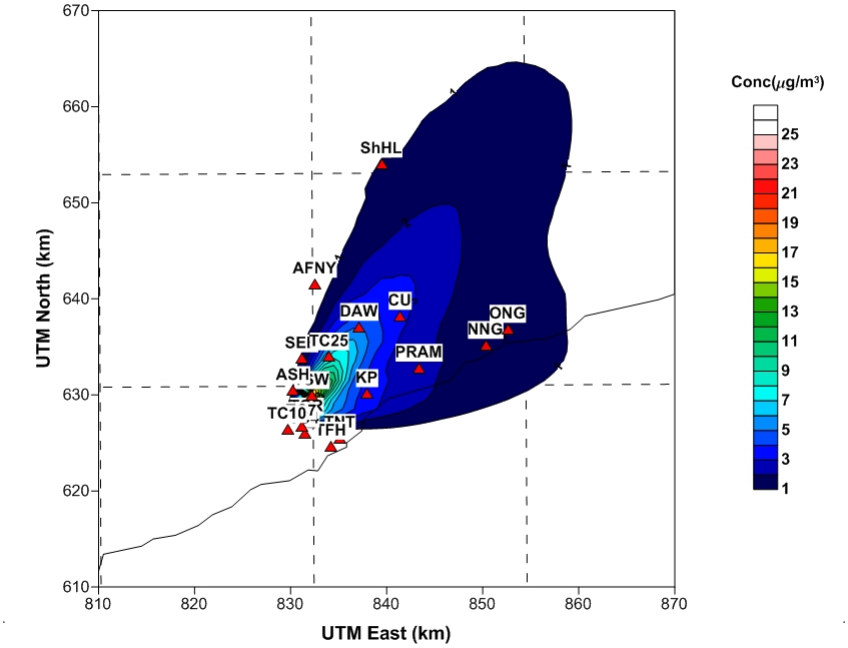


Figure 4.48: 2009 Annual Average Concentration contours of $NO_2$ in the Study Area

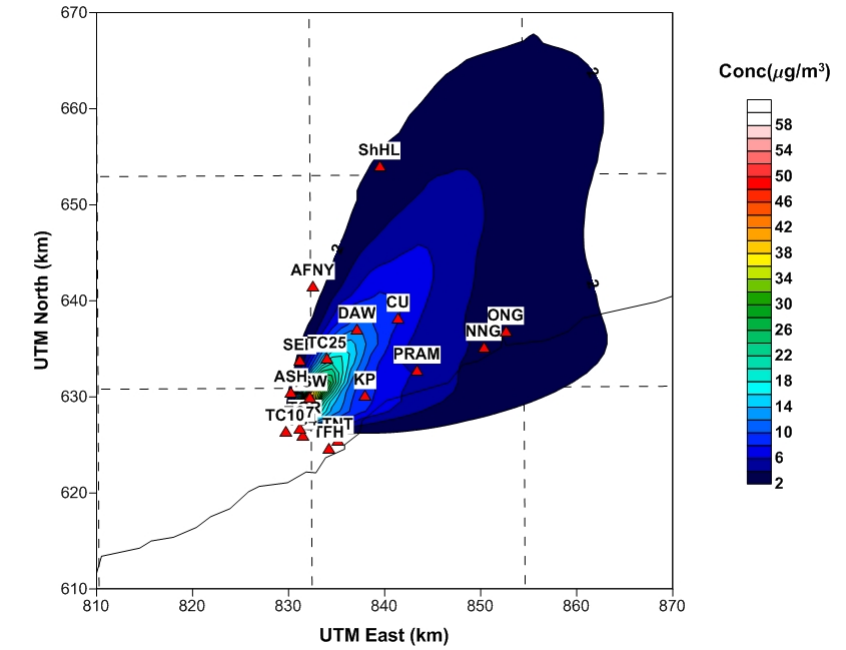


Figure 4.49: 2009 Annual Average Concentration contours of $PM_{2.5}$ in the Study Area

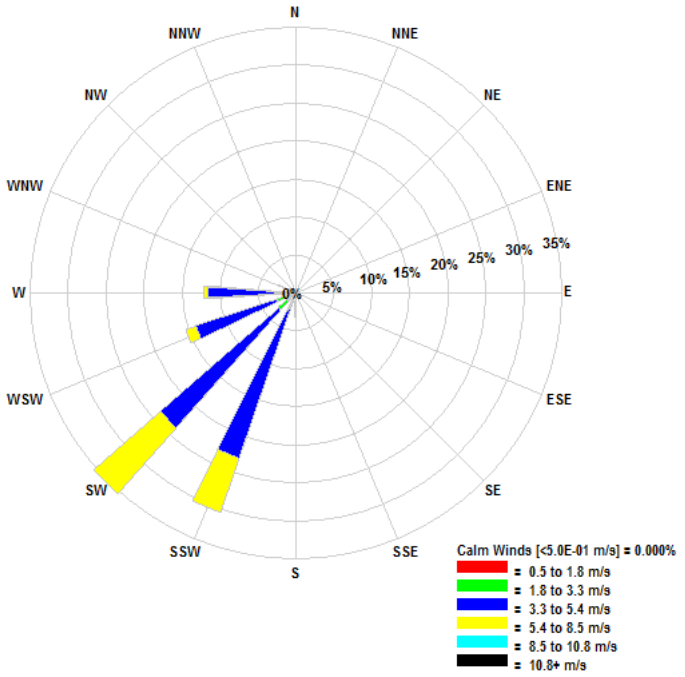


Figure 4.50: Wind Rose Depicting 2009 Surface Winds in the Study area

speed class (1.8 - 33) m/s of about 18%. Low wind speed conditions are typically associated with the worst air pollution episodes in cities (Di Sabatino et al., 2003). Therefore, predicted concentrations at the various receptors should have been higher for 2011 - 2013. This, however, was not observed. It should be recalled that emission rates from the refinery saw a steady decline from 2011 to 2013 as a result of shortfalls in crude supply. This is the reason for the low concentration contours observed within the study area.

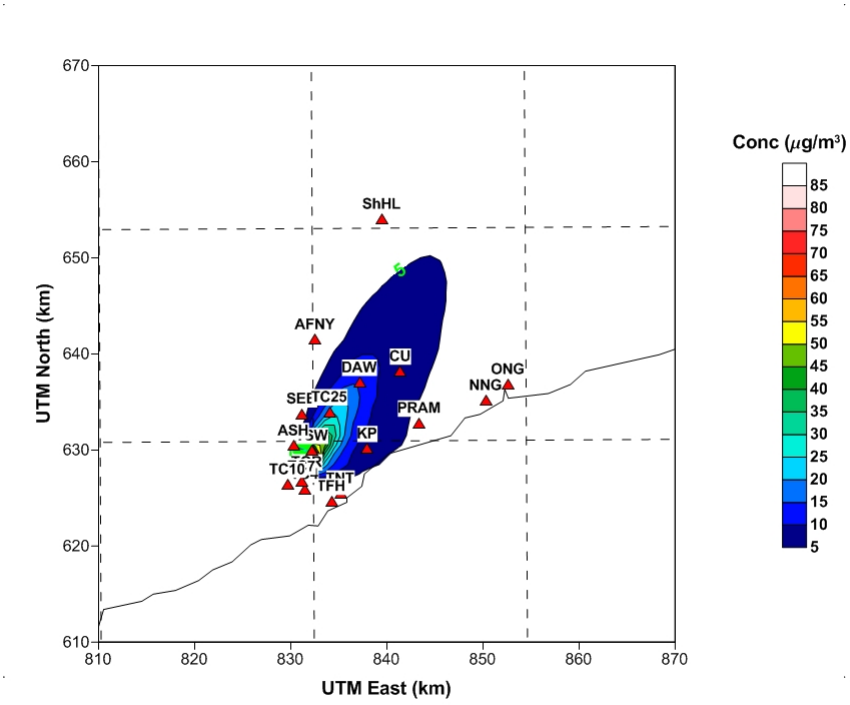


Figure 4.51: 2010 Annual Average Concentration contours of $SO_2$ in the Study Area

## 4.7 Interannual Predicted Concentrations of Emissions at Receptors

As was mentioned earlier in this chapter, receptors located within 10 - 15 km of the refinery are the most impacted by the refinery emissions. For this reason, this subsection takes another look at the annual variations in the modelled daily average pollutant concentrations at these receptors using the different emission rates estimated for the years under consideration. Results of this investigation are presented in Figs. 4.67, 4.68 and 4.69. The plots reflect the year-to-year variability in weather conditions.

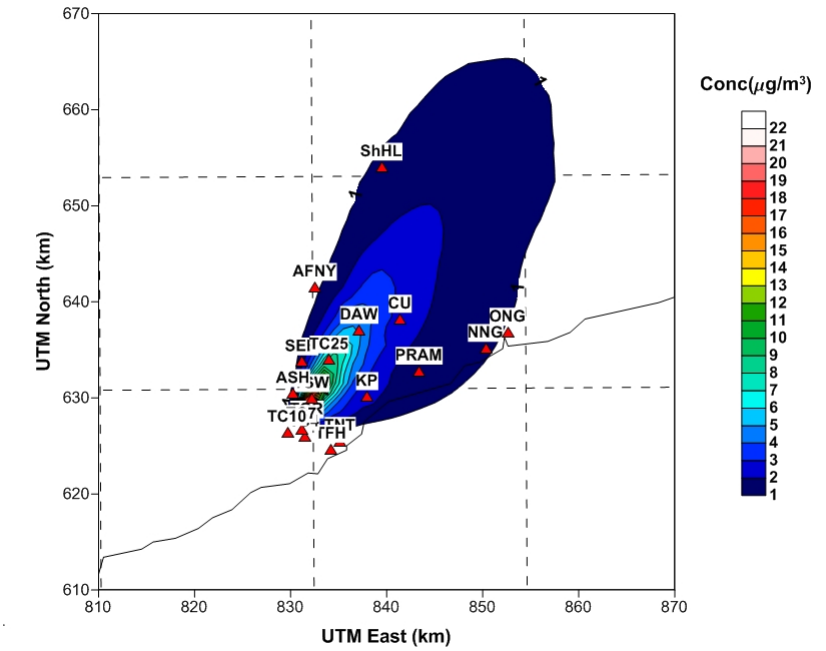


Figure 4.52: 2010 Annual Average Concentration contours of $NO_2$ in the Study Area

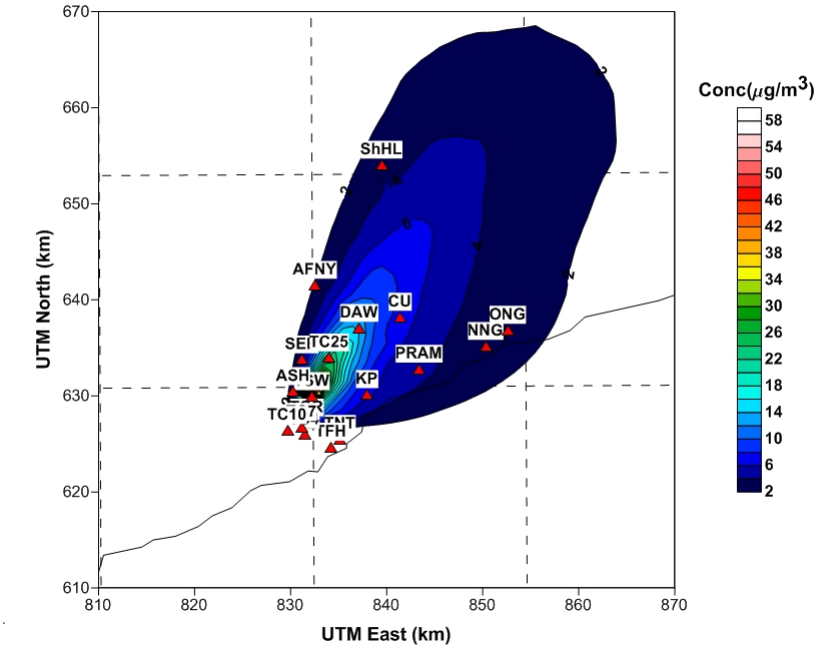


Figure 4.53: 2010 Annual Average Concentration contours of $PM_{2.5}$ in the Study Area

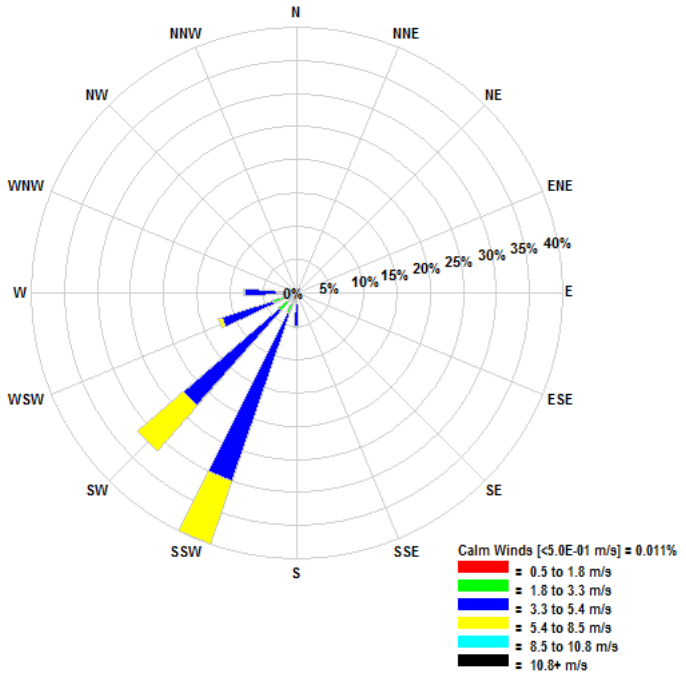


Figure 4.54: Wind Rose Depicting 2010 Surface Winds in the Study area

A look at Fig. 4.67 reveals that the highest daily $SO_2$ concentration occured at Tema Steelworks area followed by Tema Comm 25 for all the years. Concentrations at the Tema Steelworks area for years ranged from about 220 - 280 $\mu g/m^3$ with 2010 concentrations being the highest. Concentrations at Tema Comm 25 ranged between 60 - 100 $\mu g/m^3$ with the highest occuring in 2010. Other receptors recording concentrations above 50 $\mu g/m^3$ are Ashiaman and Sebrepor. The other receptors showed concentrations lower than 50 $\mu g/m^3$ except the Tema General Hospital which recorded about 70 $\mu g/m^3$ in 2013. Comparing these concentration values with WHO daily average guideline of 125 $\mu g/m^3$ for $SO_2$ (WHO (2000)), it is obvious that

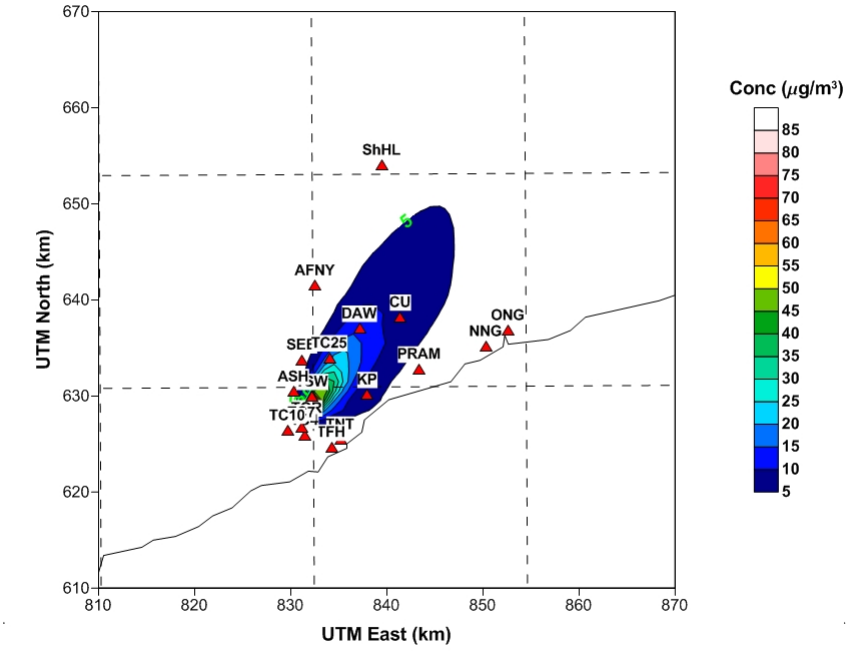


Figure 4.55: 2011 Annual Average Concentration contours of $SO_2$ in the Study Area

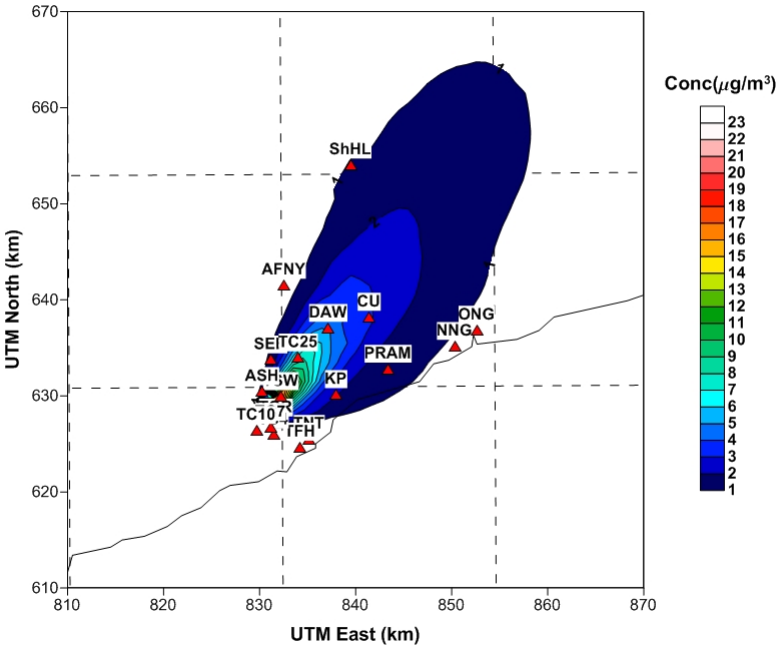


Figure 4.56: 2011 Annual Average Concentration contours of $NO_2$ in the Study Area

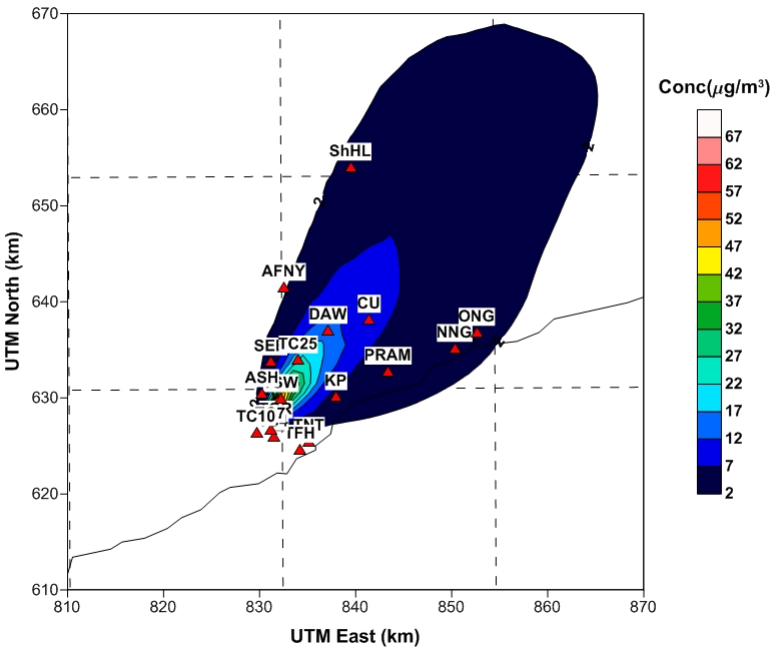


Figure 4.57: 2011 Annual Average Concentration contours of $PM_{2.5}$ in the Study Area

concentrations at the Tema Steelworks area well exceeded the regulatory limit. These concentrations also exceeded the Ghana EPA guideline values of 150 $\mu g/m^3$ for industrial areas and 100 $\mu g/m^3$ for residential areas.

From Fig. 4.68, maximum $NO_2$ concentration of about 78 $\mu g/m^3$ occured again at the Tema Steelworks after which TOR, Tema Comm 25 and Tema General Hospital follow. A comparison of the concentrations at the receptors with the WHO guideline value for $NO_2$ (50 $\mu g/m^3$) and the Ghana EPA values of 60 $\mu g/m^3$ for residential and 150 $\mu g/m^3$ for industrial areas, it can be concluded concentrations fall below these regulatory limits except the Tema Steelworks area. As far as the Ghana guideline values are concerned, the conclusion can be made that the refinery is not polluting the

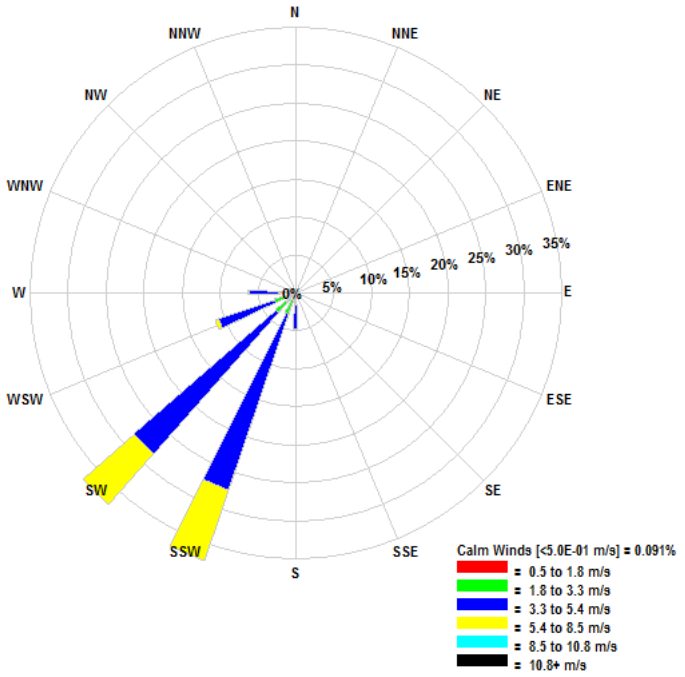


Figure 4.58: Wind Rose Depicting 2011 Surface Winds in the Study area

environment in respect of $NO_2$.

Since Ghana does not have $PM_{2.5}$ guideline values, a comparison was made with only the WHO values of 25 $\mu g/m^3$. Apart from Old and New Ningo where concentrations for all the years did not exceed this guideline value, it is quite clear from Fig. 4.69 that $PM_{2.5}$ concentrations at all other receptors exceeded the WHO guideline value. In 2013, for example, the Tema Steelworks area exceeded this value by a factor of 9 in 2013. In 2009, 2010 and 2013, concentrations at Afienya, Shai Hills, Tema Newtown, Tema Comms. 4 and 7, Tema Fishing harbour and Prampam were below

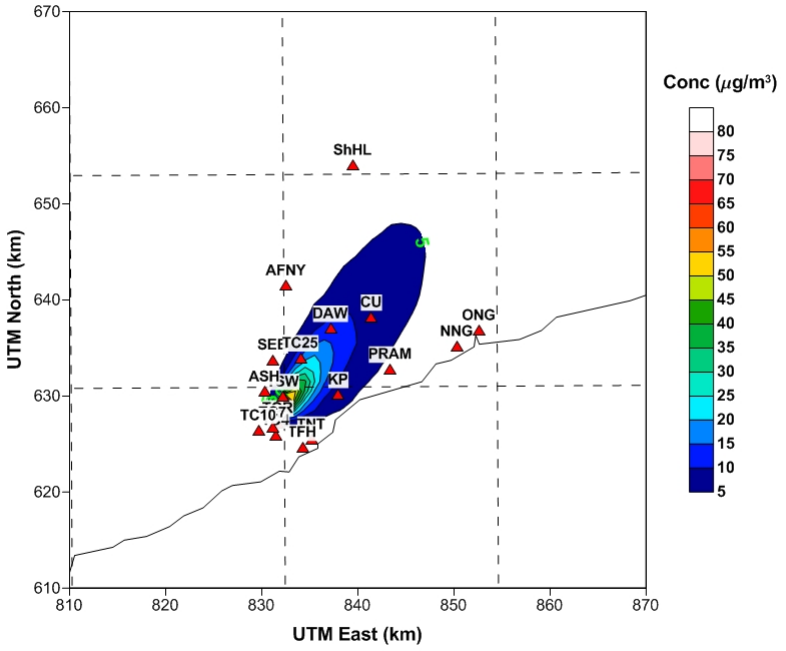


Figure 4.59: 2012 Annual Average Concentration contours of $SO_2$ in the Study Area

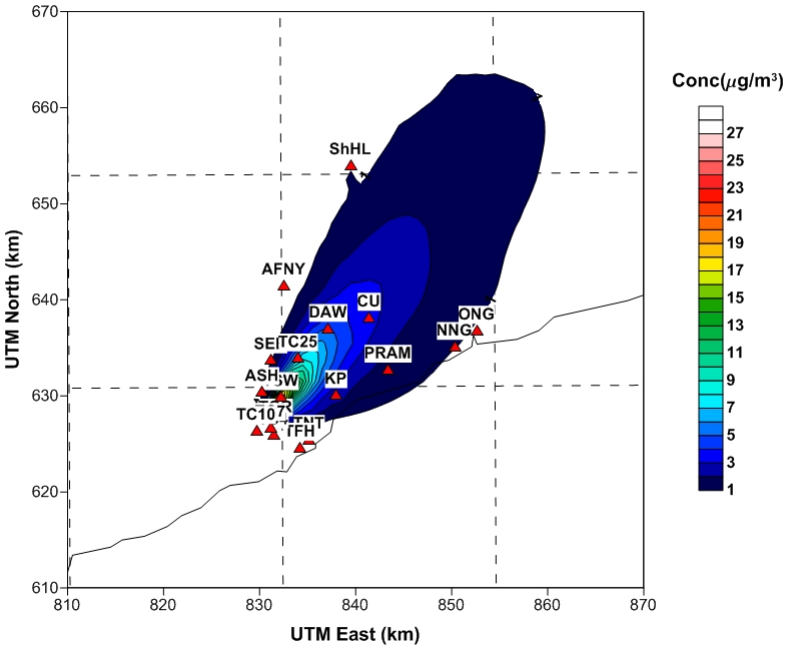


Figure 4.60: 2012 Annual Average Concentration contours of $NO_2$ in the Study Area

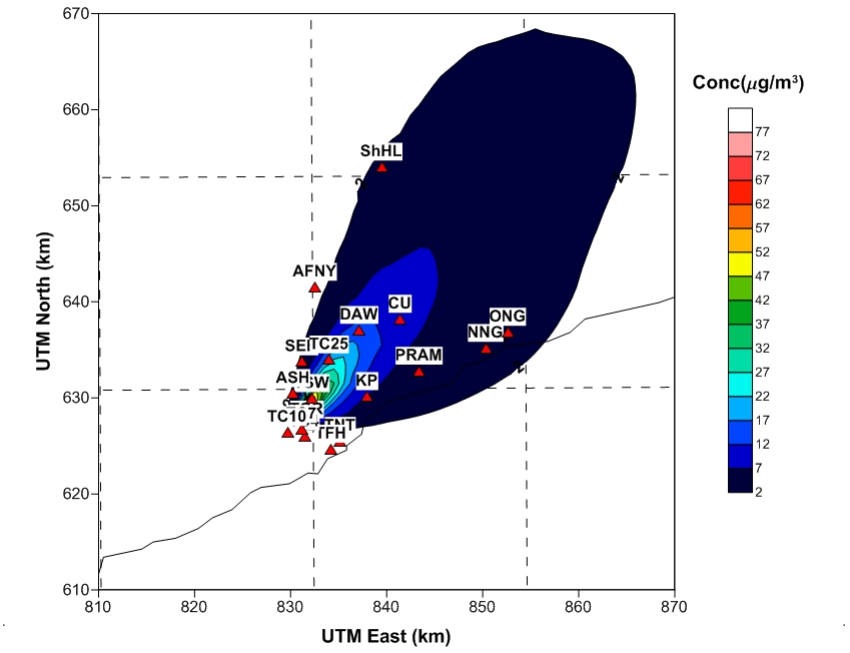


Figure 4.61: 2012 Annual Average Concentration contours of $PM_{2.5}$ in the Study Area

this guideline value. Generally, however, it is quite obvious that $PM_{2.5}$ pollution by the refinery is substantial.

## 4.8 Seasonal Variation of Pollutants

Results of seasonal variability investigations are presented in monthly average concentration plots of pollutants in 2013 at Tema Steelworks and Tema Comm. 25, Kpone and the Tema General hospital as seen in Figs. 4.70 - 4.73. Predicted monthly concentrations of the pollutants for the entire year show that highest values occured in August at Tema Steelworks and Tema Comm 25. At Kpone, highest values occured in October and in December

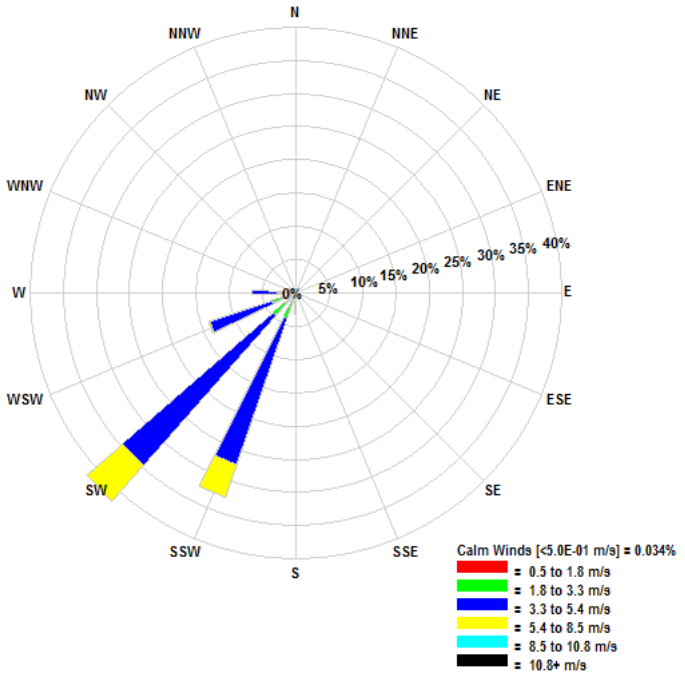


Figure 4.62: Wind Rose Depicting 2012 Surface Winds in the Study area

at the hospital. Further, it can be seen that, generally, the second half of the year during which the dry season occurs, shows slightly higher concentrations than the first half. The major wet season in the first half of the year (April-June) could be responsible for the lower concentrations of the pollutants. The effect of precipitation on atmospheric pollutants are well researched (Aleksandropoulou and Lazaridis, 2004, Davies, 1976, Pandey et al., 1992, Ravindra et al., 2003).

A particular factor that can affect pollutant distribution is the type of stability condition which is a function of temperature. During the dry and warmer months of January, February and March, the atmosphere is more

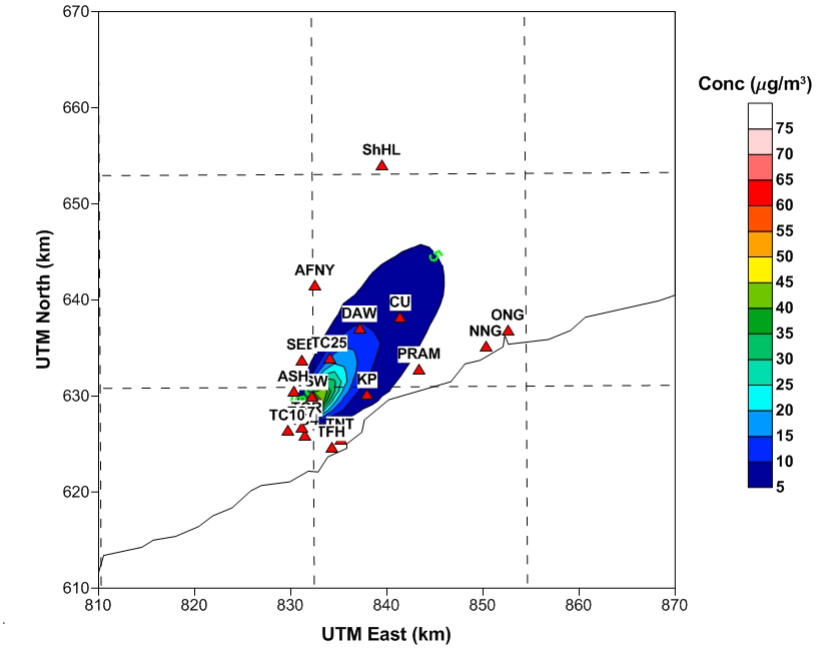


Figure 4.63: 2013 Annual Average Concentration contours of $SO_2$ in the Study Area

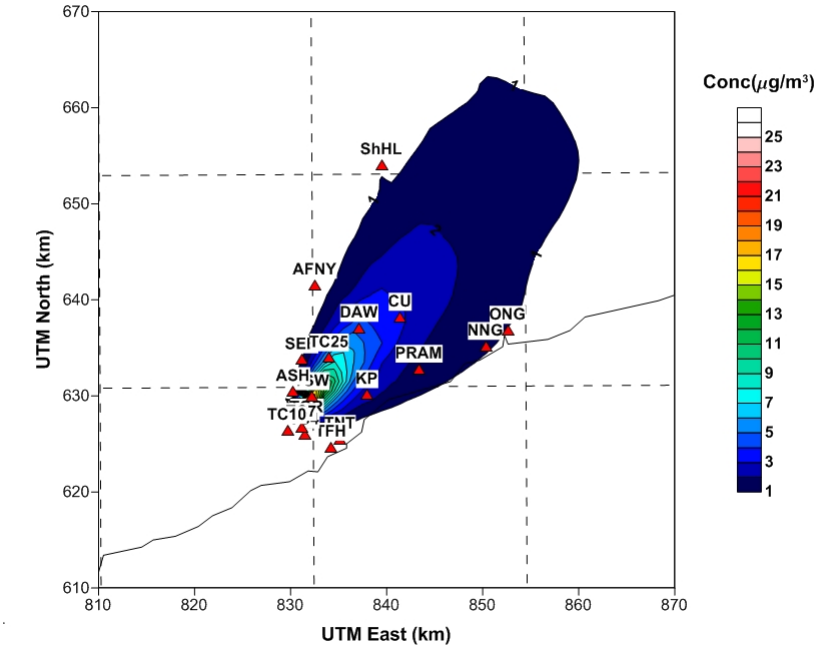


Figure 4.64: 2013 Annual Average Concentration contours of $NO_2$ in the Study Area

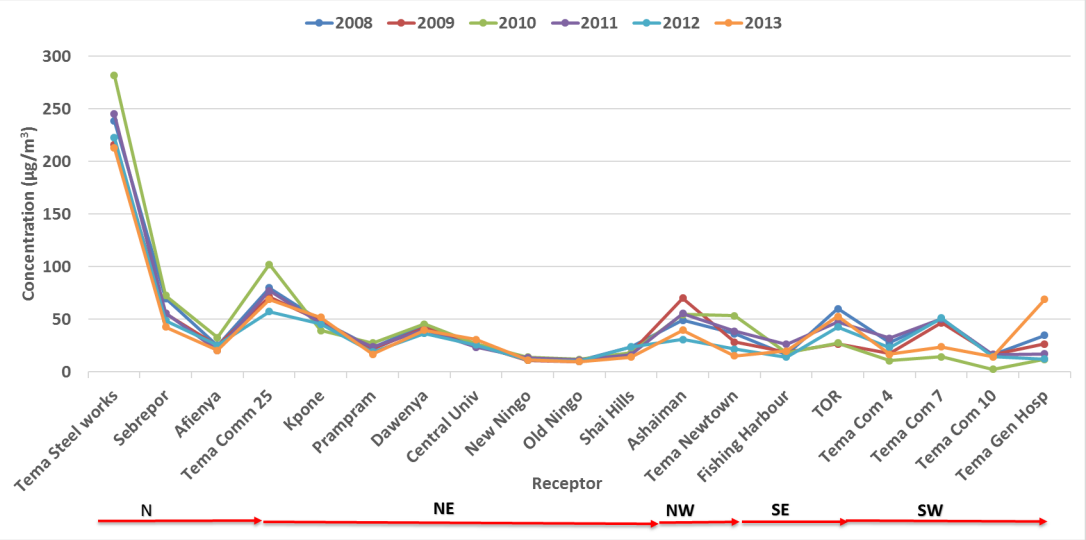


Figure 4.67: Daily Average $SO_2$ Concentrations at various receptors

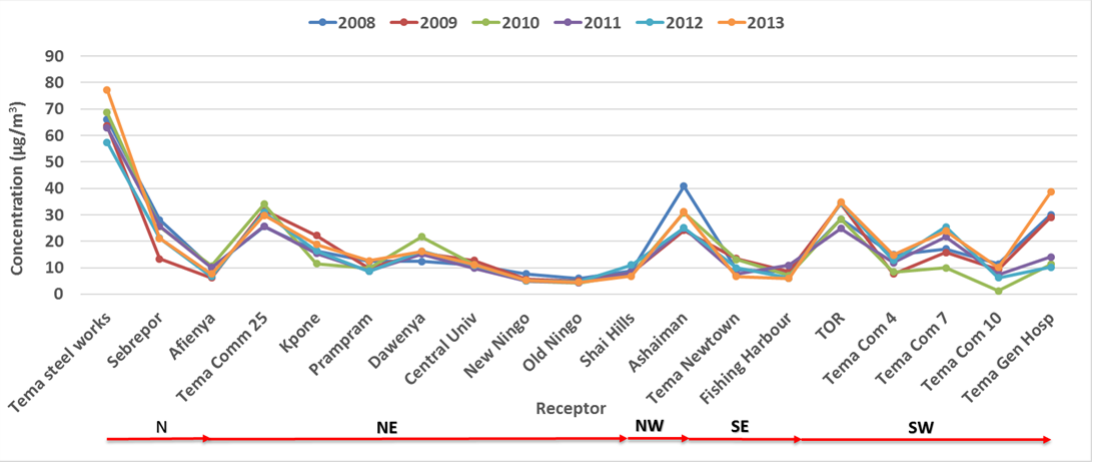


Figure 4.68: Daily Average $NO_2$ Concentrations at various receptors

unstable because of the elevated temperatures. This increases the level of turbulence, which, in turn, increases the dispersive capability of the atmosphere. As a consequence, pollutants disperse relatively rapidly in both the horizontal and vertical directions, and its ground level concentration decays over relatively short distances. The atmosphere is more stable during the cooler months of July and August due to the slightly reduced temperatures

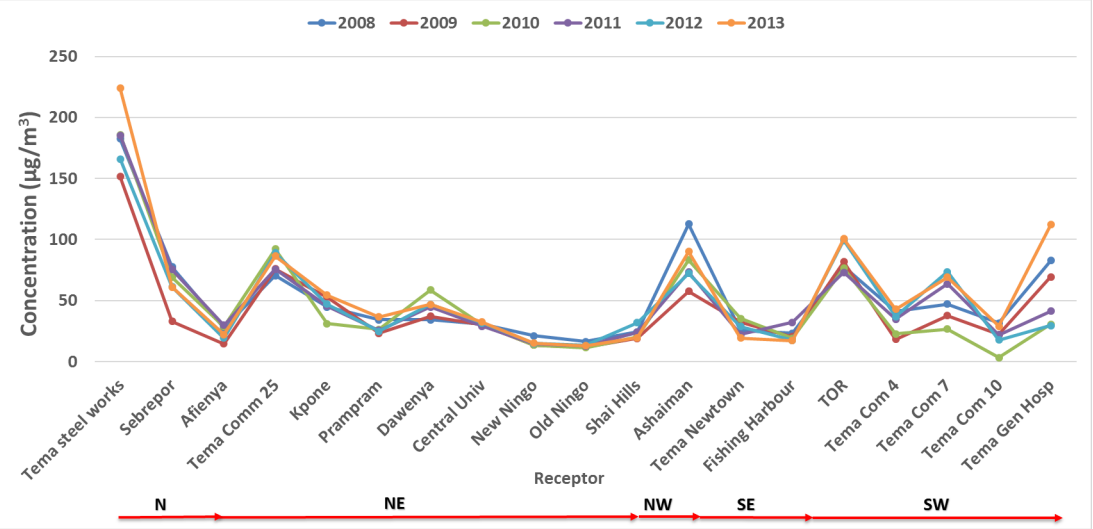


Figure 4.69: Daily Average $PM_{2.5}$ Concentration at various receptors

causing a reduction in the dispersive ability of the atmosphere. As a result, ground level concentrations of pollutants could increase as seen generally in Figs. 4.70 - 4.73. A plot showing the monthly variation of temperature over the years around the refinery is shown in Fig. 4.74.

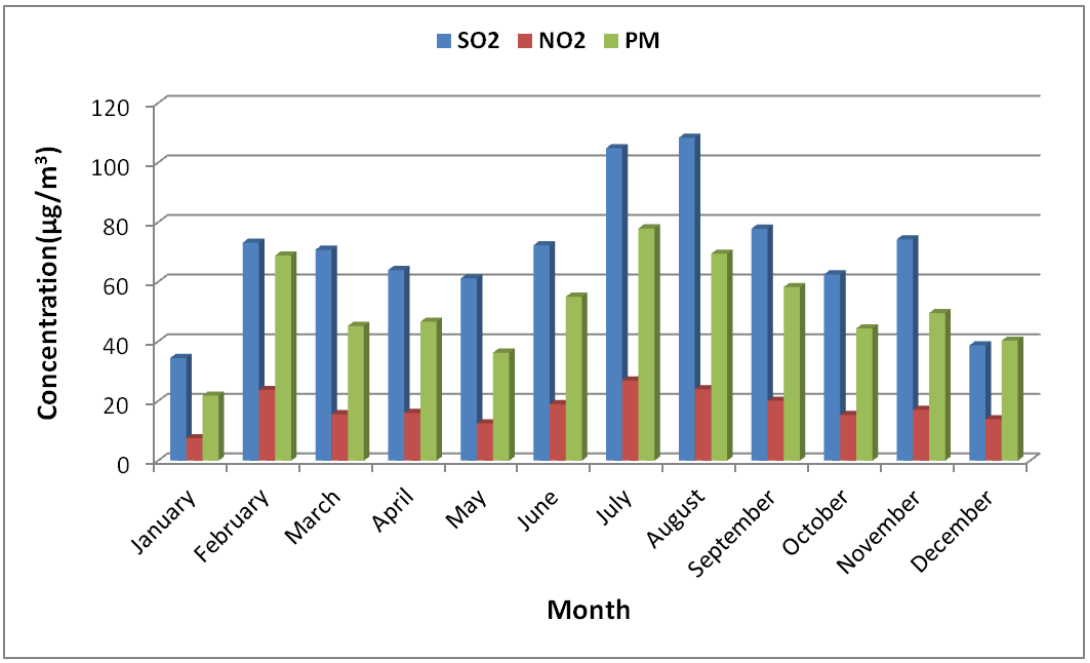


Figure 4.70: 2013 Monthly Average concentrations of pollutants at Tema Steelworks

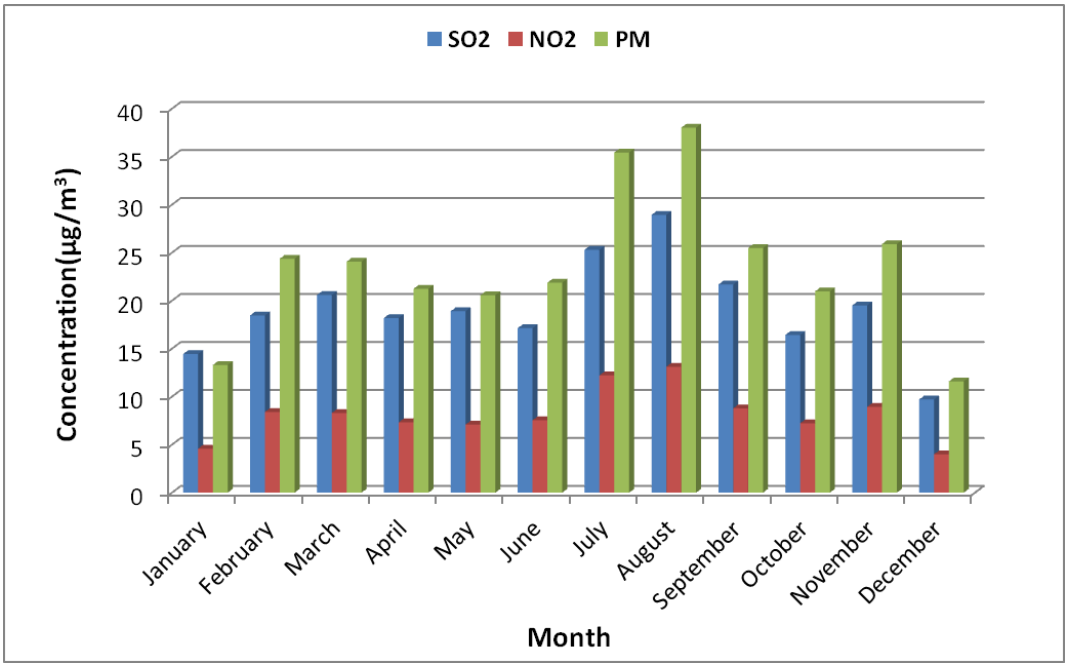


Figure 4.71: 2013 Monthly Average concentrations of pollutants at Tema Comm. 25

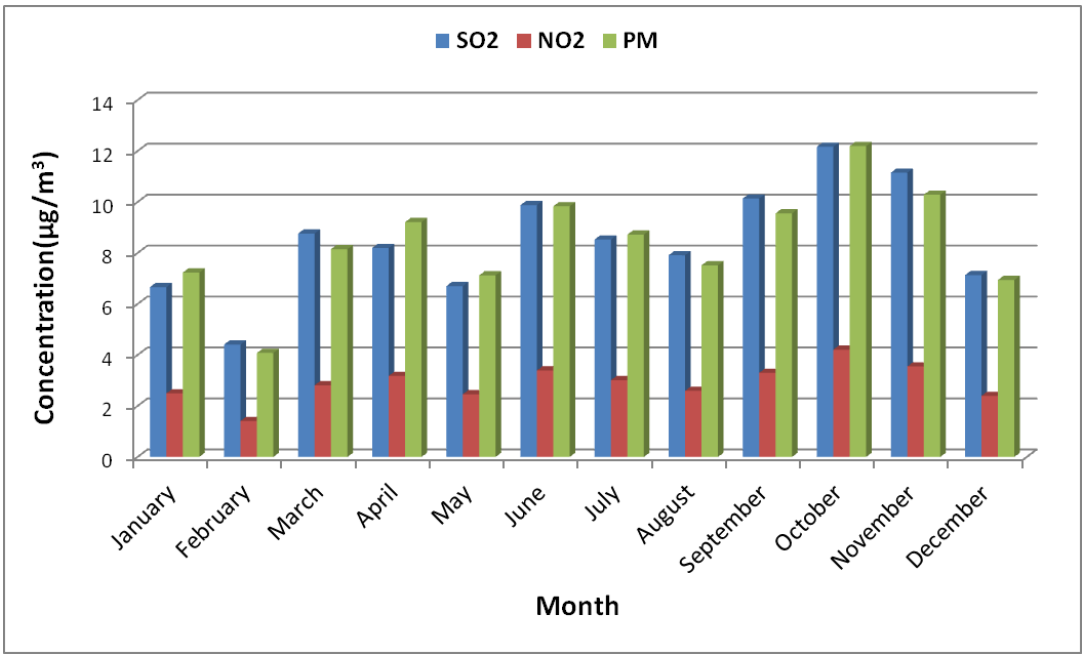


Figure 4.72: 2013 Monthly Average concentrations of pollutants at Kpone

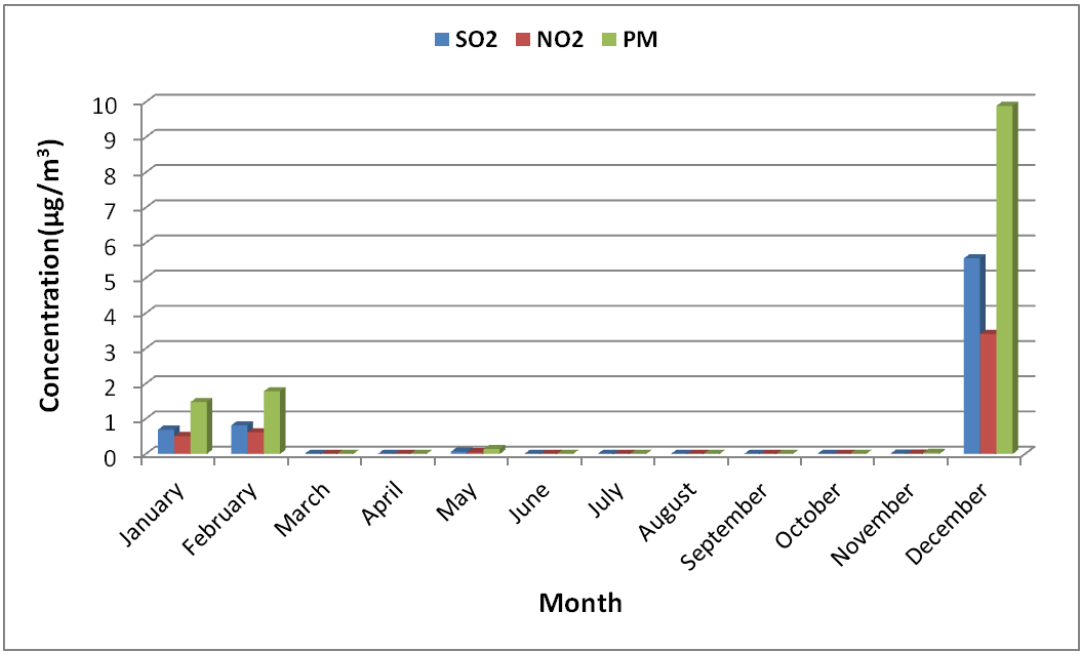


Figure 4.73: 2013 Monthly Average concentrations of pollutants at Tema Gen. Hosp

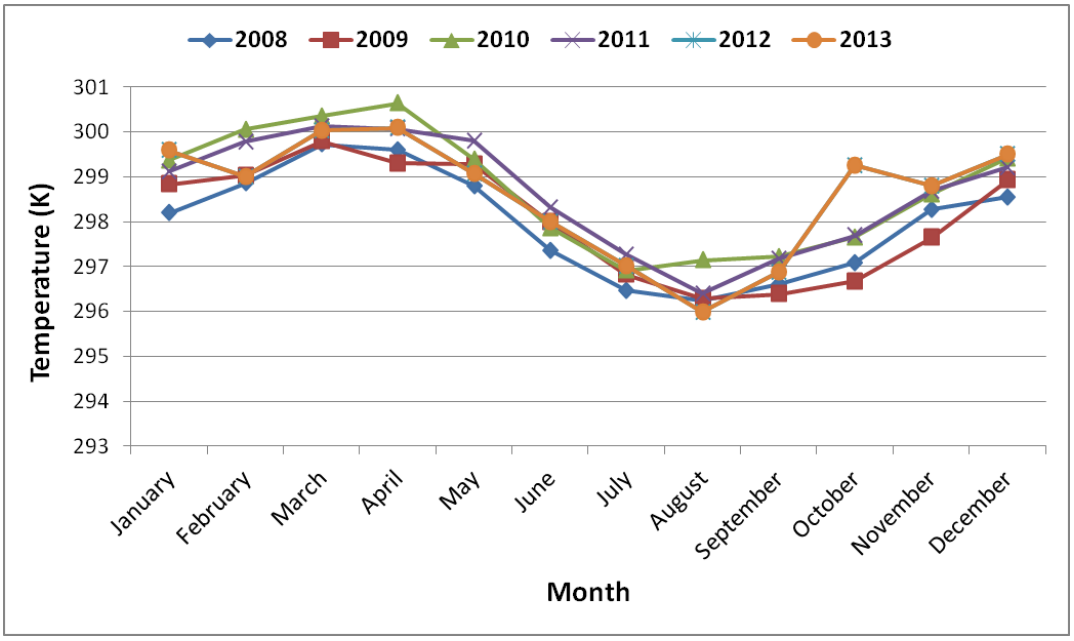


Figure 4.74: Variation of Ambient Temperature around the refinery

# Chapter 5

# Conclusions and Recommendations

## 5.1 Introduction

The overriding purpose of this study was to simulate the dispersion and transport of pollutants emitted during the processing of crude oil by TOR, in the Greater Accra Region of Ghana using the California Puff (CALPUFF) modeling system. To accomplish this goal, it became necessary to reach some prerequisite goals. The importance of air quality models in understanding air pollution and their effects was emphazised during the literature review conducted for this dissertation. Subsequent to this, it was necessary to estimate daily average emission rates from the refinery for the years under review as an important input for CALPUFF. The WRF model was

run to generate the initial meteorological data necessary to initialize CALMET model and to drive the dispersion model, CALPUFF. To validate the CALPUFF modelling system, comparisons were made between some measured and modelled data. Once these prerequisite goals were achieved, the main purpose of the research was realised. This chapter reports the conclusions and recommendations that resulted from this study.

### 5.1.1 Conclusions

The mass balance approach, which was employed to estimate the refinery pollutant emissions revealed that total $CO_2$ emissions were the highest, peaking in 2008 and followed by VOCs. Particulate matter rates were observed to be fairly constant over the years under review. The $SO_2$ and $NO_2$ emission rates were next with $NO_2$ being the least. A steady decline in emissions was observed over the years as a result of the reduction in production due to the frequent shortfalls in the refinery's crude oil supply consequently leading virtually to a halt in refinery operations in 2014 preceded by intermittent shutdowns.

To determine the radius of impact of the refinery emissions, the dispersion of $SO_2$, $NO_2$ and PM was modelled over a space of 60 $km^2$ centred nearly around the refinery was carried out. Within this space, receptor locations representing residential and health facilities, schools and industries were

identified and the maximum daily average concentrations of the pollutants at these location calculated using the CALPUFF. Meteorological data used to drive CALMET, the meteorological model, was generated by running WRF. It was concluded, based on the preliminary simulation results, that the impact of the refinery emissions was felt at receptor locations within a radius of about 20 km around the refinery. Furthermore, receptors located on the north and north-eastern parts of the refinery showed relatively higher pollutant concentrations than other parts of the study domain as a result of the predominant south-westerly winds in the study area. Conversely, south-western receptors were the least impacted by refinery emissions. A check with ambient pollutant guidelines of WHO and EPA Ghana showed that the concentrations of $SO_2$ and $NO_2$ at 36 receptors did not exceed regulatory limits. Two receptors, however, exceeded regulatory limits. Ground level concentrations of PM, however, exceeded the regulatory limits at almost all receptors.

In order to validate the modelling system, results of the meteorological and dispersion simulation were compared with measurements and observations using statistical measures. The statistical measures revealed a good agreement between model and observations leading to the conclusion that CALPUFF can be used satisfactorily for air pollution studies and for checking compliance of industrial set-ups with standards.

It should be highlighted that the utilization of CALPUFF for the simulation of dispersion of refinery emissions and for the description of air quality issues over the Tema Metropolitan Area and parts of the Accra Metropolitan area represents a useful instrument that may contribute to the establishment of environmental managing policies and to regulatory purposes.

Even though the CALPUFF modelling system has been used to successfully simulate the dispersion of refinery emissions, it is not without limitations for developing countries. The major limitation is related to the meteorological data requirements of CALMET. Calmet has switches for the use of either observations or meteorological data from a numerical weather prediction model or a combination of both, which is usually preferred. However, when observations (surface and upper air) are to be used, hourly to 3-hourly data is required. This specification of data is not available in most developing countries hence limiting its use. For example, the Ghana meteorological service could provide daily surface data and not upper air data.

### 5.1.2 Recommendations

The following recommendations are offered for related research and relevant institutions:

1. Even though the refinery emissions in almost all the receptors do not generally exceed regulatory limits, it is obvious that the inclusion of all emittors in the model will result in increased levels of pollutants which could have serious health implications on the exposed population. To be able to quantify the contributions of the other emittors within the industrial complex, their emission rates are necessary. This can be obtained through an emissions inventory campaign within the Tema Industrial area by EPA, Ghana in collaboration with all the industries. Closely linked to this, emission factors for various pollutants can also be developed.

2. The effects of refinery emissions on critical receptors, receptors located in the immediate north and north east of the refinery should be investigated through a health assessment to determine which diseases affect the populations in these receptors.

3. Despite the serious health and environmental implications of population exposure to VOCs and their strong association with ozone ($O_3$), their dispersion and transport could not be modelled. This is because of its composite nature. CALPUFF models single entities and not composites. It is therefore recommended that further research be carried out to characterise the VOCs for modelling purposes.

4. $SO_2$ and $NO_2$ are easily transformed into sulphates and nitrates in the atmosphere which are implicated in many environmental challenges and would therefore be interesting to look at closely. The effect of chemical transformation of these pollutants can be investigated using the mesopuff module in CALPUFF.

5. Real time applications using CALPUFF is recommended as this will be useful in real time analysis and prediction of plume transport and diffusion during accidental releases.

6. Since results of this research clearly indicates $PM_{2.5}$ pollution from TOR, it is important that EPA Ghana conducts regular monitoring exercises at all industries in order to enforce compliance to guidelines.

7. To reduce the error associated with emission rates input into air quality models, it is essential to use data from measurements made directly from the point source. It is therefore recommended that TOR puts in measures to ensure that flow meters are installed at various exit points.

# References

Abdul-Wahab, S. A. (2003). $SO_2$ dispersion and monthly evaluation of the industrial source complex short-term (ISCST32) model at Mina Al-Fahal refinery, Sultanate of Oman. *Environmental management*, 31(2):0276–0291.

Addo, K. A. (2013). Shoreline morphological changes and the human factor. Case study of Accra, Ghana. *Journal of Coastal Conservation*, 17(1):85–91.

Affum, H., Oduro-Afriyie, K., Nartey, V., Adomako, D., and Nyarko, B. B. (2008). Biomonitoring of airborne heavy metals along a major road in Accra, Ghana. *Environmental monitoring and assessment*, 137(1-3):15–24.

Ahuja, S. (1996). *Evaluation of MESOPUFF-II-$SO_x$ Transport and Deposition in the Great Lakes Region*. PhD thesis, University of Toledo.

Al-Fadhli, F. M., Kimura, Y., McDonald-Buller, E. C., and Allen, D. T. (2011). Impact of flare destruction efficiency and products of incomplete combustion on ozone formation in Houston, Texas. *Industrial & Engineering Chemistry Research*, 51(39):12663–12673.

Aleksandropoulou, V. and Lazaridis, M. (2004). Spatial distribution of gaseous and particulate matter emissions in Greece. *Water, air, and soil pollution*, 153(1-4):15–34.

Arku, R. E., Vallarino, J., Dionisio, K. L., Willis, R., Choi, H., Wilson, J. G., Hemphill, C., Agyei-Mensah, S., Spengler, J. D., and Ezzati, M. (2008). Characterizing air pollution in two low-income neighborhoods in Accra, Ghana. *Science of the total environment*, 402(2):217–231.

Bansah, K. J. and Amegbey, N. (2012). Ambient Particulate Matter Monitoring-A Case Study at Tarkwa. *Research Journal of Environmental and Earth Sciences*, 4(4):419–423.

Boubel, R. W., Vallero, D., Fox, D. L., Turner, B., and Stern, A. C. (2013). *Fundamentals of air pollution*, pages 291–320. Elsevier.

Briggs, G. A. (1975). Plume rise predictions, lectures on air pollution and environment impact analysis. *Am. Meteorol. Soc., Boston, USA*, 10.

Britter, R. and Hanna, S. (2003). Flow and dispersion in urban areas. *Annual Review of Fluid Mechanics*, 35(1):469–496.

Brown, R. A. (1991). *Fluid Mechanics of the Atmosphere*, volume 47, pages 197–206. Academic Press.

Brunekreef, B. and Holgate, S. T. (2002). Air pollution and health. *The lancet*, 360(9341):1233–1242.

Chan, L. and Kwok, W. (2000). Vertical Dispersion of Suspended Particulates in urban area of Hong Kong. *Atmospheric Environment*, 34(26):4403–4412.

Chandrasekar, A., Philbrick, C. R., Clark, R., Doddridge, B., and Georgopoulos, P. (2003). Evaluating the performance of a computationally efficient MM5/CALMET system for developing wind field inputs to air quality models. *Atmospheric Environment*, 37(23):3267–3276.

Cimorelli, A. J. et al. (1998). AERMOD–Description of model formulation.

Collett, R. S. and Oduyemi, K. (1997). Air quality modelling: a technical review of mathematical approaches. *Meteorological Applications*, 4(03):235–246.

Corma, A., Palomares, A., Rey, F., and Márquez, F. (1997). Simultaneous Catalytic Removal of $SO_x$ and $NO_x$ with Hydrotalcite-Derived Mixed Oxides Containing Copper, and Their Possibilities to Be Used in FCC Units. *Journal of catalysis*, 170(1):140–149.

Darko, E. and Quist, M. (2012). Low Sulphur Diesel and Refining Process, Technical and Financial Implications for Tema Oil Refinery (TOR) Limited. In *Workshop organized by National Petroleum Authority in Partnership for Clean fuels and Vehicles under the auspices of United Nation Environmental Programme (UNEP) in Accra, Ghana from September 13-14, 2012*.

Davies, T. (1976). Precipitation Scavenging of Sulphur Dioxide in an Industrial Area. *Atmospheric Environment (1967)*, 10(10):879–890.

de Leeuw, F. A., Moussiopoulos, N., Sahm, P., and Bartonova, A. (2001). Urban Air Quality in Larger Conurbations in the European Union. *Environmental Modelling & Software*, 16(4):399–414.

Demuzere, M., Trigo, R., Vila-Guerau de Arellano, J., and Van Lipzig, N. (2009). The impact of weather and atmospheric circulation on $o_3$ and $pm_{10}$ levels at a rural mid-latitude site. *Atmospheric Chemistry and Physics*, 9(8):2695–2714.

Di Sabatino, S., Kastner-Klein, P., Berkowicz, R., Britter, R., and Fedorovich, E. (2003). The modelling of turbulence from traffic in urban dispersion modelspart i: theoretical considerations. *Environmental Fluid Mechanics*, 3(2):129–143.

Dios, M., Souto, J., and Casares, J. (2013). Experimental development of $CO_2$, $SO_2$ and $NO$ emission factors for mixed lignite and sub-bituminous coal-fired power plant. *Energy*, 53:40–51.

Dresser, A. L. and Huizer, R. D. (2011). CALPUFF and AERMOD model validation study in the near field: Martins Creek revisited. *Journal of the Air & Waste Management Association*, 61(6):647–659.

EIPPCB (2012). Best Available Techniques (BAT) Reference Document for the Refining of Mineral Oil and Gas. Technical report.

England, G. C., Zielinska, B., Loos, K., Crane, I., and Ritter, K. (2000). Characterizing $PM_{2.5}$ emission profiles for stationary sources: comparison of traditional and dilution sampling techniques. *Fuel Processing Technology*, 65:177–188.

Fenger, J. (1999). Urban air quality. *Atmospheric environment*, 33(29):4877–4900.

Fernando, H. (2010). Fluid dynamics of urban atmospheres in complex terrain. *Annual Review of Fluid Mechanics*, 42:365–389.

Ferretti, M., Andrei, S., Caldini, G., Grechi, D., Mazzali, C., Galanti, E., and Pellegrini, M. (2008). Integrating monitoring networks to obtain estimates of ground-level ozone concentrationsA proof of concept in Tuscany (central Italy). *Science of the Total Environment*, 396(2):180–192.

Fishwick, S. and Scorgie, Y. (2011). Performance of CALPUFF in predicting time-resolved particulate matter concentrations from a large scale surface mining operation. In *Proceedings of CASANZ Conference from 30 July2 August,2011, Auckland*, pages 647–659.

Fowler, D., Pilegaard, K., Sutton, M., Ambus, P., Raivonen, M., Duyzer, J., Simpson, D., Fagerli, H., Fuzzi, S., Schjørring, J. K., et al. (2009). Atmospheric composition change: ecosystems–atmosphere interactions. *Atmospheric Environment*, 43(33):5193–5267.

Ghannam, K. and El-Fadel, M. (2013). Emissions characterization and regulatory compliance at an industrial complex: an integrated MM5/CALPUFF approach. *Atmospheric Environment*, 69:156–169.

G.S.S (2012). *2010 Population & Housing Census of Ghana: GA-MY*, page 5. Ghana Statistical Service.

Guilbert, J. et al. (2003). The World Health Report 2002-reducing Risks, promoting healthy life. *Education for health-Abingdon-Carfax Publishing Limited*, 16(2):230–230.

Hanna, S., Chang, J., and Strimaitis, D. (1993). Hazardous gas model evaluation with field observations. *Atmospheric Environment. Part A. General Topics*, 27(15):2265–2285.

Hanna, S. R., Strimaitis, D. G., and Chang, J. C. (1991). Evaluation of fourteen hazardous gas models with ammonia and hydrogen fluoride field data. *Journal of hazardous materials*, 26(2):127–158.

Hansard, R., Maher, B., and Kinnersley, R. (2011). Biomagnetic monitoring of industry-derived particulate pollution. *Environmental Pollution*, 159(6):1673–1681.

Harding, R., Peters, A., and Nee, J. (2001). New developments in fcc catalyst technology. *Applied Catalysis A: General*, 221(1):389–396.

Hernández, A., Saavedra, S., Rodríguez, A., Souto, J. A., and Casares, J. J. (2014). Coupling WRF and CALMET models: Validation during primary pollutants glc episodes in an Atlantic coastal region. In *Air Pollution Modeling and its Application XXII*, pages 681–684. Springer.

Hildemann, L. M., Klinedinst, D. B., Klouda, G. A., Currie, L. A., and Cass, G. R. (1994). Sources of urban contemporary carbon aerosol. *Environmental science & technology*, 28(9):1565–1576.

Holmes, N. S. and Morawska, L. (2006). A review of dispersion modelling and its application to the dispersion of particles: an overview of different dispersion models available. *Atmospheric Environment*, 40(30):5902–5928.

Holnicki, P. (2011). Uncertainty in integrated modelling of air quality.

Holtslag, A. and Van Ulden, A. (1983). A simple scheme for daytime estimates of the surface fluxes from routine weather data. *Journal of Climate and Applied Meteorology*, 22(4):517–529.

Irwin, J. S. (1983). Estimating plume dispersion-a comparison of several sigma schemes. *Journal of Climate and Applied Meteorology*, 22(1):92–114.

Jackson, P. (1981). On the displacement height in the logarithmic velocity profile. *Journal of Fluid Mechanics*, 111:15–25.

Janjic, Z. (2003). A nonhydrostatic model based on a new approach. *Meteorology and Atmospheric Physics*, 82(1-4):271–285.

Janjić, Z. I. (2002). Nonsingular implementation of the mellor–yamada level 2.5 scheme in the ncep meso model. *NCEP office note*, 437:61.

Jiménez-García, G., Aguilar-López, R., and Maya-Yescas, R. (2011). The fluidized-bed catalytic cracking unit building its future environment. *Fuel*, 90(12):3531–3541.

Jones, S., Fisher, B. E., Gonzalez-Flesca, N., and Sokhi, R. (2000). The use of measurement programmes and models to assess concentrations next to major roads in urban areas. *Environmental Monitoring and Assessment*, 64(2):531–547.

Khamsimak, P., Koonaphapdeelert, S., and Tippayawong, N. (2012). Simulated Effect of Terrain Change on Dispersion of $SO_2$ Emission Around

Mae Moh Basin. *Recent Advances in Energy,Environment and Economic Development*, pages 200–204.

Kumar, A., Luo, J., and Bennett, G. F. (1993). Statistical evaluation of lower flammability distance (lfd) using four hazardous release models. *Process Safety Progress*, 12(1):1–11.

Levy, J. I., Wilson, A. M., Evans, J. S., and Spengler, J. D. (2003). Estimation of primary and secondary particulate matter intake fractions for power plants in Georgia. *Environmental science & technology*, 37(24):5528–5536.

Liu, M.-K. and Yocke, M. A. (1980). Siting of wind turbine generators in complex terrain. *Journal of Energy*, 4(1):10–16.

Macdonald, R. (2000). Modelling the mean velocity profile in the urban canopy layer. *Boundary-Layer Meteorology*, 97(1):25–45.

Martín, J., Lumbreras, J., and Rodríguez, M. (2003). Testing flare emission factors for flaring in refineries. In *US EPA 12th International emissions inventory conference, San Diego*.

Martin, R. V. (2008). Satellite remote sensing of surface air quality. *Atmospheric Environment*, 42(34):7823–7843.

Maya-Yescas, R., Villafuerte-Macías, E., Aguilar, R., and Salazar-Sotelo, D. (2005). Sulphur oxides emission during fluidised-bed catalytic cracking. *Chemical Engineering Journal*, 106(2):145–152.

Michalakes, J., Dudhia, J., Gill, D., Henderson, T., Klemp, J., Skamarock, W., and Wang, W. (2004). The Weather Research and Forecast Model: Software Architecture and Performance. In *Proceedings of the 11th ECMWF Workshop on the Use of High Performance Computing In Meteorology*, volume 25, page 29. World Scientific.

Monin, A. and Obukhov, A. (1954). Basic laws of turbulent mixing in the surface layer of the atmosphere. *Contrib. Geophys. Inst. Acad. Sci. USSR*, 151:163–187.

Muff, R. and Efa, E. (2006). Ghana-Germany technical cooperation project: environmental and engineering geology for urban planning in the Accra-Tema area. *Explanatory notes for the geological map for urban planning*, 1(50):000.

Muller, N. Z. and Mendelsohn, R. (2007). Measuring the damages of air pollution in the united states. *Journal of Environmental Economics and Management*, 54(1):1–14.

Ofosu, F. G., Hopke, P. K., Aboh, I. J., and Bamford, S. A. (2012). Characterization of fine particulate sources at Ashaiman in Greater Accra, Ghana. *Atmospheric Pollution Research*, 3(3).

Pandey, J., Agrawal, M., Khanam, N., Narayan, D., and Rao, D. (1992). Air pollutant concentrations in Varanasi, India. *Atmospheric Environment. Part B. Urban Atmosphere*, 26(1):91–98.

Pasquill, F. and Smith, F. (1983). Atmospheric diffusion.: Study of the dispersion of windborne material from industrial and other sources. *JOHN WILEY & SONS, 605 THIRD AVE., NEW YORK, NY 10016, USA. 1983.*

Pearce, J. L., Beringer, J., Nicholls, N., Hyndman, R. J., Uotila, P., and Tapper, N. J. (2011). Investigating the influence of synoptic-scale meteorology on air quality using self-organizing maps and generalized additive modelling. *Atmospheric Environment*, 45(1):128–136.

Perez Ballesta, P., Field, R., Fernandez-Patier, R., Galan Madruga, D., Connolly, R., Baeza Caracena, A., and De Saeger, E. (2008). An approach for the evaluation of exposure patterns of urban populations to air pollution. *Atmospheric Environment*, 42(21):5350–5364.

Products, U. O. (1997). Fluid catalytic cracking process manual - process calculations,. pages 21–33, 64–68.

Protonotariou, A., Bossioli, E., Athanasopoulou, E., Dandou, A., Tombrou, M., Assimakopopoulos, V., Flocas, H., and Chelmis, C. (2004). Validation and inter-comparison of CALPUFF regulatory model to Eulerian models and measurements. An application over the greater Athens area, Greece. In *Proceedings of the 9th International Conference on Harmonisation within Atmospheric Dispersion Modelling for Regulatory Purposes*, pages 131–135.

Puliafito, S. E., Allende, D., Fernández, R., Castro, F., and Cremades, P. (2011). New approaches for urban and regional air pollution modelling and management. *Air Pollution/Book*, 1.

Qin, Y. and Kot, S. (1993). Dispersion of vehicular emission in street canyons, Guangzhou City, South China (PRC). *Atmospheric Environment. Part B. Urban Atmosphere*, 27(3):283–291.

Raupach, M. and Thom, A. S. (1981). Turbulence in and above plant canopies. *Annual Review of Fluid Mechanics*, 13(1):97–129.

Ravindra, K., Mor, S., Kamyotra, J., Kaushik, C., et al. (2003). Variation in spatial pattern of criteria air pollutants before and during initial rain of monsoon. *Environmental monitoring and assessment*, 87(2):145–153.

Rotach, M. (1994). Determination of the zero plane displacement in an urban environment. *Boundary-Layer Meteorology*, 67(1-2):187–193.

Sackey, S. S. (2012). *Development of DOAS remote sensing system for ground-based measurements of trace gas emissions in an industrial area*. PhD thesis.

Safo-Adu, G., Ofosu, F., Carboo, D., and Armah, Y. (2014). Heavy metals and black carbon assessment of PM10 particulates along Accra–Tema highway in Ghana. *International Journal of Science and Technology*, 3(8).

Schürmann, G., Algieri, A., Hedgecock, I., Manna, G., Pirrone, N., and Sprovieri, F. (2009). Modelling local and synoptic scale influences on ozone concentrations in a topographically complex region of Southern Italy. *Atmospheric Environment*, 43(29):4424–4434.

Scire, J. S., Robe, F. R., Fernau, M. E., and Yamartino, R. J. (2000a). A User's guide for the CALMET Meteorological Model. *Earth Tech, USA*, 37.

Scire, J. S., Strimaitis, D. G., and Yamartino, R. J. (2000b). A User's guide for the CALPUFF Dispersion Model. *Earth Tech, Inc*, 521:1–521.

Seigneur, C., Pun, B., Pai, P., Louis, J.-F., Solomon, P., Emery, C., Morris, R., Zahniser, M., Worsnop, D., Koutrakis, P., et al. (2000). Guidance for the performance evaluation of three-dimensional air quality modeling systems for particulate matter and visibility. *Journal of the Air & Waste Management Association*, 50(4):588–599.

Shamarock, W., Klemp, J., Dudhia, J., Gill, D., Barker, D., Duda, M., Huang, X., Wang, W., and Powers, J. (2008). A Description of the Advanced Research WRF version 3. *NCAR technical note NCAR/T-N/u2013475*.

Skamarock, W. C., Klemp, J. B., Dudhia, J., Gill, D. O., Barker, D. M., Wang, W., and Powers, J. G. (2005). A description of the advanced research wrf version 2. Technical report, DTIC Document.

Stull, R. B. (2012). *An introduction to boundary layer meteorology*, volume 13, page 2. Springer Science & Business Media.

Truhetz, H., Gobiet, A., and Kirchengast, G. (2007). Evaluation of a dynamic-diagnostic modelling approach to generate highly resolved wind fields in the Alpine region. *Meteorologische Zeitschrift*, 16(2):191–201.

Tsuang, B.-J. (2003). Quantification on the Source/Receptor Relationship of Primary Pollutants and Secondary Aerosols by a Gaussian Plume Trajectory Model: Part I Theory. *Atmospheric Environment*, 37(28):3981–3991.

USEPA (2001). Preferred and alternative methods for estimating air emissions from boilers. 2.

USEPA (2010). Available and emerging technologies for reducing greenhouse gas emissions from the petroleum refining industry. 2.1.1.

USEPA (2011). Emission estimation protocol for petroleum refineries. 2.1.1.

USGS (2010). The Global Land Cover Characterization (GLCC)Database. *NCAR technical note NCAR/TN/u2013475*.

Venkatesan, R., Mathiyarasu, R., and Somayaji, K. (2002). A Study of Atmospheric Dispersion of Radionuclides at a Coastal site using a modified Gaussian Model and a Mesoscale Sea Breeze model. *Atmospheric Environment*, 36(18):2933–2942.

Venkatram, A. (1978). An examination of box models for air quality simulation. *Atmospheric Environment (1967)*, 12(12):2243–2249.

Versteeg, H. K. and Malalasekera, W. (2007). *An Introduction to Computational Fluid Dynamics: The Finite Volume Method*, pages 1–6. Pearson Education Limited, England.

WHO (2000). *Air quality guidelines for Europe*, volume 91, pages 1–287. Second Edition,Copenhagen, WHO Regional Office for Europe.

Wieringa, J. et al. (2001). New revision of davenport roughness classification. *Proc., 3EACWE, Eindhoven, The Netherlands*, pages 285–292.

Willmott, C. J. (1982). Some comments on the evaluation of model performance. *Bulletin of the American Meteorological Society*, 63(11):1309–1313.

Wood, E. C., Herndon, S. C., Fortner, E. C., Onasch, T. B., Wormhoudt, J., Kolb, C. E., Knighton, W. B., Lee, B. H., Zavala, M., Molina, L., et al. (2012). Combustion and destruction/removal efficiencies of in-use chemical flares in the greater Houston area. *Industrial & Engineering Chemistry Research*, 51(39):12685–12696.

Zadakbar, O., Vatani, A., and Karimpour, K. (2008). Flare gas recovery in oil and gas refineries. *Oil & Gas Science and Technology-Revue de l'IFP*, 63(6):705–711.

Zannetti, P. (2013). *Air Pollution Modeling: Theories, Computational Methods and Available Software*, pages 107–130. Springer Science & Business Media, New York.

Zawar-Reza, P., Kingham, S., and Pearce, J. (2005). Evaluation of a year-long dispersion modelling of $PM_{10}$ using the mesoscale model TAPM for Christchurch, New Zealand. *Science of the Total Environment*, 349(1):249–259.

Zhao, X., Peters, A., and Weatherbee, G. (1997). Nitrogen chemistry and $NO_x$ control in a fluid catalytic cracking regenerator. *Industrial & engineering chemistry research*, 36(11):4535–4542.

Zhou, Y., Levy, J. I., Hammitt, J. K., and Evans, J. S. (2003). Estimating population exposure to power plant emissions using CALPUFF: a case study in Beijing, China. *Atmospheric Environment*, 37(6):815–826.

# Appendix A

## A Estimation of Refinery Emission Rates

### A.1 Estimation of Flue Stack Gas Rate and Composition

#### A.1.1 Combustion Air Correction to Dry Basis

To correct the combustion air to dry basis, the combined gas law equation, Eqn.(1) was used:

$$\frac{P_1 V_1}{T_1} = \frac{P_2 V_2}{T_2} \tag{1}$$

Given the following parameters (2009): $P_1$= 1 atm, $V_1 = 63882.88$ $Nm^3/hr$, $T_1$= 273 K, $P_2$ = 1 atm, $V_2$ =? $T_2$ = (120 + 273)K

$V_2 = 91963.27$ $m^3$

A Relative Humidity (RH) of 80% for Accra during the study period implies:

Moisture content = (0.017 kg $H_2O$/ 1 kg of dry air) from the Psychometric chart

Therefore, the average Volumetric Air Flow rate (Dry Basis) into regenerator = 90426.04 $m^3$/hr

Dry air density at 373 K = 0.9 kg/$m^3$

Therefore, the average mass Air Flow rate (Dry Basis) into regenerator = 81383.421 kg = 2809.61 kmol/hr with dry air molar mass of 28.966 kg/kmol

### A.1.2 Calculation of Flue Gas Rate

The flue gas rate can be calculated from the regenerator air rate. These two streams are related by the inert ($N_2$ + Ar) content which remains constant through the catalyst regeneration. From a nitrogen balance:

kmol ($N_2$ + Ar) in dry air = kmol ($N_2$ + Ar) in flue gas

(2809.61 × 0.79) kmol = Flue Gas rate × (0.82)

Therefore Flue gas molar flowrate = 2706.83 kmol/hr

### A.1.3 Flue Stack Gas Components

From the flue gas composition provided in Table 1, the $CO_2$ emission from the flue stack can be calculated.

Table 1: Flue Gas Composition

| **Component** | **$CO_2$** | **CO** | **$N_2$** | **$SO_2$** | **$NO_2$** | **$O_2$** |
|---|---|---|---|---|---|---|
| % Composition | 15.50 | 0 | 82 | 0 | 0 | 2.5 |

1. **$CO_2$**

   From the GC in the Table 1,

   $CO_2$ molar flow rate = 0.155(2706.83) = 419.56 kmol/hr

Molar mass of $CO_2$ = 44 kg/kmol is

Mass flow rate of $CO_2$ = 18460.56 kg/hr

**2. $SO_x$**

If the Density of feedstock = 907 kg/$m^3$ and the volumetric flow rate of feedstock(2009) = 72.02 $m^3$

Then the Mass flow rate of feedstock = 65322.14 kg/hr

With 1% wt of feed = sulphur content

Sulphur content = 653.22 kg

5% of feed sulphur is combusted in regenerator

Mass of combusted sulphur = 32.66 kg

Molar mass of Sulphur = 32 kg/kmol

90% of combusted sulphur reacts to form $SO_2$

Mass of combusted sulphur to $SO_2$ = 0.9(32.66) = 29.39 kg

Moles of combusted sulphur to $SO_2$ = 0.92 kmol

Based on the following stoichiometry of the reaction:

$S + O_2 \longrightarrow SO_2$ ..... (1)

Moles of $SO_2$ formed = 0.92 kmol

Molar mass of $SO_2$ = 64 kg/kmol

Therefore Mass of $SO_2$ = 0.92(64) = 58.88 kg

10% of combusted sulphur reacts to form $SO_3$

Mass of combusted sulphur to $SO_3$ = 0.1(32.66) = 3.27 kg

Moles of combusted sulphur to $SO_3$ = 0.10 kmol

Based on the following stoichiometry of the reaction:

$2S + 3O_2 \longrightarrow 2SO_3$ ..... (2)

Moles of $SO_3$ formed = 0.92 kmol

Molar mass of $SO_3$ = 80 kg/kmol

Therefore Mass of $SO_3$ produced = 0.10(80) = 8.00 kg

**3. $NO_x$**

If 0.32% of feed = elemental nitrogen

Mass of Nitrogen = 0.0032(65322.14) = 209.03 kg

15% of feed nitrogen combusted with coke on catalyst = 0.15(209.03) = 31.35 kg

Molar mass of elemental nitrogen = 14 kg/kmol

Moles of feed nitrogen combusted = 2.24479 kmol

90% of combusted nitrogen reacts to form NO

Based on the following stoichiometry of the reaction:

$2N + O_2 \longrightarrow 2NO$

Moles of NO produced = 0.9(2.24479 kmol) = 2.02 kmol

Molar mass of NO = 30 kg/kmol

Mass of NO produced = 60.47 kg

10% of combusted nitrogen reacts to form $NO_2$

Based on the following stoichiometry of the reaction:

$N + O_2 \longrightarrow NO_2$

Moles of $NO_2$ produced = 0.1(2.24479 kmol) = 0.22 kmol

Molar mass of $NO_2$ = 46 kg/kmol

Mass of $NO_2$ produced = 10.30 kg

**4. (Coke + Catalyst fines)**

**(a) Coke**

1 kg of solid particulates is produced for every 1000 kg of coke-on-catalyst (COC) combusted.(TOR Manual)

From the stoichiometry of the COC combustion kinetics below:

$2C + 11/2O_2 + H_2 + S + N \longrightarrow CO_2 + CO + H_2O + SO_2 + NO_2 + O_2$ .....(3)

Moles of $CO_2$ produced = moles of $CO_2$ in Flue gas = 419.56 kmol

Hence moles of Coke combusted = 2(419.558) = 839.12 kmol

Molar mass of coke = 12 kg/kmol

Mass of coke combusted = 10069.40 kg

Therefore Mass of coke particulates produced = 10.07 kg

**(b) Catalyst fines** At a cyclone efficiency of 99.75% and a catalyst inventory of 120000 kg (TOR Manual)

Catalyst fines lost to the air = 0.0025(120000) = 300 kg

Total Particulates = 300 + 10.07 = 310.07 kg

## A.2 Estimation of Flared Gas Composition

**1. Volatile Organic Compounds (VOCs)**

With Fuel Gas mass flow rate = 6239.0 kg and a Flare efficiency = 98% (TOR Manual)

Total VOCs in flare exit = 0.02(6239.0)kg = 124.78 kg

Average Fuel gas composition (Vol%) by GC method and volume by calculations is given in Table 2.

Then based on the stoichiometry of the reactions below, the moles and masses of the product gases are derived.

Table 2: RFCC Fuel Gas Composition

| **Component** | **Vol%** |
|---|---|
| $C_1$ | 28.0319 |
| $C_2$ | 10.46 |
| $C_3$ | 0.25 |
| Ethylene | 12.37 |
| Propylene | 1.86 |
| Butene | 1.56 |
| CO | 1.03 |
| $H_2$ | 25.85 |
| $CO_2$ | 2.197 |
| $H_2S$ | 0.4 |
| $N_2$ | 14.58 |

From the following stoichiometric combustion reactions:

$CH_4 + 2O_2 \longrightarrow CO_2 + 2H_2O$ .....(1)

$C_2H_6 + 7/2O_2 \longrightarrow 2CO_2 + 3H_2O$ .....(2)

$C_3H_8 + 5O_2 \longrightarrow 3CO_2 + 4H_2O$ .....(3)

$C_2H_4 + 3O_2 \longrightarrow 2CO_2 + 2H_2O$ .....(4)

$C_3H_6 + 9/2O_2 \longrightarrow 3CO_2 + 3H_2O$ .....(5)

$C_4H_6 + 11/2O_2 \longrightarrow 4CO_2 + 3H_2O$ .....(6)

$CO + 1/2O_2 \longrightarrow CO_2$ .....(7)

$2H_2S + 3O_2 \longrightarrow 2SO_2 + 2H_2O$ .....(8)

Total moles of $CO_2$ produced = 283.147 kmol

Mass flowrate of $CO_2$ = 283.147(44) = 12458.49 kg

**2. Total $SO_2$**

Total moles of $SO_2$ from $H_2S$ combustion = 1.35 kmol

Total mass of $SO_2$ = 86.45 kg

Tables 3 and 4 present the calculated emission rates for the years under consideration.

Table 3: RFCCU and (Total Refinery) Flare Stack Emission Rates(kg/hr)

| Emission Rate | 2008 | 2009 | 2010 | 2011 | 2012 | 2013 |
|---|---|---|---|---|---|---|
| **$SO_2$** | 87 (433) | 87 (432) | 95 (475) | 88 (441) | 81 (406) | 72 (361) |
| **$CO_2$** | 12478 (62391) | 12458 (62292) | 13695 (68478) | 12716 (63582) | 11688 (58440) | 10397 (51989) |
| **VOCs** | 125 (2500) | 125 (2496) | 137 (2743) | 127 (2547) | 117 (2341) | 104 (2083) |

Table 4: RFCCU and (Total Refinery) Flue Stack Emission Rates(kg/hr)

| Emission Rate | 2008 | 2009 | 2010 | 2011 | 2012 | 2013 |
|---|---|---|---|---|---|---|
| **$SO_2$** | 73 (366) | 64 (335) | 74 (372) | 68 (341) | 69 (347) | 69 (346) |
| **$CO_2$** | 20514 (102570) | 18460 (92302) | 18248 (91240) | 16458 (82292) | 16040 (80203) | 16079 (80398) |
| **$NO_2$** | 77 (387) | 71 (354) | 79 (394) | 72 (361) | 73 (367) | 73 (366) |
| **$PM_{2.5}$** | 311 (1037) | 310 (1034) | 310 (1033) | 309 (1030) | 309 (1029) | 309 1029) |

## A.3 Calculation of Flare and Flue Stack Exit Gas Velocities

Table 5 provides the parameters used for the calculations.

Table 5: RFCC Point Sources Parameters

| Point Source | Diameter (m) | Height (m) | Temperature (K) |
|---|---|---|---|
| **Flue Stack** | 1.28 | 60 | 513 |
| **Flare** | 0.6 | 55 | 1273 |

Given the flare gas exit temperature of 1273 K and obtaining the volumetric flow rate from the given mass rate and the cross-sectional area for the flare

diameter, the flare gas velocity is calculated as follows using flow parameters for the year 2009:

Given the flare cross-sectional area of 0.287 $m^2$, flare gas mass flow rate of 6239 kg/hr and fuel gas density of 0.8 $kg/m^3$, the volumetric flow rate can be calculated using Eqn.(2):

$$\dot{V} = \frac{\dot{m}}{\rho} \tag{2}$$

Where $\dot{V}$ is the volumetric flow rate, $\dot{m}$ the mass flow rate and $\rho$ the gas density

Volumetric flow rate = 7798.85 $m^3$

From Eqn.(3), the gas velocity can be obtained.

$$v = \frac{\dot{V}}{A} \tag{3}$$

Where v is the velocity and A the cross-sectional area of the flare.

Velocity = 7.66 m/s

The flue gas volume is determined from its moles using the ideal gas equation given by Eqn.(4).

$$PV = nRT \tag{4}$$

Where

P is the pressure,

V is the volume,

n is the number of moles,

R is the universal gas constant and

T the temperature of the gas.

Using a pressure of 101.423 kPa and the moles of flue gas of 2706.828 kmols which was calculated early on, the flue gas volume is given as:

Flue Gas volumetric flow rate = 112345.895$m^3$/hr = 31.207$m^3$/s

Given the Flue stack area of 1.127 $m^2$,

Flue Gas velocity = 24.25 m/s

Table 6: Average Exit Gas Velocities of Point Sources Used for the Simulations for 2008 - 2013

| | Exit Gas Velocity(m/s) | | | | | |
|---|---|---|---|---|---|---|
| **Point Source** | **2008** | **2009** | **2010** | **2011** | **2012** | **2013** |
| **Flare** | 7.67 | 7.66 | 8.42 | 7.82 | 7.19 | 6.39 |
| **Flue Stack** | 26.94 | 24.25 | 23.97 | 21.62 | 21.07 | 21.12 |